THE FIELD PERFORMANCE OF HIGH-REFLECTANCE SINGLE-PLY MEMBRANES EXPOSED TO THREE YEARS OF WEATHERING IN VARIOUS U.S. CLIMATES

August 2002

William A. Miller, P.E., Ph.D.
Meng-Dawn Cheng, Ph.D.
Susan Pfiffner, Ph.D.
Nan Byars, Ph.D.

Engineering Science and Technology Division

THE FIELD PERFORMANCE OF HIGH-REFLECTANCE SINGLE-PLY MEMBRANES EXPOSED TO THREE YEARS OF WEATHERING IN VARIOUS U.S. CLIMATES

William A. Miller, P.E., Ph.D.
Meng-Dawn Cheng, Ph.D.
Susan Pfiffner, Ph.D.
Nan Byars, Ph.D.

August 2002

Prepared for
The Single-Ply Roofing Institute
Needham, MA

Prepared by
OAK RIDGE NATIONAL LABORATORY
P.O. Box 2008
Oak Ridge, Tennessee 37831-6285
managed by
UT-Battelle, LLC
for the
U.S. DEPARTMENT OF ENERGY
under contract DE-AC05-00OR22725

CONTENTS

FIGURES

TABLES

ACRONYMS

BTC	Buildings Technology Center
BUR	built up roof
CDD	cooling-degree days
CL	cooling load
COP	coefficient of performance
CRRC	Cool Roof Rating Council
DOE	U.S. Department of Energy
EPA	U.S. Environmental Protection Agency
ESRA	envelope systems research apparatus
FAMES	fatty acid methyl esters
GC	gas chromatography
HDD	heating degree days
HFT	heat flux transducer
HL	heating load
HVAC	heating, ventilating, and air-conditioning
ICP-AES	inductively coupled plasma atomic emission spectroscopy
MSD	mass selective detector
NOAA	National Oceanic and Atmospheric Administration
OEM	original equipment manufacturer
ORNL	Oak Ridge National Laboratory
PLFA	phospholipid fatty acid
PVC	polyvinyl chloride
PVDF	polyvinylidene fluoride
R^2	root mean square
SHPF	seasonal heating performance factor
SPRI	Single-Ply Roofing Institute
STAR	simplified transient analysis of roofs
TiO_2	titanium dioxide
TMY2	typical meteorological year
TPO	polyethylene polyolefins

ACKNOWLEDGMENTS

The Single-Ply Roofing Institute (SPRI) and its affiliates enacted a series of User Agreements with the Buildings Technology Center (BTC) of the Oak Ridge National Laboratory (ORNL) to conduct a field study on the thermal performance of low-slope, high reflectance roofing membranes. The BTC has a long history of involvement in measuring and modeling the effects of cool roof membranes on the thermal performance of roofing systems. The BTC has documented the performance comparison of thermoset, thermoplastic, bitumen-based single-ply membranes, and ballasted membrane systems over a three-year period and has provided in this report the deliverables agreed to at the onset of the project. These deliverables are (1) documentation of the long-term energy savings for highly reflective single-ply membranes as compared to a smooth built-up, low-slope roof, (2) the development of a procedure for quantifying the benefits of single-ply membranes, and (3) the adoption and use of the procedure by the roofing industry.

The BTC thanks Carlisle, Firestone, DuroLast, JPS Elastomerics, Sarnafil, SPRI and its members for their cooperation in the completion of the field study. Our common goal is to boost the market share of single-ply membranes through the improvements in the energy efficiency and service life of these low-slope roofing systems. The support of SPRI, its members, and associates is appreciated. We have provided crucially important lifetime performance field data of single-ply membrane systems over a three-year period that will help manufacturers improve their products and further accelerate the market penetration of high reflectance "cool" roofing membranes.

ABSTRACT

Cool roof membranes can be a critical component of a proactive roof maintenance program that results in lower lifetime membrane temperatures during sunny periods. The lower membrane temperatures, in turn, reduce the air conditioning loads of the building and potentially lengthen the service life of the roofing system. If the building is located where cooling loads predominate, peak load reductions and net annual energy savings are also realized. In mixed climates with both significant heating and cooling loads, the wintertime effect reduces the energy benefit because the desirable roof heat gain in winter is diminished somewhat by the higher solar reflectance of the membrane.

Determining how exposure to the various climatic elements affects the reflectance and emittance of single-ply membranes is of paramount importance for promoting the energy efficiency and accelerating the market penetration of reflective roof products in commercial and industrial applications. Ultraviolet radiation, atmospheric pollution, microscopic growths, acid rain, temperature cycling caused by sunlight and sudden thunderstorms, moisture penetration, condensation, wind, hail, and freezing and thawing all contribute to the loss of reflectance of a roof's exterior surface. However, data describing the impact of the weather are extremely sparse simply because of the time and patience required to collect and interpret the data. Temperature, heat flow, reflectance, and emittance field data have been electronically cataloged for a full 3 years for 18 different single-ply membrane roofs exposed to the climate of East Tennessee on an outdoor test facility, the Envelope Systems Research Apparatus (ESRA).

Our results gleaned from the ESRA show that the surfaces of the white thermoplastic roof systems lost about 30 to 50% of their reflectance after 3 full years of field exposure. Our findings show that airborne particles are responsible for the loss in roof reflectance, and are also the vehicles for delivering microorganisms to the surface as these particles are deposited on the membrane. Microorganisms grow on the surface, sprouting thin root-like filaments called hyphae that are covered with enzymes. The roof becomes wet during the evening hours because the surface temperature falls below the dew point temperature of the ambient air. The enzymes dilute in the condensate and dissolve edible food from the surface of the membrane. The hyphae grow into a biological film-like mat that is hydrophilic and keeps the surface moist even when the air is dry. The hyphae also act as a net enhancing the continued deposition of dirt onto the surface, which in turn leads to larger losses in reflectance. Soiling may be exacerbated in certain thermoplastic membranes whose formulations contain edible foodstuffs for the biomass.

The cost of additional polyisocyanurate insulation required by a smooth built-up roof (BUR), constrained to have the same annual operating cost of energy as a high-reflectance roof, was compared to the cost for white thermoplastic membranes to judge the affordability of cost premiums for the membranes. Analysis showed a synergistic cost benefit because of the combined effect of R-value and reflective roofing that peaks as R-value increases from R-5 up to about R-20; however, continuing to increase R-value beyond R-20 causes the effect of insulation to mask the effect of a reflective roof. Results show that consumers in Phoenix, AZ, and Knoxville, TN, can easily afford cool membranes as compared to the additional cost of insulation for a smooth BUR.

The annual roof energy for a soiled thermoplastic membrane exposed in a predominantly cooling climate was observed to increase by 50% of the roof energy for the same thermoplastic membrane constrained to have no loss in reflectance. The increase in energy decreases through 3 years of exposure as the loss of reflectance levels off. In a more moderate climate, the cooling-energy savings are offset by the heating-energy penalty, and it appears that the ratio of cooling degree-days to heating

degree-days exceeding 0.4 may roughly represent the boundary for periodically washing cool roof membranes. Washing a reflective membrane in moderate to cooling-predominant climates will save roof energy by offsetting the impact of soiling of the membrane.

1. EXECUTIVE SUMMARY

A combined experimental and analytical study was conducted to quantify the energy savings and affordable cost premiums for cool roof membranes. The single-ply membranes tested in the study were thermoplastics, bitumen-based membranes, and thermoset membranes covered with 15 lb/ft^2 (73 kg/m^2) of ballast. The thermoplastics membranes tested were either polyvinyl chloride (PVC), polypropylene or polyethylene polyolefins (TPO). All test membranes were assigned proprietary codes. Participants knew the code only for their own roof product, and could therefore assess their system against the field of systems. The scheme kept the identity of each company's product confidential. A smooth built-up roof (BUR), Code C, was used as the base of comparison to determine energy savings in different geographic regions of the United States.

Experimental work included the initial measurement of reflectance and subsequently a measurement every fourth month. Emittance was measured annually. Field data of the temperature and heat flux were organized and plotted weekly for comparing the cool membranes against the BUR. Candidate single-ply membranes were also exposed at field sites across the country, and reflectance was measured semiannually to assess the effect of climate.

The program Simplified Transient Analysis of Roofs (STAR) was further formulated and validated against the envelope system research apparatus (ESRA) field data. STAR was coupled to the DOE-2.1E program to model a warehouse and show the annual energy savings obtainable from the candidate roof membranes from the perspective of the whole building. However, the multiplicity of building types, the diversity of the occupant's habits, the broad range of exterior surface area-to-building volume, and a building's internal loading can confound the interpretation of results developed for reflective roofing. Therefore, Petrie et al. (2001a) formulated a roof calculator for predicting the heat flow solely through the roof. STAR was used to generate the annual heating and cooling roof loads for different geographic regions within the United States. The cool roof calculator uses the computed roof loads to calculate the energy use and savings from a candidate roof membrane as compared to a smooth black roof with solar reflectance of 0.05 and infrared emittance of 0.90. The calculator computations have no interaction with the characteristics of the building and therefore eliminate the confounding building variables that can confuse measuring the performance of a roof.

1.1 CLIMATIC EXPOSURE AND CLEANING IMPACTS ON SURFACE REFLECTANCE

Three years of exposure in East Tennessee's climate soiled all white thermoplastic membranes that were field tested on the ESRA and caused about 30 to 50% loss of surface reflectance. Data from the field sites revealed that the loss in reflectance is similar across the country for test membranes J, F, and I. The dry climate in Denver, CO, showed similar drops in reflectance as observed in the predominantly heating-load climate of Joplin, MO, as well as in the colder and more humid climate of Boston, MA. However, the loss in reflectance for membranes coded A, G, K, and M was less severe at the field sites than that observed on the ESRA. The field samples were not directly adhered to roof insulation and therefore were about 15°F (8.3°C) cooler at solar noon than the same thermoplastic membranes fully adhered atop wood fiberboard and tested on the ESRA. We believe the higher peak membrane temperature observed at solar noon is the probable cause of the differences in reflectance loss.

After one full year of exposure on the ESRA, the reflectance of membranes coded A, B, F, J, K, M, P, and I dropped uniformly, and then three to six months later increased slightly. Intensity of rainfall appears to have minimal effect on the changes in reflectance. Actually, the membranes A, G, K, and M showed an accelerated loss of reflectance when the intensity of the rain was the strongest in the

summer months. Membranes A, K, and M all showed unexpected variations in reflectance, while membrane G showed a more uniform loss of reflectance with time.

The results are especially interesting for the single-ply membrane code A because its reflectance drops below 0.5 after 2 years of exposure. The U.S. Environmental Protection Agency (EPA) permits washing the membrane, and one would expect from the field data that the membrane must be washed to meet Energy Star® specifications. However, the reflectance of Code A again slightly exceeded 0.5 reflectance after the third year of exposure. Therefore, Code A just qualifies for the Energy Star logo. The individual trends of Codes A, K, and M with time are very interesting because as the intensity of rainfall increases, the losses in reflectance also increase. The three membranes show an increase in reflectance from 2.25 years of exposure to 2.5 years. Afterwards the reflectance again drops as exposure exceeds 3 years of weathering. The pattern appears to have about a 6-month cycle. In the summer, the reflectance drops; while in the winter, the reflectance increases—but the summertime drop exceeds the wintertime gain, and the cumulative loss in reflectance almost exceeds 50% after 3 years of exposure.

The intensity of the rainfall, foot traffic, biological growth, and possibly the ingredients formulated in the membranes could cause the unexpected variations. Both solid and liquid plasticizers are used in the formulation of some thermoplastic membranes to keep the material from becoming brittle and tearing. The climatic cycling of temperature is known to cause certain liquid plasticizers to migrate to the surface of the membrane, making the surface tacky; the plasticizers may also be a food source for the growth of the biomass (Griffin 2002). In either case, the effect of plasticizer should be investigated to determine its effect on the loss of reflectance of certain white thermoplastic single-ply membranes, but such a study is beyond the scope of this report.

Our findings show that airborne particles themselves are responsible for the loss in roof reflectance, and these particles are also the vehicles for delivering microorganisms to the surface as they are deposited on the membrane. Microorganisms grow on the surface forming a biological filmlike structure that is hydrophilic. Once formed, the structure forms a net that enhances the continued deposition of dirt onto the surface, which in turn leads to larger drops in reflectance. Without the surface biomass, particles will still deposit on a roof, but the drop in reflectance is less severe over time. Correlating the drop in reflectance helped substantiate our hypothesis. Regression analysis indicated that the parameters that most strongly influence the decrease in membrane reflectance were relative humidity, average daily temperature change, time, and the number of rain days. All of these parameters promote and stimulate the growth of biomass.

The results also suggest that manufacturers should check the formulation of certain thermoplastic membranes for ingredients that may promote fungal metabolism and thereby exacerbate the loss of reflectance. A judicious selection of ingredients that hinder the growth of biomass may be a key parameter for optimizing the formulation of white thermoplastic membranes for sustaining high reflectance.

Washing the membranes with commercially available cleaners almost fully restored the reflectance. For example, the highly reflective membrane Code B had developed a splotchy dull gray appearance that caused reflectance to drop about 55% after 3 years of exposure. However, cleaning almost fully restored the surface reflectance. Similar results were observed for almost all the membranes. In this 3-year, time-limited study, the results reveal that the surface opacity of the single-ply membrane limits the photochemical degradation caused by ultraviolet light present in sunlight because manufacturers have formulated the surface of their membranes to include titanium dioxide (TiO_2), a rare earth ceramic material. TiO_2 is chemically inert, insoluble, and very heat resistant. It increases surface reflectance through refraction and diffraction of the light. The light travels a shorter path and

does not penetrate as deeply into the membrane; therefore, less heat is absorbed. However, the membranes may indeed show signs of weathering after 8 to 12 years of exposure, which again is beyond the scope of this 3-year study.

The emittance of the membrane systems did not vary much from year to year. In fact, the variation in emittance was less than 5% of the average emittance for all the white thermoplastic membranes. The results are consistent with the observations of Wilkes et al. (2000) for roof coatings. The average emittance for all the white thermoplastic membranes was about 0.90 and the average standard deviation for all the membranes was about ±0.04.

1.2 THERMAL PERFORMANCE

Simulations using STAR coupled to the DOE 2.1E building code showed that the heat transmission through the roof of a warehouse having a dark BUR with R-5 insulation was about one-half of the cooling loads for the whole building. The more reflective the roof membrane remains, the lower will be its surface temperature and the less will be the load supported by the cooling plant. Therefore, the thermal performance of low-slope roofs is determined by the roof's exterior temperature, which in turn is affected by the soiling of the roof's surface. The soiling caused a drop in reflectance and caused the measured peak membrane temperature to increase from year to year as shown below in Table 1.

Table 1. The measured peak membrane temperatures for Code A, J, and C membranes exposed on the ESRA for 3 years to East Tennessee's climate

	Aug. 14–20, 1998	Aug. 6–12, 1999	Aug. 11–17, 2000	Aug. 31–Sep. 6, 2001
Code A	106.1	132.9	133.6	140.2
Code J	110.0	130.5	121.5	119.1
BUR	169.2	168.6	159.0	162.8

The peak temperature for the BUR was a measured 169°F (76.1°C) in August 1998. The maximum outdoor air temperature was about 97°F (36.1°C), and the membranes are only about 9°F (5°C) warmer than the outdoor air temperature for measurements made in August of 1998. As time progresses from year to year, the membrane's soil and the peak membrane temperatures increase. After 3 years, the surface temperature of Code A increased by about 34°F (19°C), which in turn caused the measured roof heat flow entering the building to double! On August 18, 1998, the measured daytime heat flux entering through the Code A membrane was 28 Btu/ft^2 (88 Wh/m^2). Three years later, on September 4, 2001, the heat flux had increased to 56 Btu/ft^2 (176.6 Wh/m^2). Surprisingly, just after 1 year of exposure, a 30% drop in reflectance caused the membrane temperature to increase by 27°F (15°C) for measurements taken in August 1999. The soiling of the single-ply membranes caused by climatic exposure is therefore significant because after only 1 to 3 years of field exposure, the "highly reflective" membrane (Code A) has a surface temperature that is only 22.6°F (12.5°C) lower than a BUR. As a result, the heat flux penetrating Code A increased from 25 to 50% of the flux penetrating the BUR after 3 years of field exposure in Oak Ridge, TN.

The soiling of the Code J membrane was not as severe as that observed for Code A. Initially, Code A had a higher reflectance than Code J; however, the reflectance of membrane Code J exceeded that of Code A after 3years of exposure. The soiling of the membrane J caused about a 30% loss in reflectance, which caused the peak membrane temperature to increase from 110°F (43°C) in August 1998 to about 119°F (48.3°C) in August 2001. The surface temperature of Code J was therefore almost 21°F (11.7°C) cooler than that of the Code A membrane, which in turn reduced the heat flux entering the roof. Overall, the membranes F, I, and J showed less soiling than did the membranes A,

G, and K and, therefore, performed better thermally than did membranes A, G, and K because of the higher reflectance values for F, I, and J after the 3 years of exposure.

1.3 COOL ROOF CALCULATOR

The STAR computer code was validated against the ESRA field data. The code predicts the membrane temperature within about ±5% of field measurements and predicts the daily heat flux within about ±10% when using an improved correlation for mass transfer to the roof.

Typical meteorological year (TMY2) data (NREL 1995) was used by STAR to generate cooling and heating roof loads for 235 different cities in the United States. The loads data were formulated into empirical curve fits and programmed into an algorithm. The algorithms were used for estimating the loads and the amount of energy cost savings for a reflective roof as compared to a smooth, dark BUR with the same amount of insulation but with a solar reflectance of only 0.05 and an infrared emittance of 0.90.

The relative effects of different surfaces and different amounts of thermal insulation are generally the same using the calculator and the STAR code. The average error in heating load is of the order of ±15% for the membrane Codes A, I, and H simulated for insulations levels ranging from R-5 through R-20. Results also show that the roof calculator predicts the cooling load of an R-5 roof in Phoenix, Knoxville, and Minneapolis within about ±5% of the STAR output for the membranes coded A, I, and H. Therefore, validations against STAR data showed that the calculator predicts the cooling and heating loads of roofs exposed to predominantly cooling and also predominantly heating climates within about ±10%. The calculator is also accurate for insulation levels ranging from about R-5 through R-35 (Petrie et al. 2001a).

1.4 AFFORDABLE COST PREMIUMS

For the cooling-dominated climate of Phoenix, AZ, and the mixed climate of Knoxville, TN, a highly reflective membrane yielded the maximum energy savings. With a roof insulation level of R-5, energy savings are about $\$0.37/ft^2$ per year and $\$0.13/ft^2$ per year for Phoenix and Knoxville, respectively. Increasing the R-value to R-15 drops the annual energy savings to $\$0.13/ft^2$ for Phoenix and $\$0.05/ft^2$ for Knoxville.

Table 2 shows the level of insulation needed by a smooth BUR to have the same annual operating cost as a high reflectance roof. In Phoenix, AZ, a dark absorptive BUR would need an R-value of 15.6 as compared to an R-5 roof covered with the reflective membrane Code A. In the more moderate climate of Knoxville, TN, the BUR would need R-10 as compared to the R-5 covered with the Code A membrane. Hence, ignoring radiation control almost doubles the R-value for the cooling-dominated climate of Phoenix and the mixed climate of Knoxville. Given the regional labor rates and the first cost of materials, the manufacturer's representative can use the calculator as a sales tool to demonstrate the trade-off in the cost of reflective roofing as opposed to the lower cost of BUR using more insulation to offset the increase in annual roof energy.

For example, a BUR needs an R-34.7 in Phoenix to have the same annual operating cost as a Code A membrane with R-15 insulation. Cost premiums for thermoplastic membranes were calculated by comparing the cost of the additional polyisocyanurate insulation required by the BUR to the cost for thermoplastic membranes. Analysis showed a synergy between R-value and reflective roofing as R-value increases from R-5 up to about R-20; however, continuing to increase R-value beyond R-20 causes the effect of insulation to mask the effect of a reflective roof. For Phoenix and Knoxville, a peak of about $\$0.90/ft^2$ for additional insulation occurs at about R-15 and R-18, respectively. Because thermoplastic membranes of about a 40-mil thickness cost about $\$0.40/ft^2$

Table 2. The net cost of annual energy savings and the R-value of BUR with equivalent energy costs of reflective roofs*

	Net savings ($/ft^2) vs R05E90 (BUR)			BUR equivalent R-value for net savings = 0		
Phoenix, AZ	Code A R865E928	Code I R813E947	Code H R245E805	Code A R865E928	Code I R813E947	Code H R245E805
R-5 (h·ft^2·°F)/Btu	$0.366	$0.344	$0.069	R-15.6	R-14.3	R-6.2
R-10 (h·ft^2·°F)/Btu	$0.211	$0.199	$0.040	R-30.7	R-28	R-11.2
R-15 (h·ft^2·°F)/Btu	$0.129	$0.121	$0.024	R-34.7	R-34.1	R-16.7
R-20 (h·ft^2·°F)/Btu	$0.095	$0.089	$0.018	R-35.7	R-35.4	R-26.1
R-30 (h·ft^2·°F)/Btu	$0.075	$0.070	$0.014	R-36.3	R-36.1	R-32.0
Knoxville, TN						
R-5 (h·ft^2·°F)/Btu	$0.128	$0.119	$0.027	R-10.3	R-9.8	R-5.9
R-10 (h·ft^2·°F)/Btu	$0.073	$0.069	$0.015	R-16	R-15.3	R-10.9
R-15 (h·ft^2·°F)/Btu	$0.045	$0.042	$0.009	R-30.3	R-29.2	R-16.2
R-20 (h·ft^2·°F)/Btu	$0.033	$0.031	$0.007	R-33.6	R-33.3	R-23.6
R-30 (h·ft^2·°F)/Btu	$0.026	$0.024	$0.005	R-34.9	R-34.7	R-31.5

* These simulations use initial solar reflectance, which do not include soiling of the membranes.

and thicker 80-mil membranes costs about $0.75/ft^2, a consumer could easily afford a cool membrane in Phoenix and Knoxville. Labor is not included in the analysis, but it is suspected that applying a BUR is more labor intensive than applying a single-ply membrane.

1.5 ENERGY COST INCURRED DUE TO SOILING OF MEMBRANE

The STAR code was used to generate annual roof loads for a full 3 years of exposure in Phoenix, AZ, Knoxville, TN, and Minneapolis, MN. The annual roof energy for a soiled membrane was scaled by the annual roof energy for the identical clean membrane to show the effect of soiling on the roof energy. For exposure in Phoenix, 1 year of soiling caused a 24% increase in the annual roof energy for the Code A membrane with R-15 insulation. After 2 years, the roof incurs a 51% energy increase. The increase in energy levels out through 3 years of exposure, and the net increase in annual roof energy plateaus at about 60%. For Code I membrane exposed for 3 years in Phoenix compared to a clean Code I membrane, a 31% increase is observed. Knoxville's climate is more moderate, and for Code A and I membranes with insulation levels exceeding R-10, the cooling energy savings are offset by the heating-energy penalty. It appears from the data that the ratio of $^{CDD}/_{HDD} \geq 0.4$ may roughly represent the boundary for the benefit of periodically washing cool roof membranes.

Simulations were also conducted to determine the increase in the cost of building roof energy caused by soiling of the thermoplastic membranes. What energy costs does a building owner incur before it is economically justifiable to wash the roof? Cost estimates were calculated by subtracting the roof energy for a thermoplastic membrane that soils with time from the roof energy for the same membrane that remains clean. Heating, ventilating, and air-conditioning (HVAC) equipment efficiencies and local utility rates were then applied to yield the cost data. An independent contractor would charge about 1¢ per square foot to wash a roof with a power washer. The cost of additional roof energy for Phoenix clearly justifies power washing a roof that has insulation as high as R-30 and Code A membrane. In fact, building owners can realize a net savings of about 6¢ per square foot if they wash the roof every other year for a roof with Code A membrane with R-15 insulation. The cost advantage is not as great for the Code I membrane because Code I loses only about 25% of its original reflectance as compared to the 50% loss observed for Code A membrane. In the more

moderate climate of Knoxville, the advantage for washing the roof is only about 1¢ per square foot after 3 years of exposure for the Code A membrane with R-15 insulation. Once again, the cooling-energy savings are offset by the heating-energy penalty. Washing the reflective membranes in climates having a $^{CDD}/_{HDD} \geq 0.4$ will save roof energy and is cost effective if washed every other year or every third year.

2. INTRODUCTION

Wear a white shirt on a clear, hot summer day and you're cooler than someone wearing a dark shirt. Light colors better reflect the sun's heat, while dark colors better absorb it. Similarly, light colored roof materials make for a cool roof by reflecting most of the sun's energy. Over 50% of the solar radiation received from the sun is in the visible spectrum. Temperature measurements made at Oak Ridge National Laboratory's (ORNL's) Buildings Technology Center (BTC) show that a highly reflective roof surface is typically only about 5°F (3°C) warmer than the ambient air temperature, while a dark absorptive roof can exceed the ambient air temperature by more than 75°F (40°C). Lowering the exterior roof temperature reduces the heat leakage into the building, which, in turn, reduces the air conditioning load. If the building is located where cooling loads predominate, peak load reductions and net annual energy savings occur. Savings will, however, vary with climate, internal building load, roof surface-to-building volume and the amount of roof insulation, and with the seasonal efficiency of the heating, ventilating, and air-conditioning (HVAC) system. In urban areas, reflective roofs can reduce the peak power demand and lessen the effect of urban heat islands, which in turn improves the city's air quality. Most importantly, cool roofs incur no additional costs if changes from dark absorptive to more white reflective colors are incorporated into buildings' roof maintenance schedules. Yet despite the simplicity of the cool roof concept, results of testing done under widely varying conditions are confusing industry, regulators, and consumers who do not know how to evaluate marketing claims or decide how test data apply to their situations.

2.1 RADIATION PROPERTIES

The sun generates tremendous energy, and provides about 442 Btu/h·ft^2 (1.39 kW/m^2) of electromagnetic radiation at the earth's outer atmosphere. This quantity of energy is nearly 2 horsepower, and sensors aboard NASA's satellites have shown over the 1979–99 interval that the solar radiation incident on the earth's outer atmosphere has varied only about ±0.2% (Quinn and Fröhlich 1999). Part of the solar radiation is absorbed and scattered by the earth's 90-mile-thick layer of atmosphere, which is composed mainly of air, water vapor, ozone, and dust. The rate at which radiation of wavelength λ is incident on the earth's surface per unit area of the surface and per unit wavelength interval about λ is defined as the spectral irradiance. The spectral distribution of the irradiance from the sun yields the total electromagnetic radiation incident from all possible directions and encompassing all wavelengths starting from the short wave length ultraviolet at about 200 nm through the long wave length infrared region extending beyond 2800 nm. Approximately 44% of the sun's total energy is visible to the eye, and maximum solar intensity occurs within this range. Absorbing this 44% is what makes a BUR appear black. Sunlight emits another 51% of its energy in the invisible infrared spectrum, which is sometimes divided into the near infrared (extending from beyond the red end of the visible region to about 2800 nm) and the far infrared (exceeding 2800 nm).

The solar irradiance that hits an opaque surface, such as a roof, has some of the irradiance reflected and some absorbed by the roof. Some of the absorbed energy is emitted back to the sky, and it is this emittance that regulates the release of absorbed energy. The absorptance, the reflectance, and the emittance of a roof are all surface phenomenon that occur just a fraction of a micrometer within the irradiated surface. They are expressed mathematically as ratios. The absorptance (α) determines the fraction of energy that penetrates into the surface; the reflectance (ρ) determines the fraction of incident radiation that is reflected by the surface. The emittance (ε) describes how well the surface radiates energy away from itself as compared to a blackbody[1] operating at the same temperature.

[1] A blackbody is a perfect emitter. It releases and absorbs the maximum possible amount of radiation over all wavelengths.

The material thickness of thermoplastic roof membranes is typically about 0.040 in. (1 mm), and they are therefore opaque to the incident solar radiation (i.e., no solar radiation is transmitted through the membrane). Because the membrane is opaque, the surface properties of solar absorptance and solar reflectance are related by the formula $\alpha = 1 - \rho$. For purposes of this study, the solar absorptance and the solar reflectance refer to the wavelength range from the ultraviolet at 200 nm through the near infrared at 2800 nm.

The emission of heat from a roof surface is concentrated in the infrared spectrum because at typical roof temperatures of 95 to 200°F (35 to 100°C) the emissive power occurs around the 9400 to 7760 nm range by Wein's displacement law. Thermoplastic membranes can be assumed diffuse-gray, meaning that the emittance and absorptance of the surface are (1) independent of the direction of the radiation and (2) that the emittance and absorptance do not depend on wavelength. Using Kirchhoff's radiation laws, we can relate the infrared emittance of a roof directly to the infrared absorptance of the roof as $\varepsilon_{ir} = \alpha_{ir}$. Given this relationship and the relationship of $\alpha_{ir} = 1 - \rho_{ir}$, the infrared emittance can be directly related to an infrared reflectance by $\varepsilon_{ir} = 1 - \rho_{ir}$.

Both the solar reflectance and the infrared emittance of a roof surface are important surface properties affecting the roof temperature. The solar reflectance gages the percentage of the sun's energy that a roof deflects off the building, and the infrared emittance is the percentage of infrared heat at roof temperature that a roof releases from the building. Some of the deflected and released energy is picked up by airside convective currents, which also strongly affect the roof's exterior temperature. During the evening, the emittance and the condensation of water vapor from the ambient air govern the temperature and heat flow through the roof.

We expect that in moderate to predominantly hot climates, an exterior roof surface with a high solar reflectance and high infrared emittance will reduce the exterior temperature and produce savings in comfort cooling. For predominantly heating-load climates, surfaces with moderate solar reflectance and low infrared emittance will save in comfort heating, although field data documenting the trade-off between solar reflectance and infrared emittance are sparse.

2.2 SOILING OF SINGLE-PLY MEMBRANES

Berdahl and Bretz (1997) have reported quantitative values of the solar reflectance for a few types of building materials and briefly discussed works by Taha, Sailor, and Akbari (1992) and Reagab and Acklam (1979), who published some reflectance data from field measurements of test roofs. Wilkes et al. (2000) recently completed testing 24 different roof coatings on a low-slope test stand at the BTC. Results revealed a decrease in the solar reflectance of white-coated and aluminum-coated surfaces as the time of exposure increased; however, this decrease leveled off after 2 years of exposure. The reduction was caused by surface contamination and exposure to climatic elements. Washing the roof helps; however, the roof coatings and membranes tested by Petrie did not maintain their high reflectance after washing. Wilkes et al. (2000) also observed that the emittance of the coatings did not change markedly over time, but its effect on thermal performance was intertwined with that of reflectance. Unbiased testing open to the public domain is needed to document the long-term performance of roof products because data describing the loss of reflectance are extremely sparse. Hence long-term performance is needed to develop realistic, defensible claims about annualized energy savings and affordable cost premiums.

To the authors' knowledge, information on the weather's impact on the change in reflectance and emittance of roof materials is limited. Further, the trade-off between climate and reflective roofs has only recently been investigated because of the time and patience required for documenting the weather's impact on exterior roof surfaces.

3. FIELD TEST FACILITY

The BTC is a U.S. Department of Energy (DOE) National Users Facility, and is collaborating with industry in developing comprehensive data for accelerating the market penetration of cool roof materials. Our research includes a broad range of cool roofing systems, including membranes, coatings, and metal panels. The roofing industry is keenly interested in documenting whether their products can reduce the space conditioning requirements for commercial applications. Our approach seeks industry accepted and technically viable procedures to fairly compare various commercially available roof systems and to promote the increased use of energy-efficient roof products by consumers.

3.1 ENVELOPE SYSTEMS RESEARCH APPARATUS

SPRI and several members of SPRI enacted user agreements with the BTC to study the effect of climatic exposure on the surface properties of single-ply membranes. SPRI and its affiliates field-tested for 3 years their single-ply, low-slope roofing systems on the western half of the envelope systems research apparatus (ESRA) (see Fig. 1). AISI, NamZAC, MBMA, MCA, and NCCA are using the eastern half of the ESRA to test unpainted and painted metal roofing.

The ESRA is a one-level, air-conditioned test building that is oriented east-west for exposing large areas of roof products (see Fig. 1). A low-slope roof was built on the ESRA to conduct side-by-side testing of roofs under the same solar irradiance and climatic conditions. The slope was set for a ¼-in. of rise for every 12-in. of run (i.e., 1.2° slope). Approximately half of the ESRA roof (35 ft by 40 ft) is subdivided into ten sections. Each section or lane is part of a roof system that consists of a metal deck, a 1-in.-(25.4-mm) thick piece of wood fiberboard laid on the deck, another ½-in.-(12.7-mm) thick piece of wood fiberboard placed atop the 1-in.-(25.4-mm) thick piece, and a mechanically attached single-ply membrane. The metal deck is made of 22-gage (0.030-in. or 0.76-mm-thick) galvanized steel. The deck's ribbing is narrow, about 1½ in. (38.1 mm) wide. Two-by-fours were laid atop the metal deck at about every 4 ft on center, and attached to the deck using standard decking fasteners as shown in Fig. 2. The two layers of wood fiberboard were placed between the two-by-four partitions making the ten test lanes. Similar membrane materials were overlapped a few inches within a test lane and across test lanes and welded together using a hot air gun as shown in Fig. 3. Parapets were used to divide some of the test lanes where the differences in roof material required special techniques to fasten the material to the roof (Fig. 4).

3.2 SINGLE-PLY MEMBRANES UNDER FIELD TEST

Test membranes were assigned proprietary codes known only by the ORNL principal investigator. Participants in the SPRI users agreement knew their own code but not the identity of other test participants, so participants could assess their system against the field of systems while still keeping the performance of their company's product confidential. A built-up roof (BUR) was used as the base of comparison to determine energy savings. The BUR is made of several layers of alternating bitumen and bitumen-saturated felt paper as shown in Fig. 5. The BUR is coded C. The completed assembly for the test membranes exposed on the ESRA is displayed in Fig. 6.

3.3 FIELD SITES

Samples of the test panels were prepared for field exposure at different locations across the country to quantify the effect of climate on the weathering of the single-ply membranes. Table 3 lists the different exposure sites, and Fig. 7 shows the setup at one site in Saginaw, MI. The participants selected ten different roof membranes. These field samples use the same codes as were used by the membranes that were field tested on the ESRA. The codes are given in Table 4.

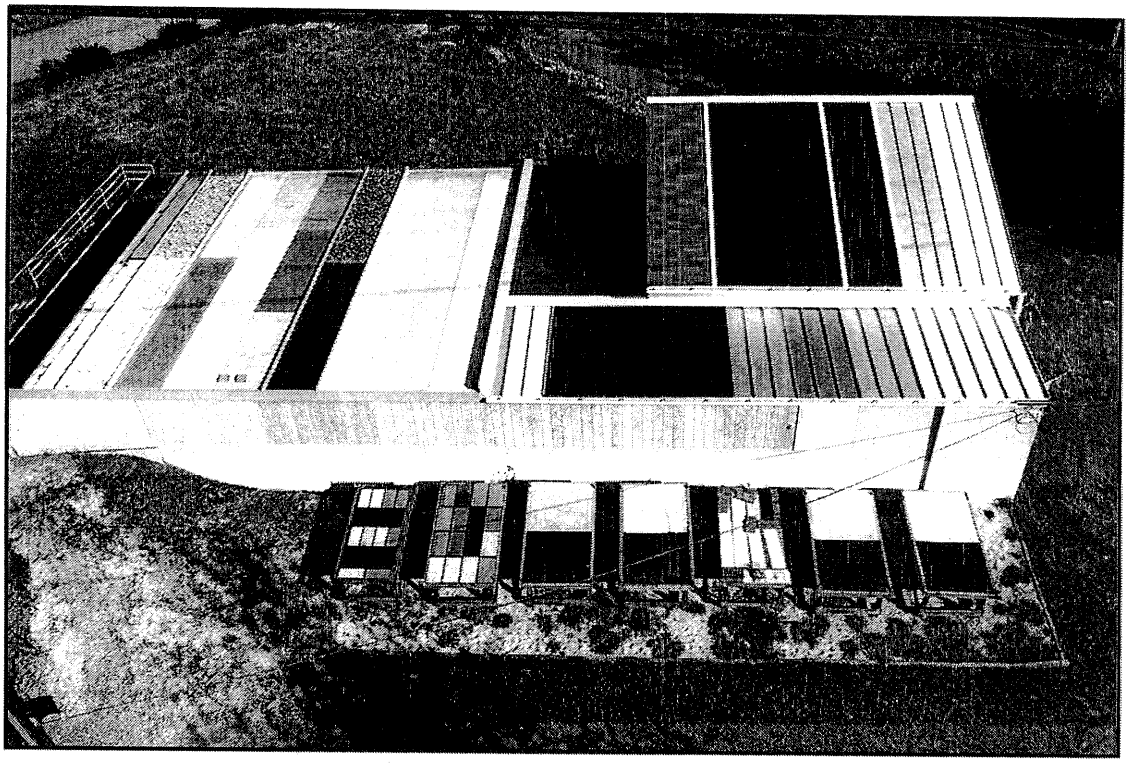

Fig. 1. The envelope systems research apparatus is used for testing roof manufacturer's best products.

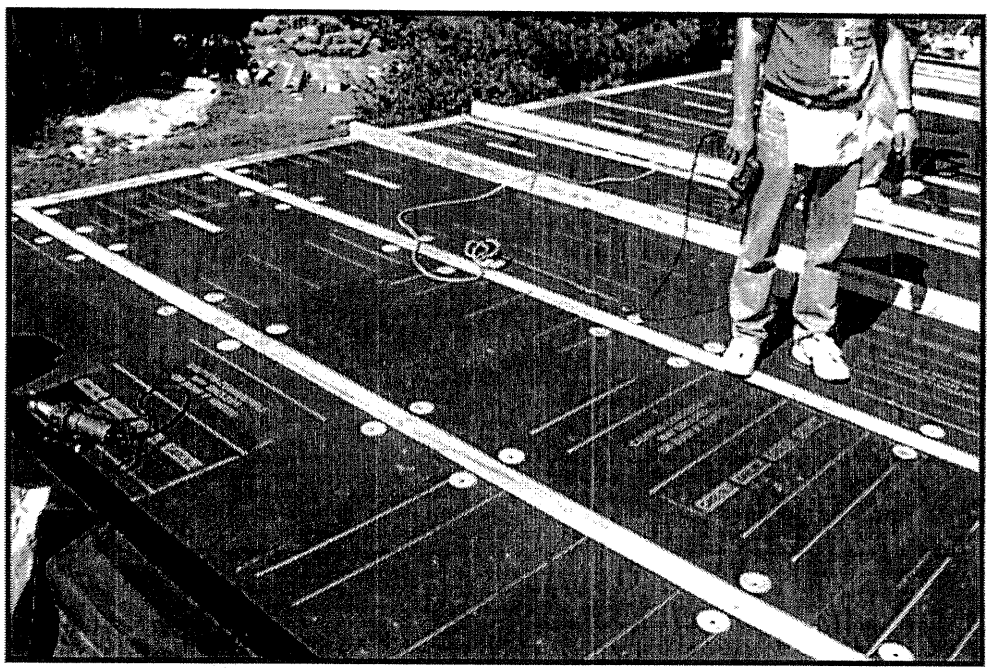

Fig. 2. The test roofs cover a lane about 40 in. (1 m) wide, and each lane has 1½-in. (0.04 m) of wood fiberboard under the roof membrane.

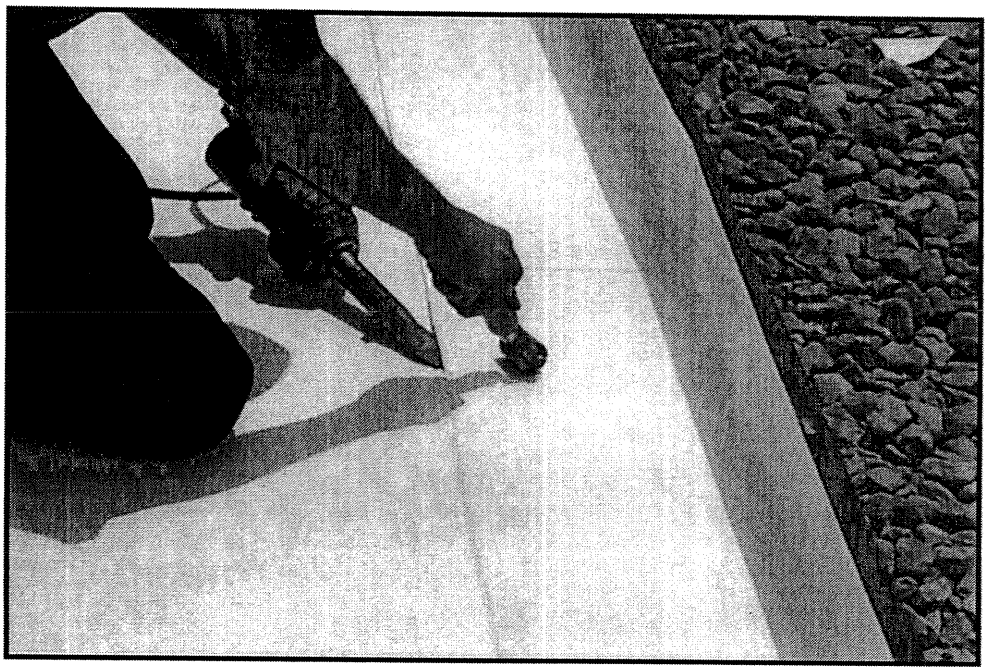

Fig. 3. Membranes made of similar material were fastened using standard low-slope roof practice.

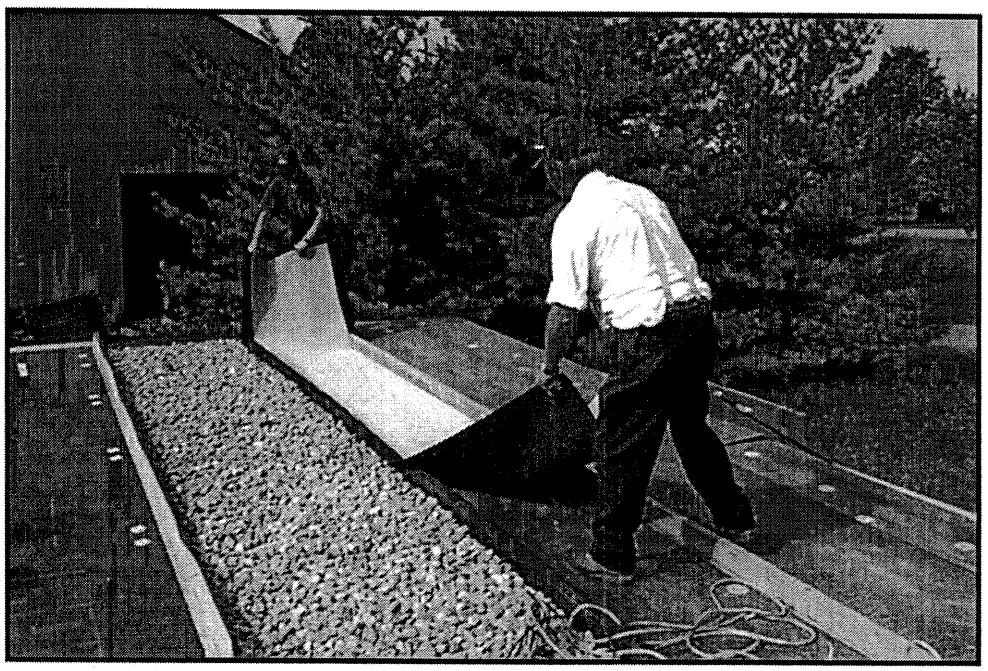

Fig. 4. Parapet walls were used to separate unique roof systems.

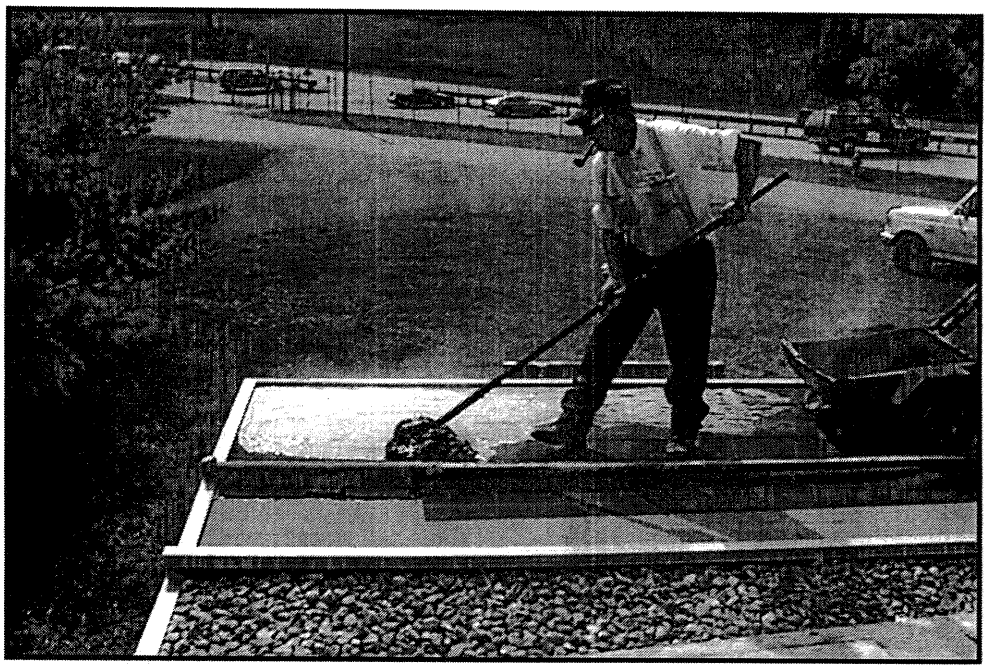

Fig. 5. The BUR is made of four alternating layers of bitumen and bitumen-saturated felt paper.

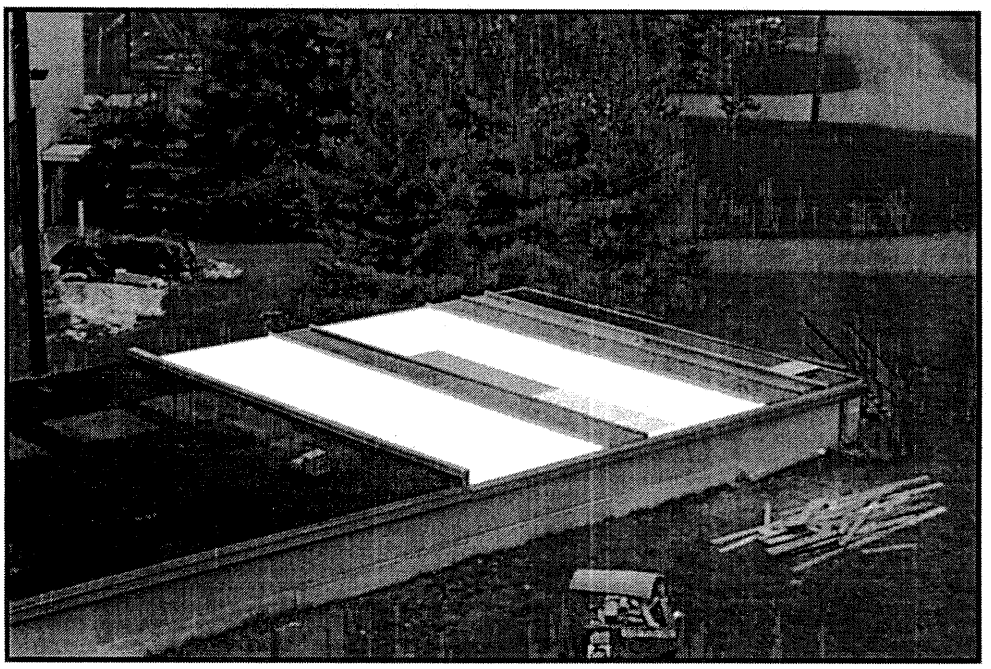

Fig. 6. We completed installation of the single-ply membranes in July 1998.

Table 3. Field sites selected for weathering of single-ply membranes

Location	Zip code	Site descriptive	Local contact	Responsible company
Littleton, CO	80127	Cold and dry	Joel E. Hazy 303-978-3576	Johns Manville 10100 W. Ute Ave P.O. Box 625005
Joplin, MO	64801	Moderate	Kerri Eden 417-624-6644 ext. 2305	Tamko Roofing Products 220 West Fourth Street
Saginaw, MI	48601	Cold and wet	Al Janie 800-248-0280	DuroLast Roofing, Inc. 525 Morley Drive
Fullerton, CA	92832	Humid and warm	Joe Malpezzi 717- 245-7056	Carlisle SynTec Inc. Post Office Box 7000
Canton, MA	02021	Cold and wet	James Rubenacker 781-828-5400	Sarnafil Roofing 100 Dan Road
North Hampton, MA	01060	Cold and wet	Bob Banas 413-584-9208	JPS Elastomerics 82 Conz Street

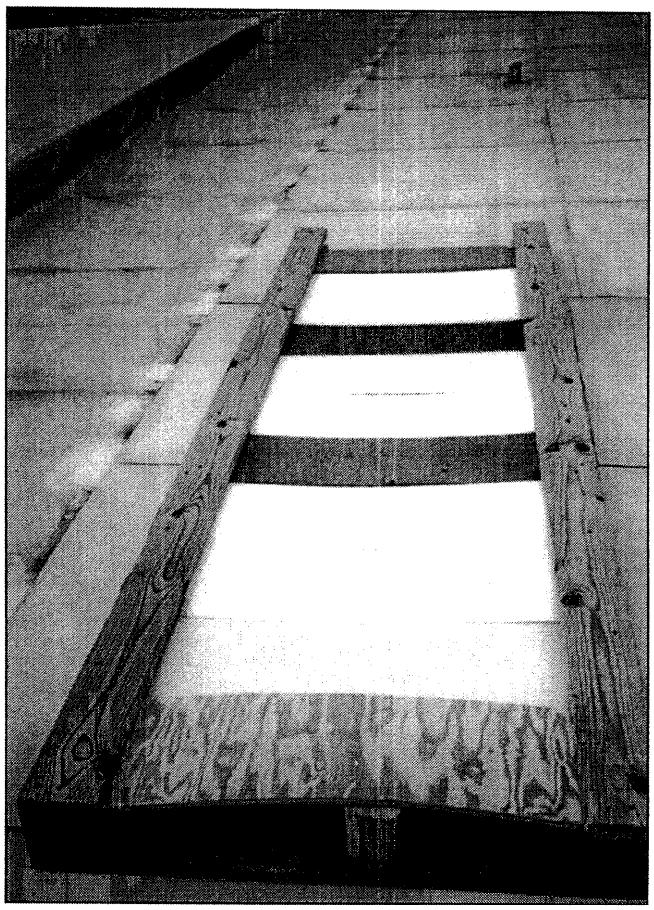

Fig. 7. Membranes at the Saginaw, MI, exposure site.

Table 4. Codes of membranes exposed at field sites across the country

Codes	L	I	J	R/S	F	A	G	B	H	K

Field testing was conducted at a slope of ¼-in. rise for every 12-in. of run for all membranes exposed at all sites. We tested an additional set of membranes at 2 in. of rise for every 12 in. of run at the Saginaw, MI, site. To do a regression analysis for predicting the drop in reflectance required weather data. We collected weather, pollution, and surface radiation data and correlated the drop in reflectance of the samples tested at the various sites.

3.4 INSTRUMENTATION

Heat flux transducers and type T copper constatan thermocouples are strategically placed in all of the ESRA test roofs to measure the heat flow and the temperature distribution through the insulation (Fig. 8). The thermocouples are placed in the ESRA's indoor ambient, attached to the top side of the metal deck, taped between the two layers of fiberboard, and taped atop the surface of the ½-in.-thick (12.7-mm) piece of wood fiberboard. A 2-in. (50.4-mm)-square slot with a depth of 0.18 in. (4.6 mm) was routed into the top of the 1-in. (25.4-mm) wood fiberboard for the placement of a heat flux transducer (HFT) as shown in Fig. 9.

3.4.1 Temperature and Heat Flux

All transducers were calibrated before being installed into the low-slope assembly. Type T copper constatan thermocouples were fabricated from the same spool of wire and calibrated in situ in a constant temperature bath. The in situ calibrations corrected for the effects of signal conditioning through the analog-to-digital cards of the data acquisition system (DAS). Each HFT was calibrated according to ASTM standard C518 (ASTM 1998). The HFT was placed in a 12- by 12-in. (0.305- by 0.305-m) guard made from the same lot of wood fiberboard as used in construction of the low-slope assembly. The sandwich of ½-in.-thick (12.7 mm) wood fiberboard, the HFT, and 1-in.-thick (25.4 mm) wood fiberboard was then placed in a heat-flow metering apparatus to develop a calibration that corrects for the shunting of heat flow around the transducer. The manufacturer states

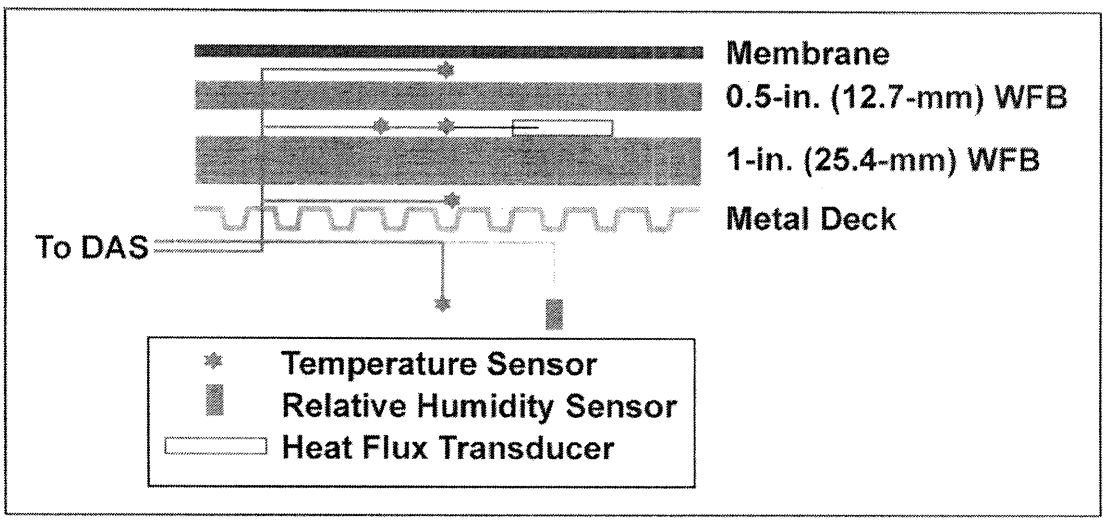

Fig. 8. Thermocouples and heat flux transducers are embedded into the low-slope test roofs on the ESRA.

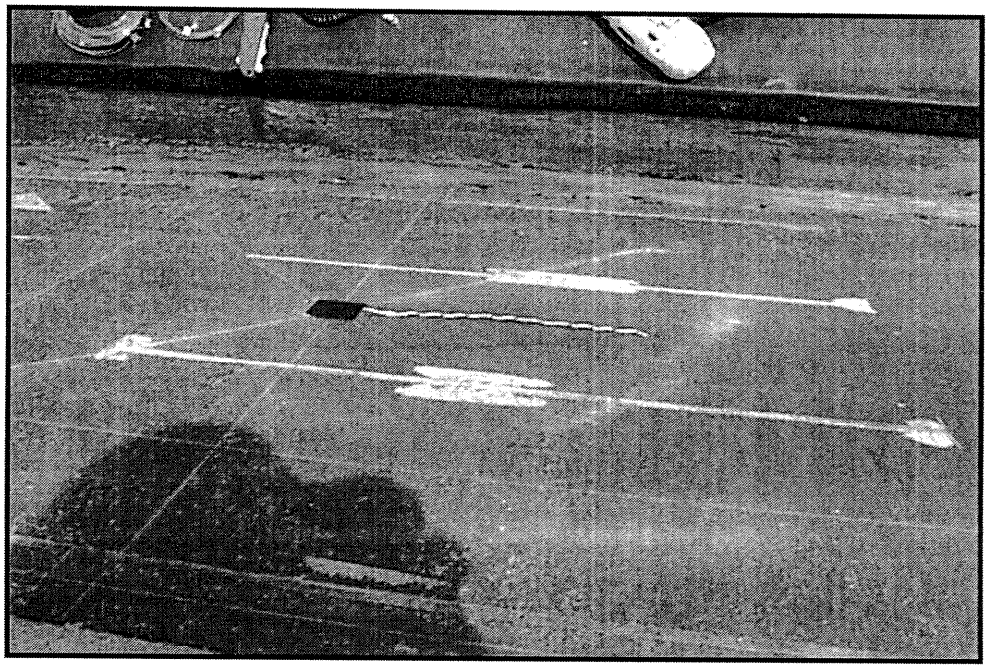

Fig. 9. A slot is routed from the 1-in (0.025-m) thick wood fiberboard for the heat flux transducer.

accuracy as ±1% of full-scale reading with a sensitivity of about 1.3 Btu/hr·ft^2 per mV of signal (4.1 W/m^2 per mV). Our calibrations showed them to be accurate within ±5% of the instrument's reading. The two thermocouples taped between the two layers of fiberboard are located 2 in. (50.4 mm) and 4 in. (101.6 mm) away, respectively, from the HFT to check for any horizontal temperature gradients.

Using a computational heat conduction code, simulations were made to check the magnitude of horizontal heat flows in the plane of the roof. Predictions showed the effects were small and extend no more than a few inches in from the break between low-slope test lanes. The horizontal heat flow is 2% of the vertical heat flux along the top of the ½-in.-thick fiberboard (12.7 mm) at a distance 3 in. (76.2 mm) away from the interface of two adjacent test lanes. The lateral heat flow drops to less than 1% of the vertical flow 6 in. from the interface. Our instrumentation is placed in the center of each test lane and is about 24 in. (0.61 m) from an adjoining test lane. Therefore, axial effects are judged insignificant. Also, the temperatures measured about 2 in. (50.4 mm) and 4 in. (101.6 mm) away from the HFT show no lateral gradients. We conclude that the heat flux is indeed one-dimensional as required by the HFT.

3.4.2 Solar Reflectance

We used two different but portable instruments to measure the solar reflectance. The Devices and Services reflectometer (ASTM 2002) was used to measure the solar reflectance of the single-ply membranes, whose surfaces were smooth. The device uses a tungsten halogen lamp to diffusely illuminate a sample of about 1-in. diam. Four detectors measure the reflected light in different wavelength ranges. The four signals are weighted in appropriate proportions to yield the total hemispherical reflectance. The device is accurate to within ±0.003 units (Petrie et al. 2001b) through validation against the ASTM E-903 method (ASTM 1996).

An albedometer instrument was used to measure the reflectance of the test roofs on the ESRA having ballast rocks. The instrument uses a precision spectral pyranometer that is sensitive to radiant energy in the spectrum ranging from 0.28 to 2.8 μm. The instrument is intended for use when the sun's zenith angle to the normal from a surface is less than 45°. ASTM E-1918 (ASTM 1996) describes the procedure used to measure the reflectance. Basically, the pyranometer is used only on clear, cloudless days from about 10 a.m. to 2 p.m. The dome of the pyranometer is positioned facing directly upward to measure the total irradiance from the sun. The pyranometer is then rotated to face directly down and measure the reflected solar radiation from the low-sloped roof surface. The solar reflectance then is the ratio of the reflected radiation to the incoming radiation.

3.4.3 Infrared Emittance

The infrared emittance of the different single-ply membranes varies very little; the average emittance for all the membranes is about 0.90. However, the emittance does impact roof temperature and is almost as important as reflectance. We used a portable emissometer to measure the infrared emittance using the procedures in ASTM C-1371 (ASTM 1997). The device has a thermopile radiation detector, which is heated to 180°F (82°C). The detector has two high-ε and two low-ε elements and is designed to respond only to radiation heat transfer between itself and the sample. Because the device is comparative between the high- and the low-ε elements, it must be calibrated in situ using two standards, one having an emittance of 0.89, the other having an emittance of 0.06. Kollie, Weaver, and McElroy (1990) verified the instrument's precision as ±0.008 units and its accuracy as ±0.014 units in controlled laboratory conditions.

3.4.4 Weather Station

The BTC has a weather station that electronically records the incident solar flux, the long wave radiation beyond 3 μm, the ambient dry bulb temperature, the ambient air relative humidity, the barometric pressure, the wind speed, the wind direction, and the rain. The data are scanned every 10 s and averaged over 15 min.; averages are written to an electronic file. The weather data were used to develop correlations of the change in reflectance using regression analysis. A sample of the weather data as used in the analysis is seen in Table 5. The weather data for the analysis of the membranes at the other sites (Boston, MA, Fontana, CA, Jacksonville, FL, Joplin, MO, North Hampton, MA, Saginaw, MI) were obtained from the National Oceanic and Atmospheric Administration (NOAA).

Table 5. Weather database for the ORNL campus: the data are running averages calculated between respective reflectance measurements with the exception of the days incurring rainfall

Time of reflectance measurements, days	Dry bulb temperature, C	Temperature change, C	Relative humidity, %	Barometric pressure, inches Hg	Solar radiation, W/m^2	Occurrence of rain noted between time of reflectance measurements, days	Rainfall inches	Ozone, ppm	Carbon monoxide, ppm	Particulate matter, 10 ug/m^3	Wind speed, mph
98	22.45	9.60	72.24	29.15	219.71	16	5.94	0.073	1.18	38.02	2.74
205	7.94	10.50	76.95	29.22	92.02	39	15.44	0.048	1.63	30.89	3.01
259	6.61	11.06	65.69	29.14	145.93	19	6.23	0.049	1.15	25.09	3.71
348	18.80	11.14	69.81	29.09	245.83	29	12.62	0.064	0.92	34.57	3.68
412	24.34	10.03	77.86	29.10	247.11	19	12.35	0.072	0.98	44.18	2.84
477	16.46	13.50	71.61	29.13	191.75	15	3.85	0.056	1.26	33.28	2.69
588	5.27	9.96	66.86	29.18	105.26	28	10.97	0.048	1.42	28.32	3.23

3.4.5 Data Acquisition

A 700 MHz Pentium III computer was programmed using FIX DMACS version 7.1 software supported by Windows version 98. The code scans all instruments every 15 s and electronically records averages at 15-min. intervals to a historical database within the FIX DMACS hierarchy. Data are retrieved weekly from the historical database and written to a spreadsheet for combination with the weather data and preparation for further analysis with simulation computer codes.

3.5 SURFACE CONTAMINANT MEASUREMENTS

Nature does add many constraints to the performance of roof material. These constraints include ambient air quality and meteorological conditions. Constraints are interrelated and may be amplified, causing difficulty in prediction. For example, a cold front brings in precipitation and improves local air quality by exchanging the polluted air mass in an urban area with a fresh clean air mass from another region. The precipitation, on the other hand, may act to clean the roof surface thereby rejuvenating its reflectance. The water that came with precipitation may provide an opportunity for the growth of microorganisms and enhanced deposition of airborne dusts leading to reflectance reduction. The sensitivity of roof reflectance to the environment has barely started being explored and is far from being understood.

3.5.1 Particle Characterization Using an Inductively Coupled Plasma Spectrometer

Surface samples of airborne particulate matter lying on the test roofs were collected using premoistened Berkshire wipes to collect samples from each thermoplastic roof type over a square area of 2 ft by 2 ft (0.61 m by 0.61 m). A wipe was applied in an "S" wiping pattern using only hand pressure. The wipe was folded in half with the exposed side placed on the interior of the fold. We then repeated the S wipe at a 90° angle to the first pattern to collect a sufficient amount of sample. The wipe was stored in a plastic sealed bag and transported to the analytical laboratory. A typical sample of the Code J thermoplastic roof shows in Fig. 10 that the sample contains a large amount of dust.

Two types of wipes were used to collect samples. The first was a 9 in. by 9 in. (0.23 m by 0.23 m) Berkshire (catalog # LB1240909-48) wipe that has very low background levels of the elements S, Si, Al, Ca, Fe, Mg, Mn, and Ni. This type of wipe sample was acid digested following the EPA's "Acid Digestion Method for Metal Analysis, #3005A." A 100-mL solution of the dissolved metal species was analyzed using inductively coupled plasma atomic emission spectroscopy (ICP-AES) having a detection limit of more than 0.01 mg/L. A blank wipe was used to calibrate the ICP-AES to account for metal concentrations preexisting in a new wipe. The above digested solution was also analyzed for sulfate content by an ion chromatograph equipped with a conductivity detector. The analytical uncertainties for elements are ±5%. We expect the total uncertainty is about ±20%, including both analytical and sampling components.

The second type of wipe, a Gelman Sciences (P/N 66211) quartz filter, was used to determine the carbon contaminants on the test roofs. Each wipe was 8 in. by 10 in. (0.20 m by 0.25 m) in area, and was a high-purity, binder-free filter that contains negligible carbon. The dust samples were scraped off the quartz wipes and analyzed using LECO CN-2000 total organic carbon analyses. External standards (soil samples provided by LECO) were used for the calibration, and the measured carbon contents were then converted to total carbon content for each wipe. A new wipe was also used as a blank to check for any carbon residues in the wipes.

3.5.2 Biomass Analysis Using Gas Chromatography and Mass Spectrometry

Phospholipid fatty acid (PLFA) analyses were performed at the Center for Biomarker Analysis at the University of Tennessee to determine microbial biomass and community structure present on the test

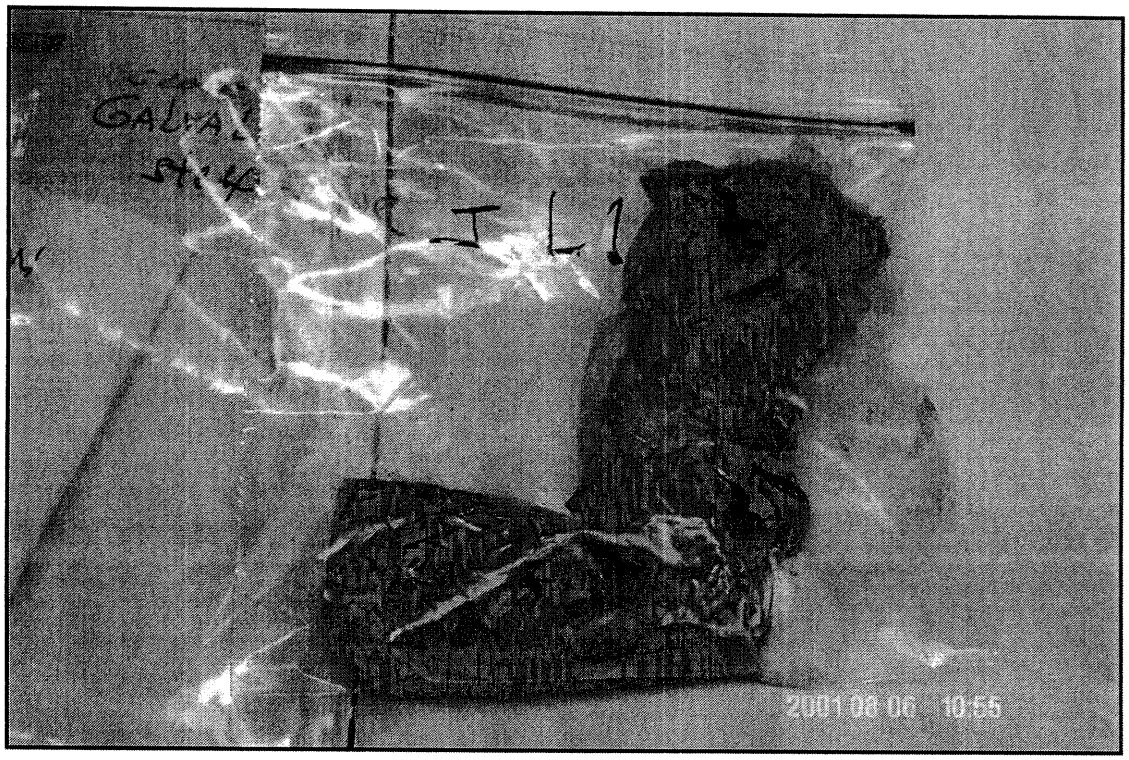

Fig. 10. Berkshire wipe samples were stored in zip lock bags for transport to an analytical laboratory.

membranes and metal roofs. Glass fiber filters (Whatman GF/D) were individually wrapped in aluminum foil and heated to 842°F (450°C) for 4 h to remove organic contaminants. The filters were wetted on site with deionized water, which had been treated with chloroform to remove any lipids. The wetted filters were wiped over a 7.8 in. by 7.8 in. (0.20 m by 0.20 m) section of the roof surface to remove particulate matter. Each sample was reinserted back into its aluminum foil envelope and placed in a labeled plastic seal-tight bag. The samples were then placed in a cooler containing dry ice to immediately freeze and preserve them; samples were frozen at -40°F (-40°C) until extracted.

PLFAs were analyzed using the procedures described by White and Ringelberg (1998). After extracting the filters by a modified single-phase chloroform-methanol-phosphate buffer procedure (Bligh and Dyer, 1959; White et al., 1979), the total extractable lipid was fractionated on a silicic acid column. The polar lipid fraction was collected and transesterified into fatty acid methyl esters (FAMES) by mild alkaline methanolysis for gas chromatography (GC) analysis (Guckert et al., 1985; White and Ringelberg, 1998).

GC analyses of FAMES was performed with a Hewlett Packard 5890 gas chromatograph equipped with a ZB-1 nonpolar dimethyl-polysiloxane capillary column having 164 ft (50 m) length, 0.01in. (0.25 mm) ID, 0.00001 in. (0.25 μm) film thickness, a flame ionization detector, and a split injector using the technique described by Ringelberg et al. (1997). The FAMES were dissolved in hexane, containing heneicosanoic acid methyl ester as the internal standard. The temperature protocol is as follows: the initial temperature of 165.6°F (60°C) is held for 2 min, ramped at a rate of 18°F (10°C) per min to 328°F (150°C), held at 328°F (150°C) for 2 min, and then increased at a rate of 5.4°F/min (3°C/min) to a final temperature of 619°F (312°C). An equal detector response was assumed for all

components and identifications were made by comparison of chromatographic retention times to standards (Matreya Inc., Pleasant Gap, PA). The peak areas of each PLFA are quantified based on the peak area and concentration (50 pmol/L) of the internal standard. The identities of the FAMES were verified using gas chromatography and mass spectrometry. The biomass measurements of total pmol/cm^2 were converted to bacterial cell counts using the conversion of $2.5 \cdot 10^4$ cells per pmol PLFA (Balkwill et al. 1988).

Mass spectral verification of all lipid moieties was accomplished using a HP5971 mass selective detector (MSD) interfaced with a HP5890 series II GC equipped with a ZB-1 nonpolar dimethyl-polysiloxane capillary column 197 ft (60 m) long, 0.01 in. (0.25 mm) ID, and 0.000004 in. (0.1 μm) film thickness. The temperature protocol for this analysis was as follows: the initial temperature of 238°F (100°C) was immediately ramped 18°F/min (10°C/min) to 328°F (150°C), held at 328°F (150°C) for 1 min, and then increased at a rate of 5.4°F/min (3°C/min) to a final temperature of 565°F (282°C). The MSD was run at 70 eV, using positive ion electron impact ionization.

4. EXPERIMENTAL RESULTS

Prior studies conducted with roof coatings at ORNL revealed that the solar reflectance decreases significantly in the first 2 years of weathering (Byerley and Christian 1994; Petrie et al. 1998). Low-slope membrane manufacturers are therefore keenly interested in documenting the drop in reflectance. They also want to better understand the causes of the drop in reflectance because the U.S. Environmental Protection Agency (EPA) and the Cool Roof Rating Council (CRRC) are both implementing energy-performance rating systems. The EPA has its Energy Star® Roof Products Program to help consumers identify energy-efficient, cost-effective roofing. Manufacturers enter a memorandum of understanding with the EPA and may display the Energy Star® logo if their product meets Energy Star® specifications for low-slope roofing. The roof covering a low-slope roof must have an initial solar reflectance of at least 0.65, and the reflectance must be greater than 0.50 after 3 years of exposure, after cleaning, on the low-slope roof. Reflectance data for three existing roofs for 3 years of exposure must be documented, and one of the roofs must be located within a major urban area. The CRRC provides the consumer with certified product data. However, it allows requirements for reflectance and emittance to come from the state building codes.

4.1 FIELD EXPOSURE ON THE ESRA

Reflectance measurements of the membranes exposed on the ESRA were done every 3 months during the 3½-year study. The results of these measurements are shown in Fig. 11. Each membrane is described generically using an RxxEyy designation. Rxx states the percentage of solar hemispherical reflectance of the new sample, 100 being a perfect reflector. Eyy defines the percentage of infrared hemispherical emittance of the new sample, 100 being the emittance of a blackbody. For example, the BUR is labeled R05E90 (Fig. 11). Its brand new properties are therefore 0.05 reflectance and 0.90 emittance. The descriptive nomenclature helps readers quickly compare roof products and also lets them observe the change in surface properties over time from their brand new values. Table 6 identifies the RxxEyy designations for the different coded membrane systems tested on the ESRA. The coded membranes are listed in descending order of their reflectance from the highest to the lowest value. Thermal property data were also measured for several of the membranes. The material thickness, density, and thermal conductivity are also listed in Table 6.

The membrane Code G (R85E90) is the only membrane whose reflectance dropped uniformly over the 3 years of exposure (Fig. 11). After 1 full year of exposure, the reflectance of membranes coded A, B, F, J, K, M, N, P, and I drop inconsistently. A drop in reflectance is followed 3 months later by a slight rise and is different from the drop observed in membrane G. The intensity of the rainfall, foot traffic, biological growth, and possibly the ingredients formulated in the membrane could cause the unexpected variations. Further investigation under laboratory conditions is required to determine the magnitude of reflectance loss caused by the parameters identified in this study.

The results are especially interesting for the thermoplastic membrane Code A (Fig. 11). The reflectance of this membrane drops below 0.5 after 2 years of field exposure. However, it again slightly exceeds 0.5 after the third year of exposure. Rainfall is not necessarily the reason for the increasing amount of reflectance. Very possibly the formulation of the membrane and/or biological growth may affect the surface and allow intermittent collection and release of dust. The data implies that the rain simply washes the surface when the surface is less tacky. If, however, rainfall had not helped wash the surface of the roof product, it would not meet the Energy Star® qualification without further cleaning. The EPA does allow washing of the roof, and the results show that certain roof materials will require washing to meet the EPA's Energy Star® criterion.

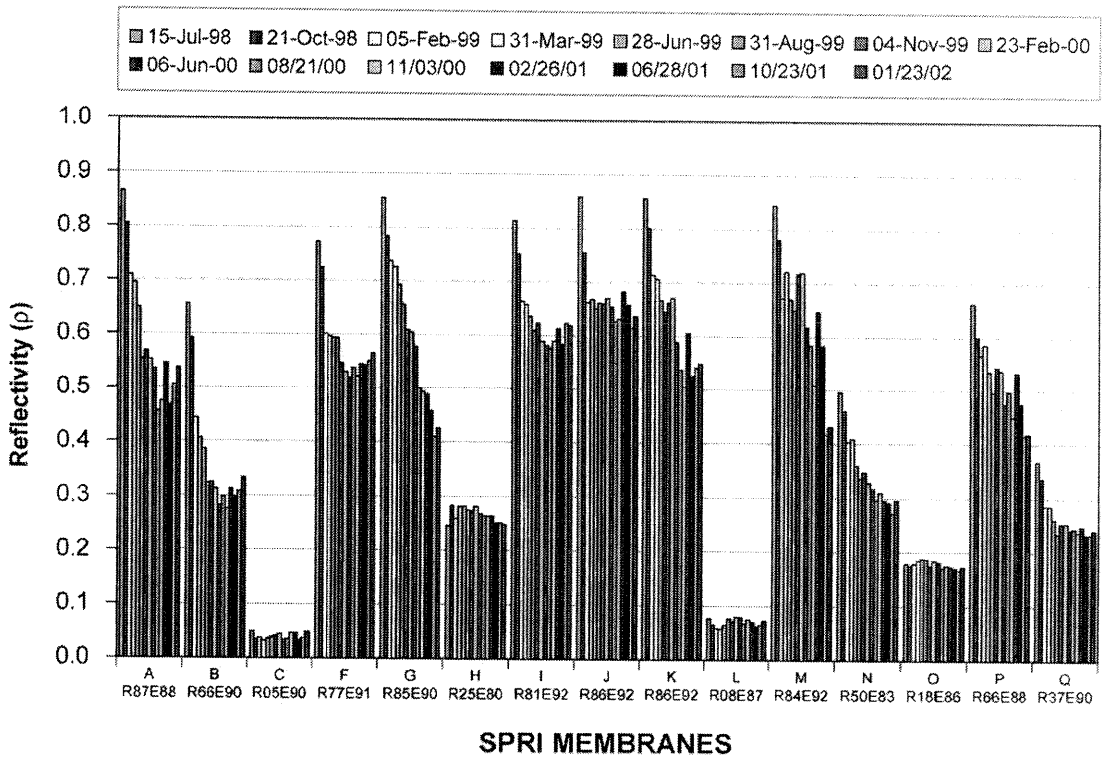

Fig. 11. Reflectance measures taken for the membranes exposed on the ESRA.

Table 6. Designations for the single-ply membranes field-tested on the ESRA

Code	Reflectance (ρ)	Emittance (ε)	Identifier	Thickness, in	Density, lbm/ft^3	Thermal conductivity, Btu·in./(h·ft$^{2.0}$F)
A	0.865	0.928	R87E88	0.036	74.1	0.79
J	0.859	0.919	R86E92	0.044	59.0	1.19
K	0.856	0.920	R86E92	0.058	81.9	1.10
G	0.854	0.933	R85E90	0.045	82.4	1.00
M	0.844	0.920	R84E92			
I	0.813	0.935	R81E92	0.042	58.9	0.65
R	0.793	0.855	R80E86	0.047	72.3	1.80
F	0.772	0.935	R77E91	0.041	63.5	1.32
P	0.664	0.875	R66E88			
B	0.655	0.901	R66E90	0.045	77.6	0.96
N	0.496	0.830	R50E83			
Q	0.368	0.904	R37E90			
E	0.358	0.900	R36E90			
S	0.327	0.900	R33E90			
H	0.245	0.805	R25E80	0.161	66.4	1.01
O	0.179	0.860	R18E86			
L	0.075	0.867	R08E87	0.045	70.6	1.96
C	0.049	0.900	R05E90			

* To convert thermal conductivity to W/(m·°C) multiply Btu·in./(h·ft$^{2.0}$F) by 0.1442279

The reflectance of the BUR, R05E90, and of Code L, R08E87 showed increases with time due to the accumulation of dust (Fig. 11). The dust has a higher reflectance than does the asphalt and therefore causes the surface reflectance of the BUR to slightly rise. The reflectance meter is accurate to ±0.003 reflectance points. The variation in reflectance measurement over 3½ years is ±0.006 reflectance points for the BUR. Therefore about half of the variation in reflectance for the BUR could be caused by instrument error. Settling of dust on the roof and the subsequent washing by rain are within the precision of measurement for the BUR.

Membranes Codes H and O show a slight increase in reflectance during the first year of exposure, but gradually drop over the remaining 2½ years of the study. With exception of membranes A, G, K, and M, the major drop in reflectance occurs within the first 2 years of exposure (Fig. 12). The vertical bars in Fig.12 represent monthly precipitation. Also, the variation of monthly precipitation has little effect on the drop in reflectance. The reflectance of the membranes A, G, K, and M continues to drop past 2 years of weathering. Although membranes A, G, K, and M have the highest initial reflectance, the reflectance of the membranes F, I, and J each finished higher than A, G, K, and M after 3 years of exposure.

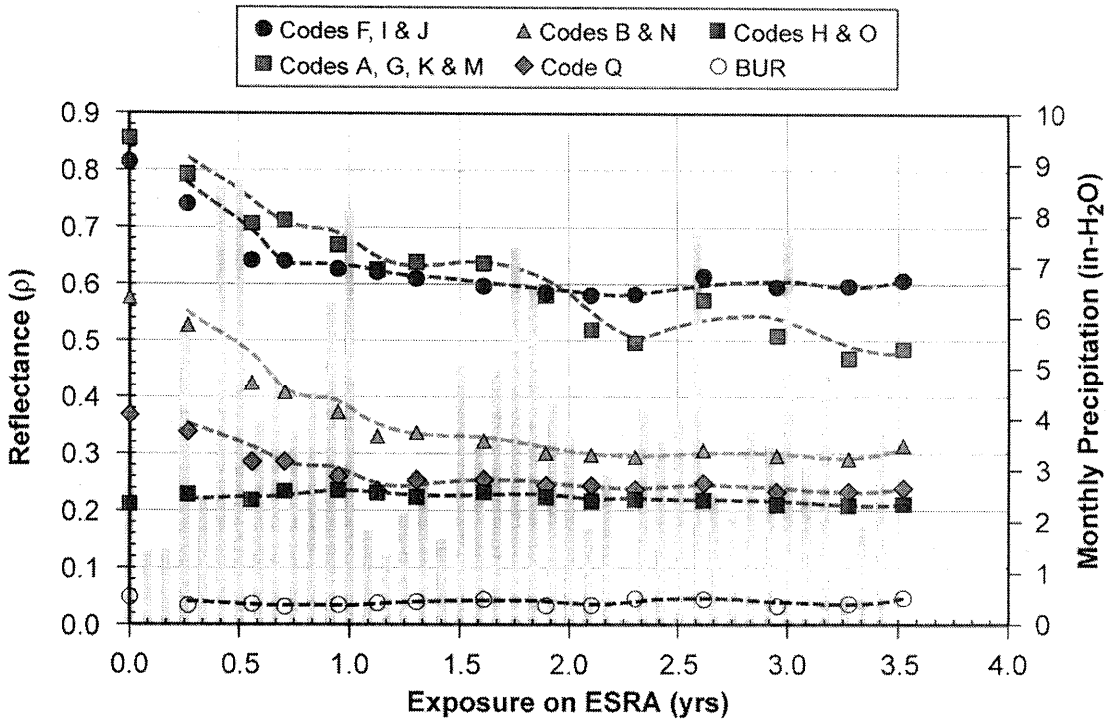

Fig. 12. The amount of precipitation has little effect on the reflectance of the membranes exposed on the ESRA.

Membranes F, J, and I lost about 25% of their original reflectance after 3 years of exposure (Fig. 13). The bars in Fig. 13 represent the daily maximum precipitation per month to show the intensity of rainfall. Again, the intensity of the rainfall appears to have minimal effect on the changes in reflectance. Actually, membranes A, G, K, and M show the largest loss in reflectance when the intensity of the rain was the strongest. At roughly 1¾ years of exposure, days having roughly 3.5 in. of rainfall occurred in consecutive months. Afterward the reflectance of membranes A, G, K, and M dropped an additional 15%, yielding a total reflectance drop of 40%. Membranes A, K, and M all show unexpected variations in reflectance, while membrane G shows a more uniform drop with time

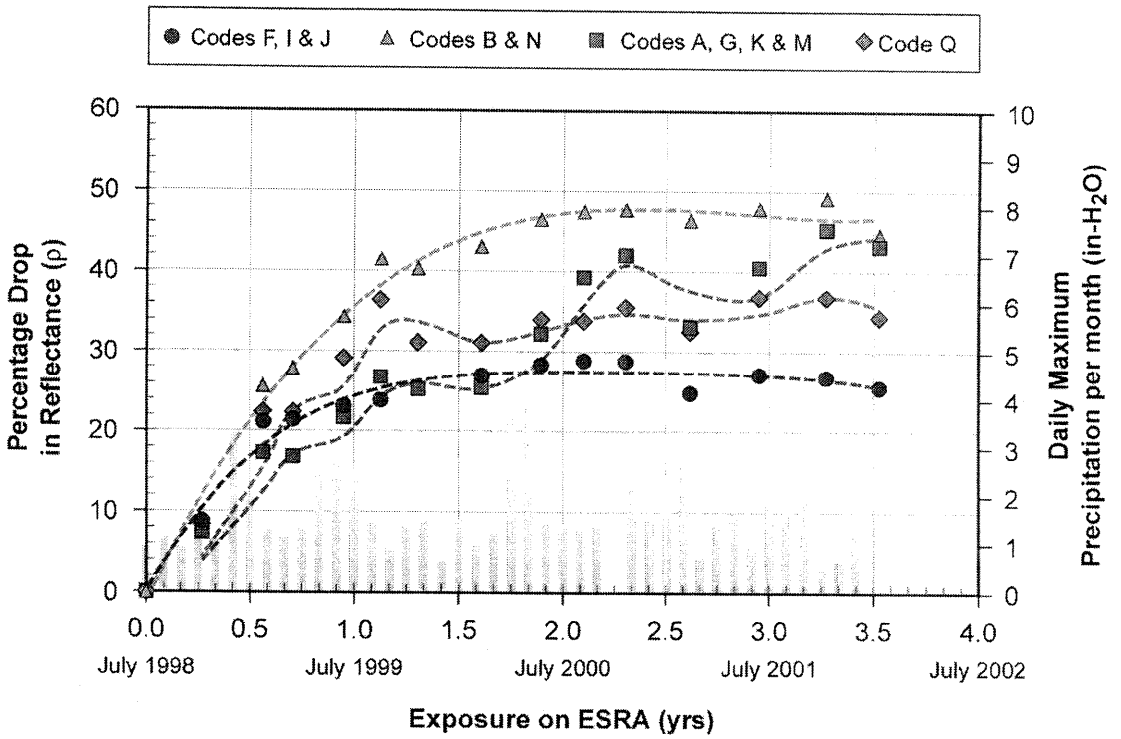

Fig. 13. The reflectance drops from 30 to 50%; however, the intensity of rainfall has little effect.

(Fig. 14). The individual trends with time are very interesting because as the intensity of rainfall increases so does the loss in reflectance increase for membranes A, K, and M. The three membranes show an increase in reflectance from 2¼ years of exposure to 2½ years. Afterwards, the reflectance again drops as exposure reaches 3 years of field exposure. The cyclic pattern occurs after 2 years of exposure and appears to have a 6-month period with more loss of reflectance in the warm summer months than in the winter.

The reasons for the unexpected variations are not fully understood, but may very well be caused by the effects of biological growth and by the effects of plasticizers in some of the membranes. The climatic cycling of temperature is known to cause certain liquid plasticizers to migrate to the surface of the membrane, making the surface tacky. If the plasticizer is a food source, its presence on the surface will further stimulate biomass growth (Griffin 2002). Manufacturers formulate thermoplastic roof products with liquid plasticizer to improve the flexibility of the membrane over a wide range of service temperatures. Adding extra liquid plasticizer improves the pliability of the membrane in cold weather applications; however, exposing the same product to higher temperatures can cause the liquid plasticizer to diffuse to the surface making the membrane feel sticky (Griffin 2002). Hence, the effect of plasticizer should be investigated to determine its effect on the loss of reflectance of certain white thermoplastic single-ply membranes, but this investigation is beyond the scope of this report.

Membranes B and N had the largest drop in reflectance. It was nearly 50% after 3 years of field exposure. Hence after 3 years of exposure in East Tennessee's climate, the loss in reflectance ranges from about 25% to a maximum drop of 50% of the reflectance for new materials.

Reflectance studies were also conducted on ballasted roof systems field tested on the ESRA. The reflectances of these test roofs were measured using an albedometer on clear days between of 10 a.m.

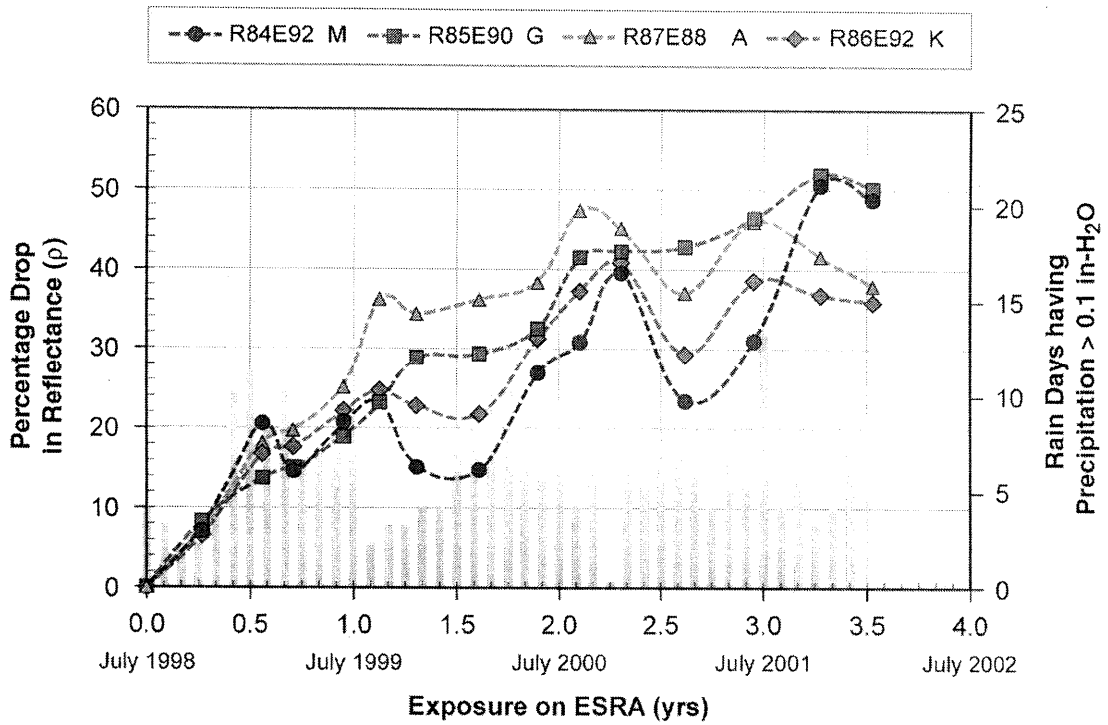

Fig. 14. Cyclic changes in reflectance observed for thermoplastic membranes field-tested on the ESRA.

and 4 p.m. Reflectance for Codes E and S did not change, and the variation in measurement is within ±0.01 reflectance points, which is about the accuracy of the instrument. The reflectance of the ballast rock systems, Codes E and S, are therefore not affected by the climatic elements. Ballast system R was spray painted with a white reflective coating. Its initial reflectance was 0.59. After 3½ years of field exposure, the reflectance dropped 34% to a reflectance of 0.39. The drop in reflectance levels off after 2 full years of exposure for Code R (Fig. 15). Interestingly, birds would turn over the ballast rock in search of food. The under side of the rock was not painted, and as a result, the reflectance dropped. The paint itself drops in reflectance; however, it contributes only about 10% to the total 34% drop.

The emittance of the membrane systems did not vary much from year to year. In fact, the variation in emittance was less than 5% of the average emittance for all the white, thermoplastic membranes. The results are consistent with the observations of Wilkes et al. (2000) for roof coatings. The average emittance for all the white, thermoplastic membranes was 0.90 and the average standard deviation for all the membranes was about ±0.04. As a group, electric nonconductors are characterized by high values of infrared emittance. Pond water, paper, concrete, plaster, oil-based paints, and oak plank are typical examples having $\varepsilon \geq 0.90$. Polished metals, however, have an emittance ranging from as low as 0.05 to as high as 0.50. The reason metals have a low emittance while opaque nonmetals like membranes have a high emittance is due in part to the rough, unpolished surface of the nonmetal. The surface properties of reflectance and emittance for metals are described by electromagnetic theory; however, opaque nonmetals are not well described by electromagnetic theory. Highly polished metals exhibit low emittance because of two traits, the index of refraction and the extinction coefficient, for the surface that typically yields a normal emittance (ε_n) ≤0.10.

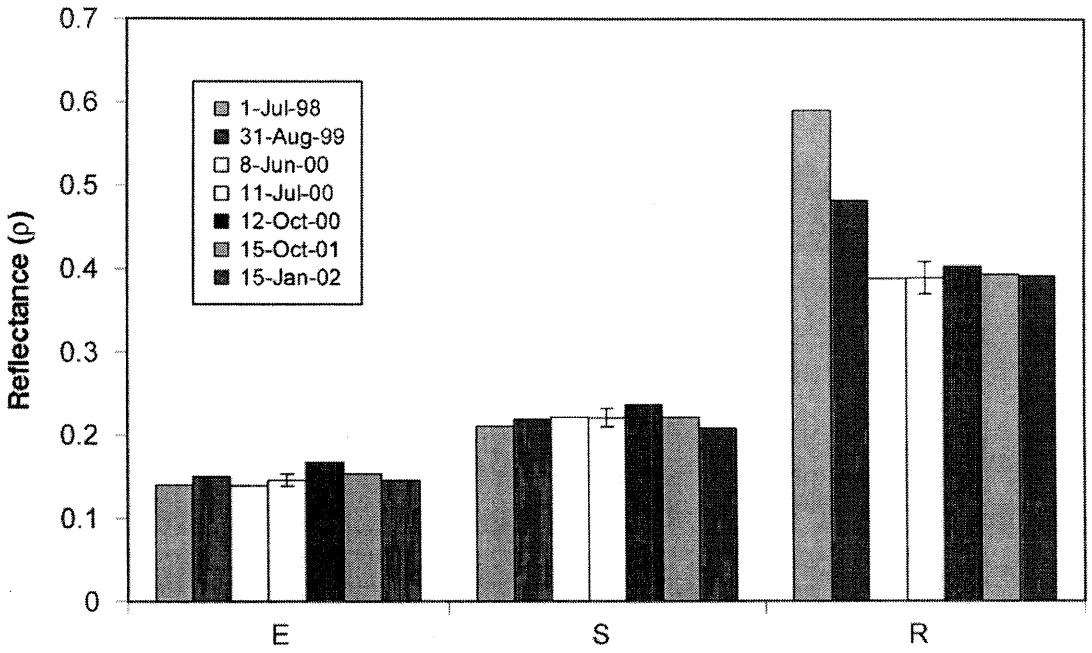

Fig. 15. Ballast roofs on the ESRA.

4.2 SAMPLES EXPOSED AT FIELD SITES ACROSS THE UNITED STATES

The samples of the test panels (see Table 4 for the codes) exposed to the different climates (see Table 3 for the list) showed significant differences among membranes. Each sample was attached to plywood backing that was about 1½ ft wide by 4 ft long. All samples at the test sites were simply laid atop a low-slope roof and oriented facing south; slope was set at ¼ in. rise for every 12 in. of run. Reflectance data for the membranes coded A and K show that the reflectance of these materials exposed across the country is higher than the reflectance for the same materials weathered on the ESRA (Fig. 16). After about 6 months of exposure, all materials show a degradation of about 15% in reflectance. However, after 3 years of exposure, the samples on the ESRA showed 15% more degradation than did the samples weathered across the country.

We believe the discrepancy is due to the type of thermoplastic membrane and also due to the setup of the field samples as compared to actual installation. The field-tested thermoplastic and thermo-set membranes were fastened to ½-in.- thick (0.0127-m) plywood and placed on the roofs of commercial buildings. Recall Fig. 7 where an air gap existed between the sample membrane and the low-slope roof of a building used for exposing the samples. The air gap under the plywood let the field membranes sense a lower membrane temperature than would be observed for the same membrane directly adhered to roof insulation and deck. Computer simulations revealed that at solar noon, the peak membrane temperature of a field sample was about 15°F (8.3°C) cooler than the membrane temperature of the same thermoplastic membrane fully adhered to roof insulation and the deck. It is speculated that the lower membrane temperature reduced the migratory diffusion of liquid plasticizer used in membranes A and K. In other words, the ESRA membrane Code A dropped 45% from its fresh-from-the factory value while the samples across the country only dropped 30% because the field samples incurred a cooler peak temperature. Therefore, less plasticizer diffused to the surface and the surface was less tacky. It stayed cleaner. For Code K, the ESRA membrane incurred a 38% reduction, while field samples had just 18% loss in reflectance.

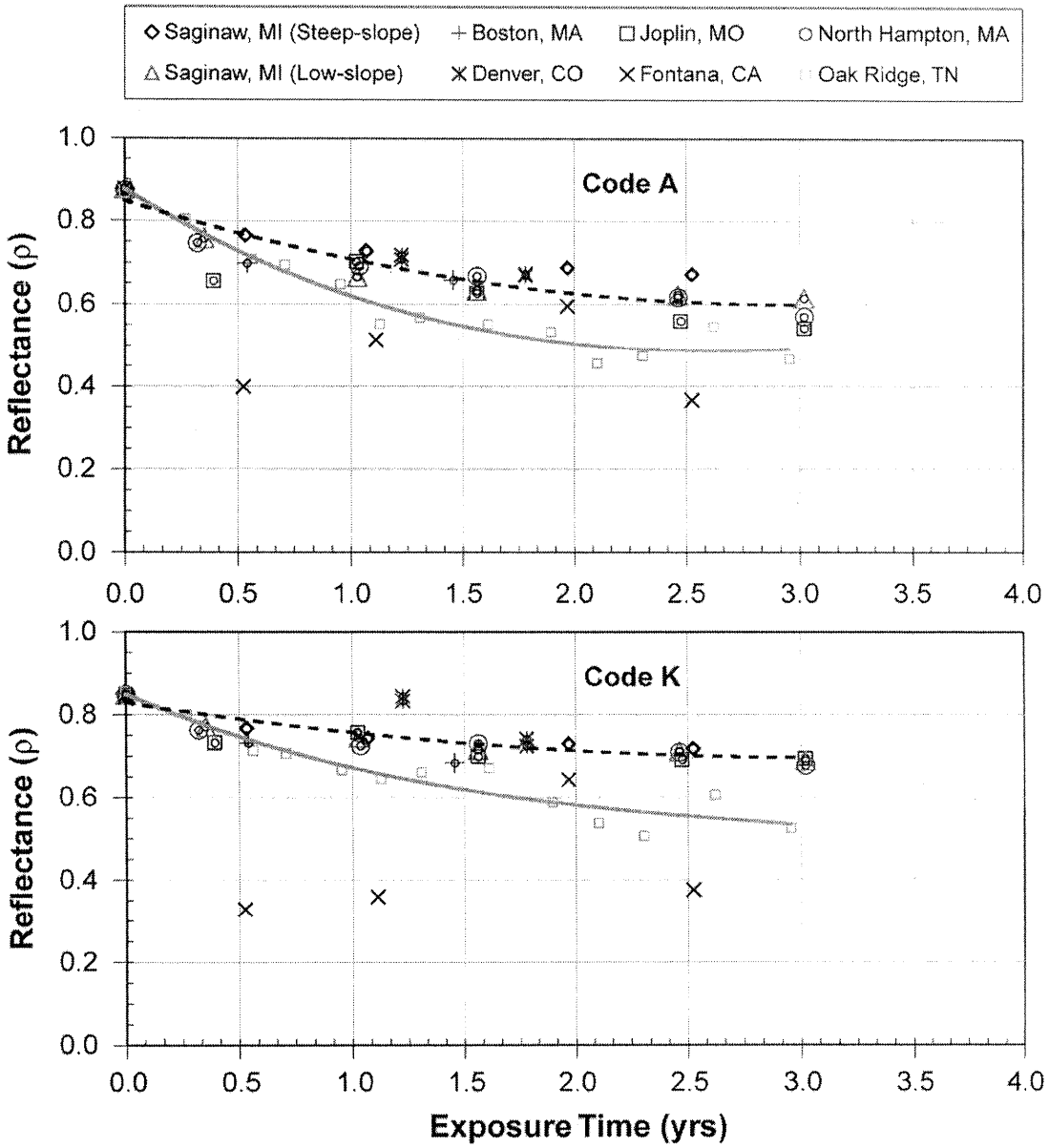

Fig. 16. Field samples A and K have similar reflectance drops, but differ from samples exposed on the ESRA.

Also interesting is the uniformity of the drop in reflectance for the field samples A and K. The dry climate in Denver, CO, showed similar drops in reflectance as observed in the predominantly heating-load climate of Joplin, MO, as well as in the cold and humid climate of Boston, MA (Fig.16). Membranes F, J, and I also showed the same uniformity in the reflectance drop for samples exposed across the country (Fig. 17). Unlike membranes A, G, K, and M, membranes F, I, and J have similar drops in reflectance for the samples exposed on the ESRA as compared to the same samples in the field across the country. Also, while the reflectance of membranes A, G, K, and M starts higher than that of F, I, and J, the measured reflectance after 3 years of exposure for F, I. and J exceeds that of A, G, K, and M. The results show that for the ESRA field site that membranes F, J, and I are not as susceptible to soiling as membranes A, G, K, and M.

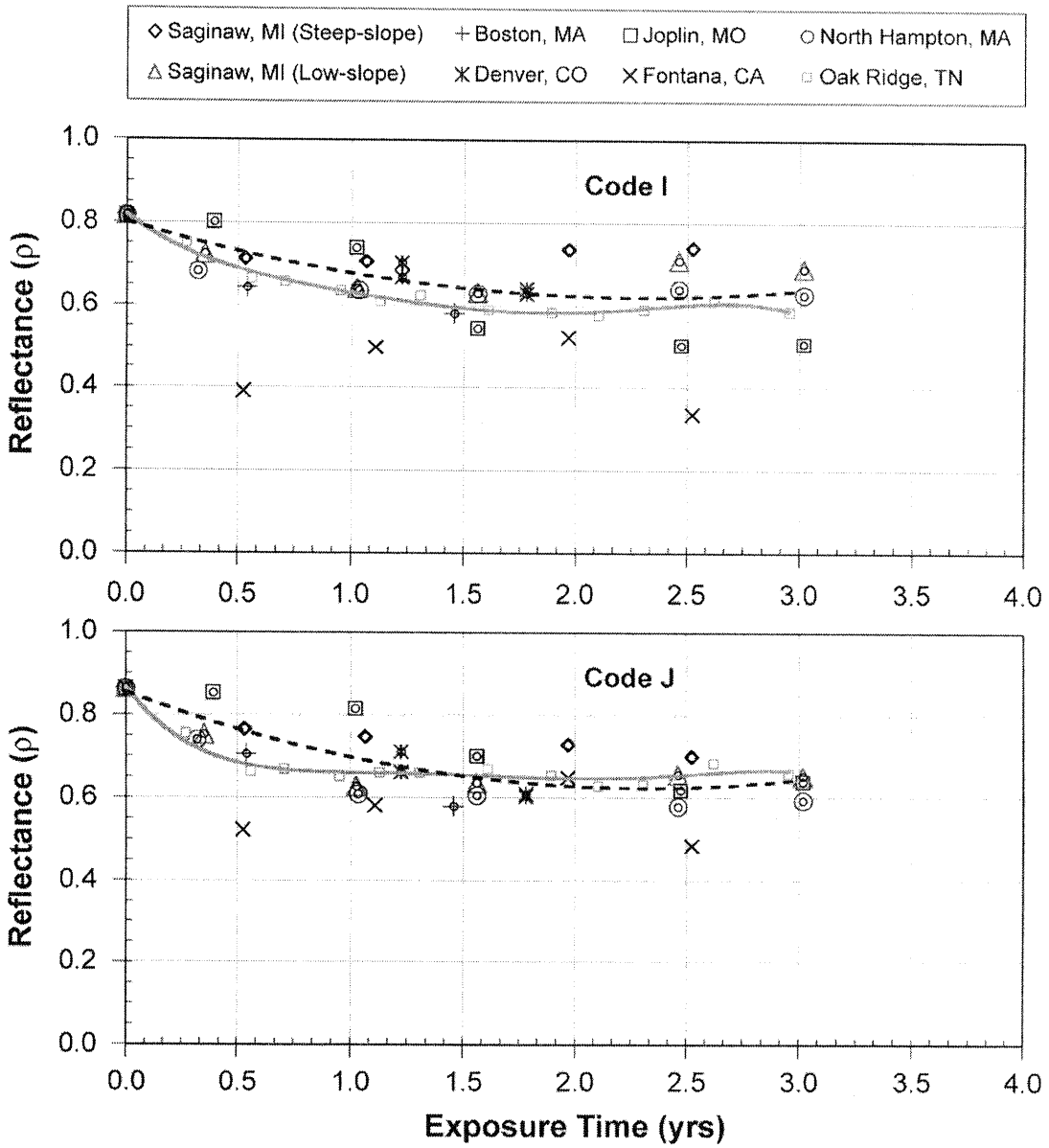

Fig. 17. The loss of reflectance is similar for field samples J and I exposed to various climates across the United States.

4.3 CORRELATION OF REFLECTANCE

A statistical analysis program[2] was used to develop a model for forecasting the loss of reflectance of the thermoplastic membranes and to give insight into the climatic factors that affect the reflectance of the roofing membranes. We formulated and validated a correlation between the change in membrane reflectance and the climatic data (Table 5) that included daily temperature, daily temperature change, relative humidity, barometric pressure, number of days of rain, total precipitation, ozone, particulate matter, carbon monoxide, total solar radiation, UV radiation, wind speed, and wind direction. The

[2] StatGraphicsPlus

correlation coefficients developed by statistical analysis showed significant variation, especially as the membranes were all grouped together or analyzed by membrane material or brand. We conducted multiple regression analysis to determine the combination of effects of the climatic parameters. The parameters which gave the highest correlation coefficient when grouped together were time, relative humidity, average daily temperature change, solar radiation, and number of rain days, with a root mean square error[3] (R^2) of 0.57 for all the membranes. Barometric pressure, particulate matter, CO, ozone, average temperature and wind speed had little effect on the loss of reflectance.

The regression fits improved as more specific groupings of membrane material or brand were analyzed as compared to a fit of all the membranes. The results indicate that the roofing membranes correlate best by brand rather than by material. The finding implies that each manufacturer's formulation of material is affected slightly differently by the climatic elements. For example, two membranes made by the same manufacturer showed root-mean square error (R^2) values of 0.88 and 0.83. When the same data is regrouped and analyzed by material with the same model, the R^2 drops to roughly 0.60.

In formulating the correlation (Eq. 1), we averaged the climatic data over the period of time between reflectance readings (approximately 3 months) and fit the averaged climatic data against the percentage of change in membrane reflectance over the given time interval. The equation and correlation coefficients (Table 7) that describe the best correlation using the weather parameters to predict the change in membrane reflectance for all and several of the membranes grouped together are as follows:

$$\Delta R = C_1 + C_2\,[\text{Days}] + C_3\,[\text{RH}] + C_4\,[\text{Solar}] + C_5\,[\text{Rain Days}] + C_6\,[\Delta T]\ \rho_{aged} = \rho_{new} + \Delta R \qquad (1)$$

where:

ΔR	Represents the percentage change in reflectance over the number of days of exposure,
Days	Represents the number of days of exposure to the climatic elements,
RH	Represents the relative humidity averaged over the number of days of exposure,
Solar	The solar radiation (W/m^2) averaged over the number of days of exposure,
Rain Days	The cumulative number of days of rain over the number of days of exposure,
ΔT	The daily temperature change (°C) averaged over the number of days of exposure.

Table 7. Correlation constants for regression analysis of single-ply membranes tested on the ESRA

	Bias C_1	Days C_2	RH C_3	Solar C_4	Rain days C_5	ΔT C_6
All Membranes	-0.190565	- 0.0001196540	0.00445855	0.000099192	0.00301695	- 0.0119601
A, B, G, N, Q	-0.263915	- 0.0000846798	0.00577443	0.000155005	0.00297988	- 0.0144526
A, G, K, M	-0.266381	- 0.0000382624	0.00538368	0.000146431	0.000678006	- 0.00866035
Q, N, P	-0.262271	- 0.0001156250	0.00603492	0.000160721	0.00451447	- 0.0183142
J, F, I	-0.199009	- 0.0001670020	0.00436974	0.000315678	0.00133509	0.000977091

Figure 18 shows a plot of the measured reflectance versus the reflectance calculated from the correlation developed using a multiple regression analysis for all the membranes at the Oak Ridge, TN, site. A linear least squares equation is fit to these results (Fig. 18). The scatter of measurements about the linear fit of the data shows that the average absolute error between the correlation and the data is 6.8%. Therefore the correlation is an accurate predictor of the loss of reflectance for all the thermoplastic membranes.

[3] The root mean square error describes the goodness of fit of the regression equation. It measures the percentage variation in the fit. As example, an R^2 of 0.75 explains 75% of the total variation in the data.

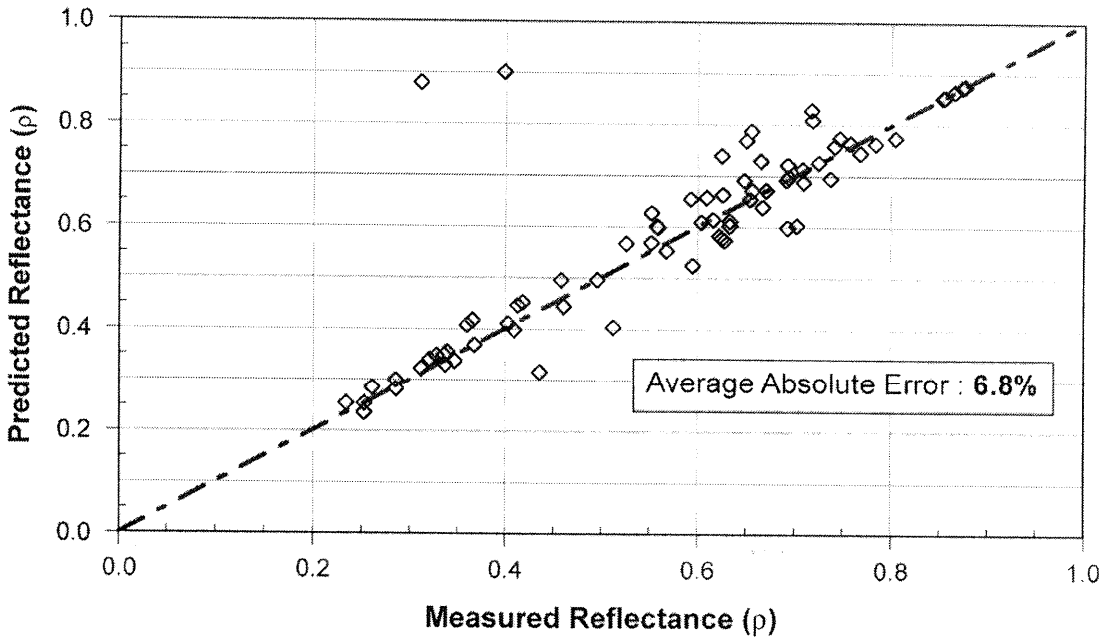

Fig. 18. Correlation of reflectance versus the measured reflectance for all the thermoplastic membranes at field sites and the ESRA.

In summary, the weather parameters that appear to have the greatest effect on the change in membrane reflectance are time, relative humidity, rain days, temperature change, and solar radiation. Relative humidity, rain days, and average ambient air-temperature change have the greatest influence on the statistical model. A curve fit using days and days squared fits the data well because the loss of reflectance tends to follow a parabolic curve with time. The fact that relative humidity and the number of rain days are important regression variables gives some insight into the mechanisms causing the loss of reflectance. Relative humidity and the number of rain days may imply that the amount of time the membranes remain wet is significant for understanding the mechanism causing the loss of reflectance. Wet or moist conditions are conducive to the growth of biomass, which will be discussed in Sect. 4.5 of this report.

4.4 CLEANING MEMBRANES

An original equipment manufacturer (OEM) provided the BTC with samples of a white thermoplastic membrane material that the OEM had exposed to weathering in the south central United States. Each year the OEM would place samples in a weathering farm to judge the durability of the membrane. The exposure time of the samples ranged from 1 to 7 years. The BTC measured the reflectance of these samples and observed that the reflectance dropped from about 0.8 to about 0.5 (Fig. 19). The 38% degradation in reflectance was not necessarily uniform; however, the OEM's samples probably varied from year to year as formulations were modified to improve the product. We cleaned the samples using 409® cleaner·degreaser and observed that all the samples were restored to their original reflectance (Fig. 19). This result reveals that the surface opacity of this thermoplastic membrane limited the photochemical degradation caused by ultraviolet light present in sunlight for 7 full years of exposure.

Given the finding for the OEM's product, the test roofs on the ESRA were washed and reflectance measurements made to determine whether the surface reflectance could be restored to its original

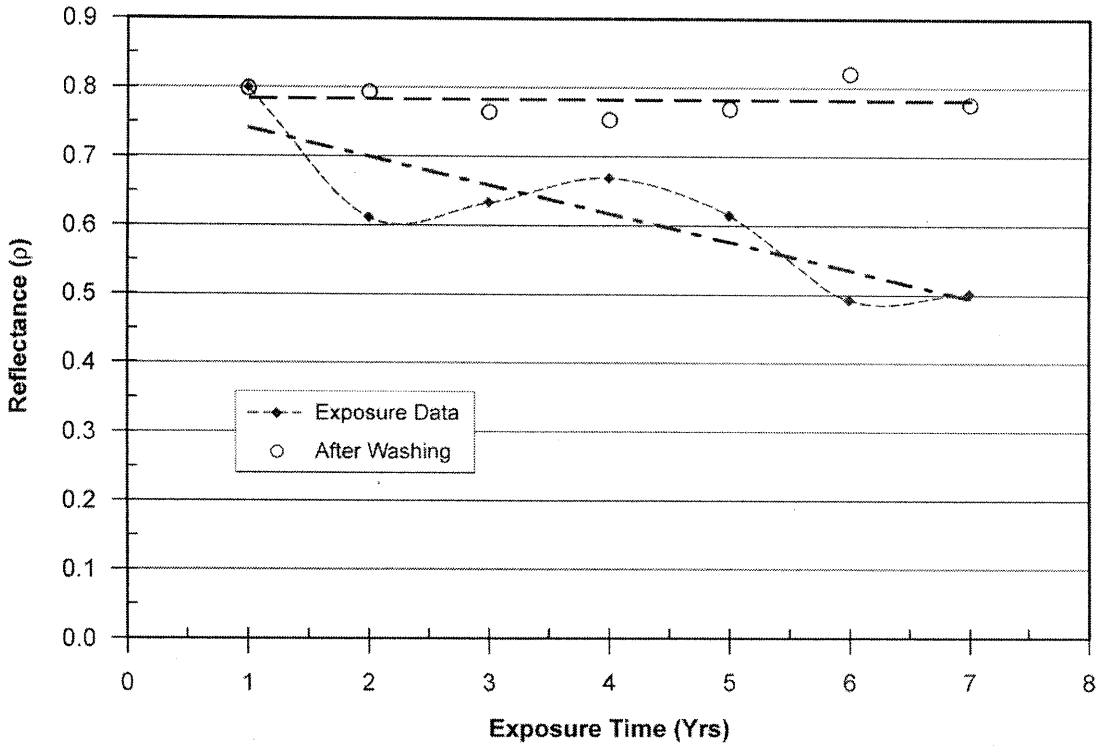

Fig. 19. Washing of test membranes shows the material impervious to solar irradiance after 7 years of exposure in south central United States.

value. Water, 409® cleaner-degreaser, trisodium phosphate (TSP), and cleaning liquids Restore and Rennovate, sold by Ken Barlow Inc., were applied to small areas of about 1 ft (0.305 m) in diam on each test membrane. A soft brush was used with the TSP cleaner; all other cleaning agents were applied with a soft cloth. The cleaners were allowed to react with the soiled surface for about three minutes before wiping the surface with another water saturated soft cloth.

Again the results were pleasantly surprising, because the washing almost fully restored the reflectance (Figs. 20 and 21). For membrane Code B, all cleaners, with the exception of water and TSP, restored 98% of the surface's reflectance (Fig. 20). Membrane B had developed a splotchy dull gray appearance that degraded reflectance about 55%. Cleaning almost fully restored the surface reflectance of all the thermoplastic membranes as typified by Code K (Fig. 21). Table 8 lists the restoration of reflectance after cleaning all thermoplastic membranes field tested on the ESRA. The average restoration in reflectance for all membranes (Table 8) is about 95% of the original reflectance for each sample. The results are significant and show that the thermoplastic membranes are impervious to the effects of solar irradiance within the first 3 years of climatic exposure. Ultraviolet light has had little short-term effect on the reflectance. Manufacturers have formulated their membranes with titanium dioxide (TiO_2), a rare earth ceramic material. Titanium dioxide is processed from rutile and is the most important white pigment currently used in the manufacturer of paints, plastics, and roof membranes. TiO_2 is chemically inert, insoluble, and very heat resistant. It increases surface reflectance through refraction and diffraction of the light. The light travels a shorter path and does not penetrate as deeply into the membrane; therefore, less heat is absorbed. Note however that the membranes may indeed show signs of weathering after 8 to 12 years of exposure. It would be very

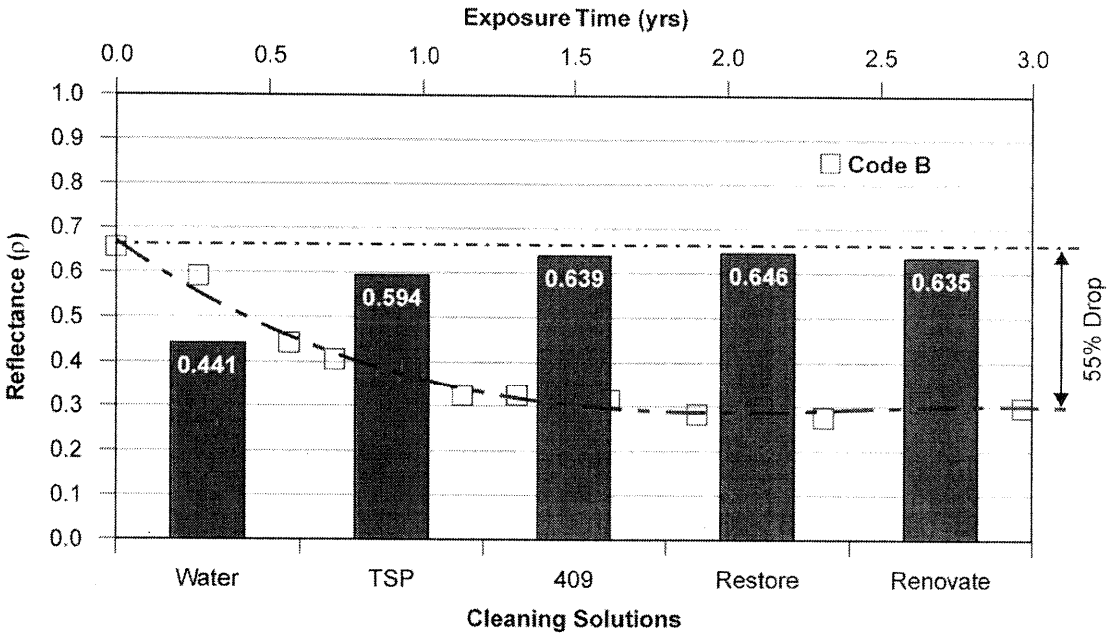

Fig. 20. Washing of Code B membrane restored 98% of its original reflectance.

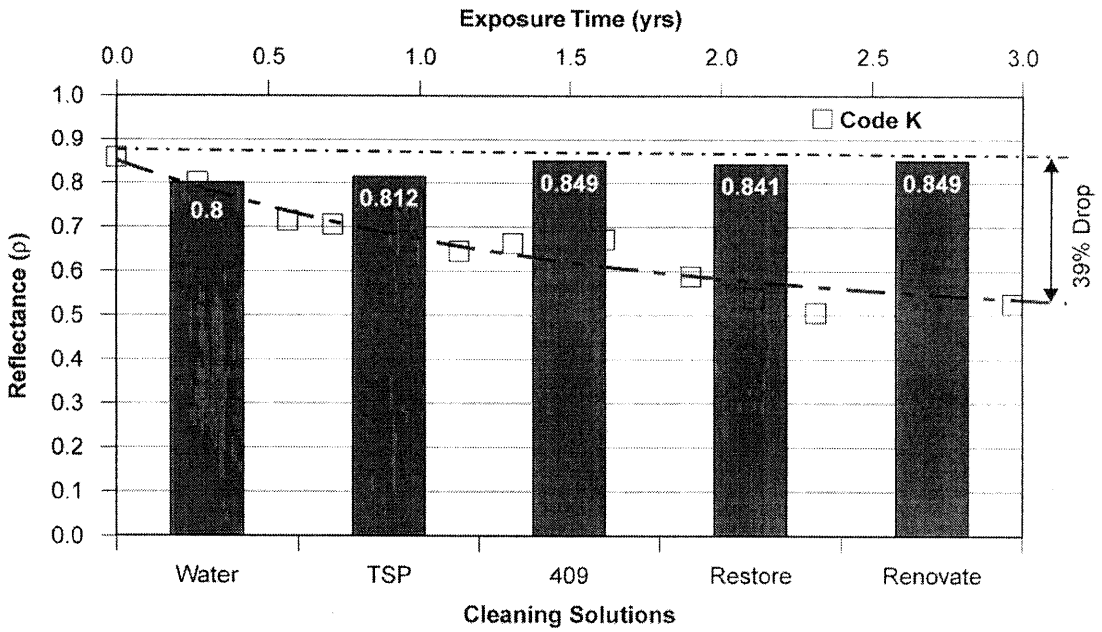

Fig. 21. Code K was almost fully restored after washing.

Table 8. The restoration of reflectance (%) for the membranes exposed on the ESRA

	A, G, K, M	B, N	F, I, J
Water	77.1%	60.6%	57.7%
Trisodium phosphate (TSP)	92.6%	89.6%	85.0%
409 cleaner • degreaser	94.7%	94.9%	95.0%
Restore (2 min)	97.1%	95.6%	91.5%
Renovate (5 min)	98.3%	95.5%	92.8%

interesting to determine if the surface opacity of the thermoplastic membranes field tested at ORNL continue to limit the photochemical degradation caused by ultraviolet light as compared to the thermoplastic membrane field tested for 7 years by the OEM.

4.5 AGENTS CAUSING THE DROP IN REFLECTANCE

The results gleaned from 3 years of field testing on the ESRA show that the solar reflectance of several of the highly reflective, thermoplastic membranes lost almost 50% of their original reflectance. The reduction is caused by surface contamination that soils the roof. Our findings show that airborne particles themselves are responsible for the loss in roof reflectance, and are also the vehicles for delivering microorganisms to the surface as they are deposited on the membrane. Microorganisms grow on the surface, sprouting thin root-like filaments called hyphae that are covered with enzymes. During the evening, a roof will become wet as the surface temperature falls below the dew point temperature of the ambient air. The enzymes covering the hyphae go into solution in the condensate and dissolve edible food from the surface of the membrane. The solution of nutrients migrates into the microorganism because of the difference in osmotic pressure between the nutrient-rich solution and the microorganism. The biomass begins to thrive if the food source is plentiful and the moisture high. A colony forms on the roof surface, and the hyphae grow into a biological filmlike mat that is hydrophilic and keeps the surface moist even when the air is dry. The hyphae act as a net enhancing the continued deposition of dirt onto the surface, which in turn leads to larger losses in reflectance. Soiling may be exacerbated in certain thermoplastic membranes whose formulations contain edible foodstuffs for the biomass. Correlating the drop in reflectance substantiated our hypothesis. Regression analysis (discussed in Sect. 4.3) indicated that the parameters that most strongly influence the decrease in membrane reflectance were relative humidity, average daily temperature change, and the number of rain days. All of these parameters affect the moisture content on the roof, which promotes and stimulates the growth of biomass.

The results suggest that manufacturers should check the formulation of their membranes for ingredients that may promote fungal metabolism and thereby exacerbate the loss of reflectance. A judicious selection of ingredients that hinder the growth of biomass may be a key strategy for optimizing the formulation of white thermoplastic membranes to sustain high reflectance.

4.5.1 Biomass

The Biomarker Analysis Center at the University of Tennessee conducted an ester-linked phospholipid fatty acid (PLFA) analysis to determine whether microorganisms were growing on the test membranes. PLFA is an effective technique to measure microbial biomass and determine the community structure when bacteria, algae, or fungi are present on the membranes. The analysis includes solvent extraction of roof samples for organics and the separation of the recovered lipids into lipid classes. A healthy cell contains polar lipids, and the polar lipids in microbes are phospholipids. By identifying the phospholipids, which are merely organic matter, we can identify and quantify the biomass.

Microbiologists use a shorthand nomenclature for labeling fatty acid organic molecules. The fatty acid is abbreviated by the number of carbon atoms (A), a colon, the number of unsaturations (B) followed by the omega symbol (ω) followed by the number of carbons (C) from the methyl end of the molecule to the position of the unsaturation (e.g., A:BωC) (White and Ringelberg, 1998).

The PLFA analyses revealed a range of total biomass for the roofing materials from 8360 to 46,400 pmole/ft^2 ($9{\cdot}10^4$ to $5{\cdot}10^5$ pmol/m^2), representing $1.9{\cdot}10^{12}$ to about $9.3{\cdot}10^{10}$ cells/ft^2 ($2{\cdot}10^{13}$ to about $1{\cdot}10^{11}$ cells/m^2). The highest biomass was seen for membrane Code M and the lowest biomass values were measured on Code Q and for a clear-coated acrylic Galvalume® metal roof. Eight of the thirteen roof samples exhibited biomass values exceeding about $9.3{\cdot}10^{16}$ (10^{18} pmol/m^2). The major PLFA, 18:2ω6, ranged from 56–72% of the total PLFA profiles for all the thermoplastic membranes (Fig. 22). This finding is very important because the PLFA 18:2ω6 is a fungal indicator lipid. The other major PLFAs were 18:1ω9c, 16:0, and 18:1ω7c, which are precursors to 18:2ω6 (Fig. 22). Fungi are ubiquitous, prevalent in soil, on plants, and in air. Total spore concentrations of 85 to 285 spores/ft^3 (3000 to 10000 spores/m^3) are found in the air (Armstrong 2002). A comparison made for fungal and bacterial biomass for each membrane shows the fungal influence predominant in the microbial community (Fig. 23). Even though the conversion factor to cells overestimates the fungal biomass, it is evident that the microbial community present on the roofing materials is largely a fungal community.

We compared the thermoplastic membranes to painted metal roof materials in order to observe potential differences between membrane and metal materials. The averaged PLFA profile and biomass was used to represent all the membranes. The biomass for the acrylic-coated Galvalume® metal roof, containing zinc, was significantly less than that for the white-painted polyvinylidene

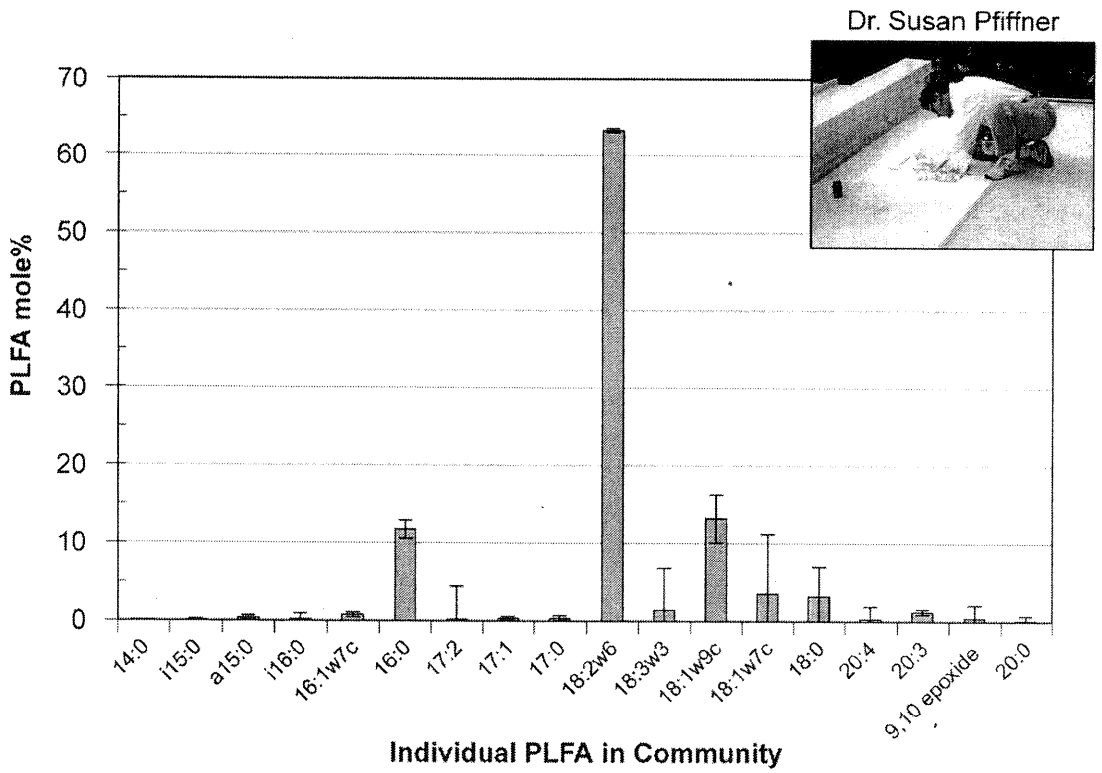

Fig. 22. Analysis verified that all the ESRA test membranes had a phospholipid fatty acid that is a fungal indicator.

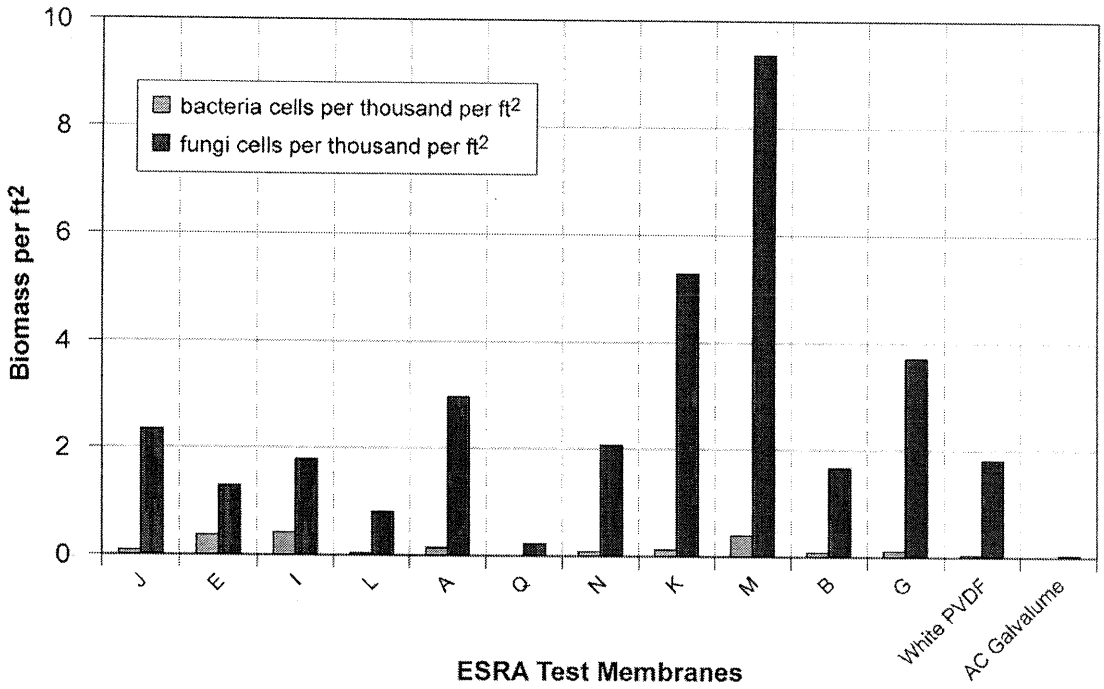

Fig. 23. The community biomass ranged from 10^6 to 10^8 cells per ft^2; grassland soils contain significantly more bacteria than fungi.

fluoride (PVDF) galvanized steel roof or the thermoplastic membranes (Fig. 24). In addition, this low biomass sample had a distinctly different community profile, in which the major PLFAs were 16:0 and 18:0. These PLFA are general fatty acids that are ubiquitous in the environment and are often found at higher relative percentages in low biomass samples. The low biomass and minimal microbial community structure for the clear-coated Galvalume metal roof indicates that the zinc inhibited the microbial community. Changes in soil microbial community upon exposure to zinc have been previously documented, but the effect of the fungal community varies and is not well understood (Frostegård et al.1996, Bååth et al.1998, Kelley et al. 1999). The comparison to the acrylic coated Galvalume strongly suggests that manufacturers should investigate compounding their thermoplastic membranes with appropriate ingredients to resist biochemical attack from fungal biomass.

The white-painted PVDF galvanized steel roof and the thermoplastic membranes had the same level of viable biomass. However, the reflectance of the white-painted PVDF steel only lost about 10% of its fresh-from-the-factory value as compared to the 30 to 50% loss for the thermoplastic membranes. The difference is believed due in part to the difference in surface finish of the two roof covers. Thermoplastic membranes have a more coarse surface finish than do white-painted PVDF metals. The hyphae from the colony of fungi can more easily attach themselves to the thermoplastic membranes; they cannot penetrate or easily attach themselves to the painted PVDF metal. Hence we believe the biomass and contaminants clinging to the biomass wash off the painted metal more readily than they wash off the thermoplastic membranes.

4.5.2 Airborne Contaminants

Airborne particulate matter comes from many sources such as soil and road dusts, emissions from internal combustion engines and fossil-fueled power plants (termed man-made aerosols), as well as pollens from trees and grass (termed natural aerosols). Particulate matter settles on a roof surface.

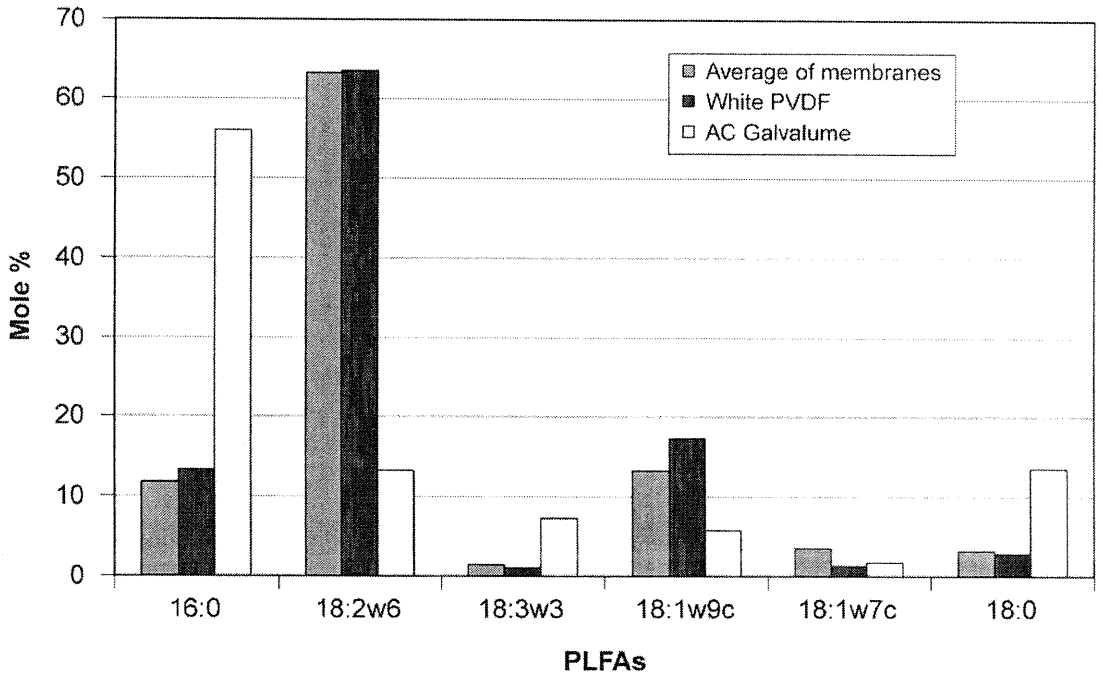

Fig. 24. The membranes and AC Galvalume® have very different community profiles.

Depending on the chemical content and the size of the particles, incoming solar radiation can be reflected back to the atmosphere or be absorbed and re-emitted in a different wavelength. The light scattering and absorption processes occur within a few microns of the surface, but they determine the roof reflectance. Our findings show that the long-term loss of reflectance appears to be determined by the ability of the particulate matter to cling to the biomass that adheres to the roof, resisting being washed off by rain.

Samples were collected from several of the thermoplastic membranes that were field tested on the ESRA (see Sect. 3.5.1). The elemental composition of the dust was analyzed using an inductively coupled plasma spectrometer (ICP) to detect elements that are typically found in the ambient air. Table 9 lists the concentration of the elements found on the painted metal and thermoplastic roof samples. The data in this table show that the samples contain high levels of the crustal elements Si, Al, Ca, Fe, Mn, and Mg. The amounts of crustal elements in the samples J, F, and I are not uniform. Sample J has consistently high amounts of crustal elements. Sample I contains the lowest concentration of elements. Sample J had a higher biomass content that did I (Fig. 23). Samples M and G show consistently higher levels of Si, Al, Fe, and Mg concentrations than J, F, and I, indicating that the dust retention capacities for M and G are possibly greater than for the other roof samples. Samples A, M, and G also had the largest concentrations of biomass (see Fig. 23), indicating a possible link between the biomass and the dust found on the thermoplastic membranes.

Interestingly, the sulfate levels found in the M and G samples are lower than those found in J and A. Samples F and I were found to have negligible amounts of sulfate. Sulfate is the major light-reflecting component in the man-made atmospheric aerosols and would produce some light scattering on the roof surface to boost reflectance. Ni is typically of anthropogenic origin; the data here, however, suggest that the amount of this element in deposited particles is small.

Table 9. Composition of contaminants on the roof samples (mg/ft^2)*

Sample name	SO_4	Si	Al	Ca	Fe	Mg	Mn	Ni
AC Galvalume®	0.482	0.650	0.208	0.036	0.238	0.029	0.002	0.001
WH PVDF	0.152	0.745	0.065	0.017	0.126	0.013	0.001	0.002
J	0.694	2.435	0.242	0.207	0.325	0.074	0.004	0.001
F	0.000	1.270	0.194	0.058	0.278	0.096	0.003	0.001
I	0.000	0.820	0.202	0.037	0.184	0.059	0.002	0.001
A	0.455	2.100	0.536	0.027	0.736	0.090	0.005	0.001
M	0.127	3.660	0.746	0.043	0.862	0.121	0.006	0.001
G	0.191	3.625	0.719	0.051	0.822	0.113	0.006	0.001

* To convert composition to mg/m^2, multiply mg/ft^2 by 10.76391.

Samples were also analyzed for the total carbon existing on the thermoplastic membranes. We did not separate elemental carbon from organic carbon because our instrument was not equipped to differentiate elemental from particle-bound organic carbon molecules. Carbon, especially elemental carbon, is the most significant light-absorbing species embedded in man-made atmospheric aerosols. Organic carbon represents the other remaining fraction of the total carbon measured on the thermoplastic membranes. Organic carbon has little effect on light absorption. Hence, the effect of the biomass on the roof membranes would not directly affect the reflectance of the membrane. The crustal elements clinging to the biomass reduces reflectance. For example, if a roof surface were partially covered with carbon soot, the reflectance of this surface would be substantially reduced (Berdahl, Akbari and Rose 2000). It is also important to remember that elemental carbon is only a fraction of the total carbon in atmospheric aerosols.

Annual carbon emissions in the United States are estimated to fall in the range of 1 to 18.6 mg/ft^2 (10 to 200 mg/m^2). The total carbon concentrations detected on the test roofs (Table 10) show that samples J, A, M, and G all have concentrations within the range of carbon emissions expected nationally. Codes J, A, M, and G also have the greatest concentrations of fungal biomass (Fig. 23).

Table 10. Carbon analysis results

Sample name	Concentration (mg/ft^2) *
AC Galvalume®	0.579
WH PVDF	1.351
J	4.041
F	0.795
I	0.562
A	3.065
M	1.735
G	2.095

* To convert concentration to mg/m^2, multiply mg/ft^2 by 10.76391.

Reflectance data were collected about the same time that the samples of roof contaminants were swiped from the thermoplastic membranes. The concentrations of sulfur and crustal elements and total carbon were fit against the reflectance of the membranes to show the correlation (or lack of it) with the chemical variables. In Fig. 25 the y-axis is a log scale that holds the value for the chemical

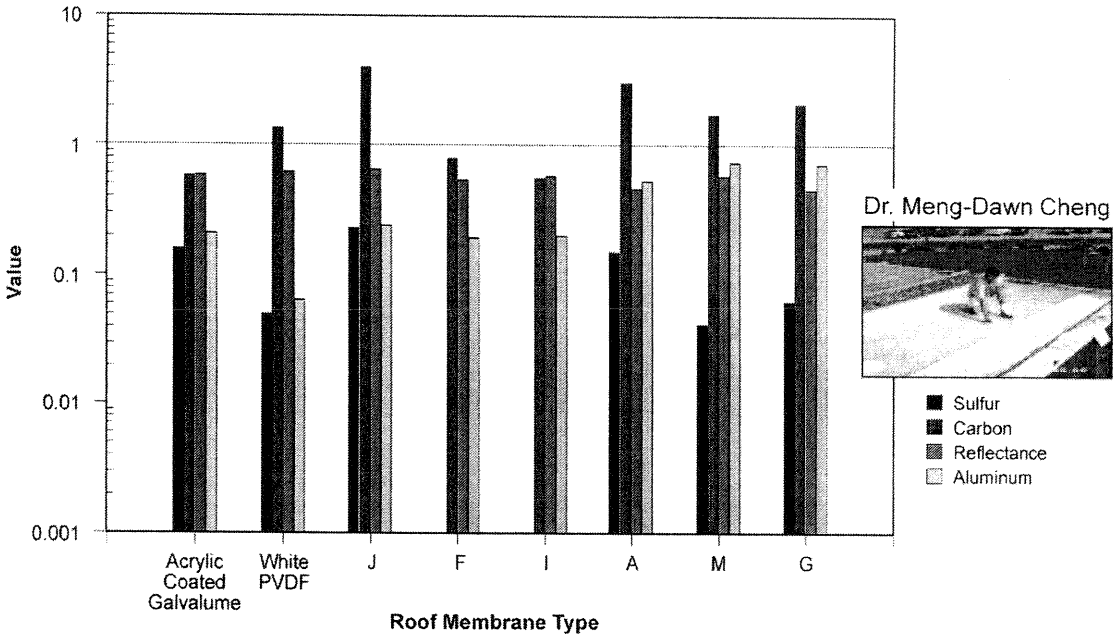

Fig. 25. Dr. Meng-Dawn Cheng identified and qualified several air borne contaminants on the metal and single-ply membrane roof systems.

concentrations of particles and the reflectance values. The reflectance measurements for different membranes on this particular date appear to be quite similar, although the chemical composition varies significantly for the different membranes. In comparison with biological data discussed earlier (Fig. 24), the biomass content on the acrylic-coated Galvalume was virtually zero because of the zinc treatment applied to the metal roof. Assuming that the carbon concentration on the acrylic coated Galvalume roof was mostly elemental carbon, we speculate that more than half of the carbon on the white-painted PVDF and Codes J, A, M, and G was of organic origin. The elemental carbon is not the main element causing the loss of reflectance on these coded membranes. Rather, the crustal elements that are held by the biomass cause the loss of reflectance.

To further support our hypothesis, we used the concentrations of each element from all roof membranes and correlated the concentrations with reflectance. Table 11 shows the correlation coefficients. A positive coefficient implies that the element increases reflectance while a negative coefficient implies a loss in reflectance with increasing amounts of the constituent element. A coefficient near zero implies the element has little effect on the surface reflectance. The relationship between the reflectance and individual elements across all membrane types shown in the Table 11 indicates that the surface reflectance is correlated with crustal elements such as Si, Al, Ca, Fe, Mg, Mn, and Ni but not with carbon (C). Sulfur from SO_4 shows a positive influence and increases reflectance as expected.

Table 11. Correlation of elements detected in samples collected from all membrane surfaces: reflectance is correlated as a function of the concentration of the detected elements

S	Si	Al	Ca	Fe	Mg	Mn	Ni	C
0.21	-0.36	-0.61	0.472	-0.64	-0.53	-0.57	0.334	-0.01

The correlation coefficients of reflectance with Si, Al, Fe, Mg, and Mn were all negative, indicating that the higher the crustal element level (possibly dustier), the lower the reflectance value.

The findings based on the above contaminant study of biomass and aerosols show that airborne particles soil the roof membrane and are the vehicles depositing microorganisms (spores) on the surface of the thermoplastic membranes. When a spore lands on a roof surface, the enzymes that cover the outside of the spore mix with moisture on the roof and dissolve edible nutrients for the spore. The mixture is drawn into the spore by osmotic pressure, and the spore begins to sprout thin root-like filaments called hyphae. The hyphae are coated in enzymes and dissolve more nutrients for the fungus to thrive on. Ester-linked phospholipid fatty acid (PLFA) analysis proved that a fungal indicator was prevalent on all the membranes and painted metal roofs. Filamentous fungi like *Aspergillus niger* or *Trichoderma reesei* are prolific secretors of enzymes and are probably the detected biomass. Their hyphae grow thickly, digging into the surface and forming a protective mat that keeps the surface moist even when the surrounding ambient air and membrane appear to be dry. However, the zinc coating on the acrylic coated Galvalume kept the biomass population low. We believe the hyphae grow into a biological filmlike mat that is hydrophilic. It uses the moisture that condenses onto the membrane during the evening hours when the temperature of the membrane drops below the dew point temperature of the ambient air. The hyphae also act as a net enhancing the continued deposition of dirt onto the surface, which in turn leads to larger losses in reflectance. Soiling may be exacerbated in certain thermoplastic membranes whose formulations contain edible foodstuffs for the biomass. Hence, the effect of the organic carbon is indirect. It serves as a host for crustal and carbon elements to adhere to the roof and is not easily washed off by rainfall. Surface finish of the roof membrane may be extremely important because the coarse texture may provide attachment sites for the biomass to cling to the membrane if not penetrate it over time. Correlation of the elements deposited on the test roofs shows that the crustal elements cause the loss in reflectance on the thermoplastic roof membranes. The effect of elemental carbon is minor.

4.6 MEMBRANE TEMPERATURE AFFECTED BY REFLECTANCE DROP

A building's comfort cooling and heating system uses purchased energy to offset the thermal energy gained or lost through the roof. The roof thermal load is directly related to the solar irradiance absorbed by the building. The more reflective the roof, the lower will be its surface temperature and the less will be the roof load imposed on the cooling plant. So determining how soiling affects the reflectance of the membranes is of paramount importance for predicting and documenting the effect of weather on the temperature of the thermoplastic membrane, which in turn yields useful information about the durability of the membrane.

The reflectance of the membrane Code A dropped almost 50% after 2 years of exposure (Sect. 4.1). The drop in reflectance caused the measured peak membrane temperature to increase from 100°F (38°C) in August 1998 to about 140°F (60°C) in September 2001 for data collected near solar noon on days having nearly the same outdoor air temperature and solar irradiance (Fig. 26). The 40°F (22°C) increase in surface temperature caused the measured heat flow leaking into the building to double! On August 18, 1998, the measured daytime heat flux entering through Code A membrane was 28 Btu/ft^2. Three years later, on September 4, 2001, the heat flux had increased to 56 Btu/ft^2. After one year of exposure, a 30% drop in reflectance caused a membrane temperature increase of 36°F (20°C) for measurements taken in August 1999. The soiling of the thermoplastic membranes is therefore significant, because after only 1 to 3 years of field exposure the highly reflective membrane, Code A, has a surface temperature that is only 20°F (11°C) lower than a BUR (Fig. 26). The heat flux penetrating Code A increased from 25 to 50% of the flux penetrating the BUR after 3 years of field exposure in Oak Ridge, TN.

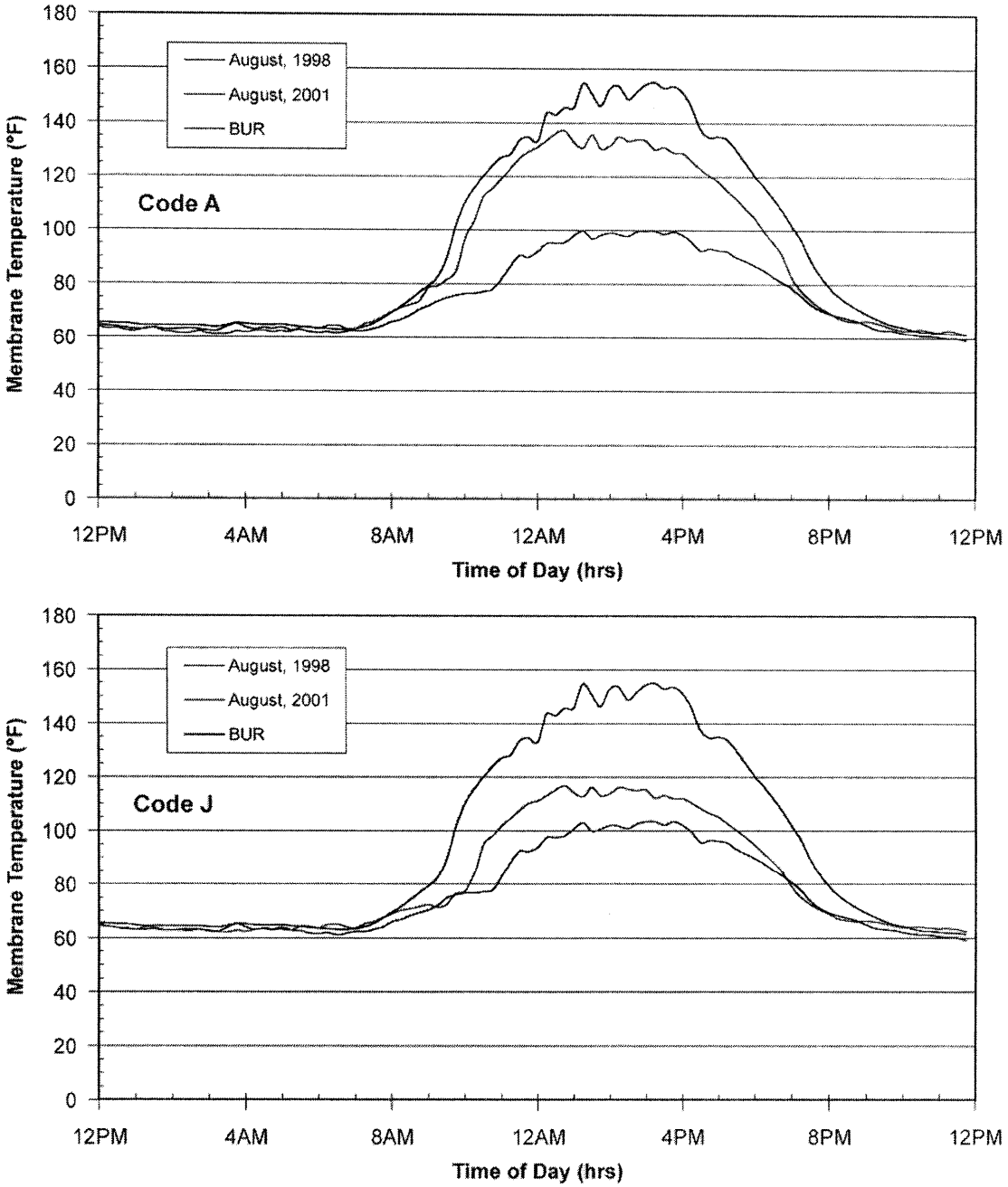

Fig. 26. A 50% drop in reflectance for Code A caused the peak membrane temperature to increase 40°F (22°C) for August days having similar outdoor air temperature.

The Code J membrane was not as soiled as was Code A after 3 years of field exposure. Initially, Code A had a higher reflectance than Code J, but because of soiling by airborne contaminants, the reflectance of membrane Code J exceeded Code A after 3 years of exposure. Soiling of the membrane J caused a 24% drop in reflectance (see Sect. 4.1). The reflectance degradation caused the peak membrane temperature to increase from 100°F (38°C) in August 1998 to about 110°F (43°C) in August 2001. However, for the September day in 2001, the surface temperature of Code J was almost

30°F (17°C) cooler than that of the Code A membrane (Fig.26), which in turn reduced the heat flux. Code J absorbed a flux of 39 Btu/ft^2 on September 4, 2001, as compared to 56 Btu/ft^2 for Code A. Therefore membranes F, J, and I performed better thermally than did membranes A, G, K, and M, because of their superior resistance to soiling.

5. THE FORMULATION AND VALIDATION OF THE STAR COMPUTER CODE

Large, open floor areas on one level characterize many current industrial and commercial buildings. Single-story buildings have a large ratio of exposed exterior surface-to-floor area, and the roof is roughly 85% of the exposed exterior (Baker 1980). A very gradual roof slope of about 1.2° for drainage of precipitation is typical of commercial roofing. The gradual slope allows the placement of mechanical and air-conditioning equipment, which saves the building owner useful floor space. Historically, the roof is built up with multiple layers of a felt paper applied to several applications of bitumen. Such roofs, called built-up roofs (BURs), can offer excellent waterproofing and can provide a long service life. However, the roof is the major source of heat leakage because of its large, exposed surface area and dark, heat-absorptive characteristic coupled with the demand for comfort cooling within the building.

In the summer, the higher the roof temperature, the greater the potential for heat leakage into a building, and the greater the burden on the air-conditioning system. For example, the exterior daytime temperature of a BUR can exceed 180°F (82°C) in predominantly hot climates. In winter, the lower the roof temperature, the greater the potential for heat leakage from the building, and the greater is the energy consumed for comfort heating.

5.1 SIMPLIFIED TRANSIENT ANALYSIS OF ROOFS (STAR)

Low-slope roofs are constructed of metal decking that support a layer of insulation and a single-ply membrane or BUR cover. The heat flow entering or leaving a low-slope roof is driven by the exterior surface temperature of the roof, which in turn is affected by the surface properties of solar reflectance and infrared emittance of the membrane, the amount of roof insulation, and the exposure of the surface to the climatic elements. The heat flow through any layer of the roof is calculated using Fourier conduction heat transfer, provided the temperature distribution is known through the roof.

A numerical computer code, termed STAR, is used to solve for the temperature profiles through the roof. It allows the radiation and mass transfer energy terms to be included in the boundary condition at the exterior surface. Wilkes (1989) formulated the code using the discretization techniques presented by Patankar (1984). The code models the transient one-dimensional heat flow through the exterior roof cover, through multiple layers of roof insulation, and through the supporting subframe (e.g., a metal deck). The model accounts for temperature-dependent thermal properties. The energy equation in time and one-dimensional space is linearized into a collection of simultaneous algebraic equations. The equations are fully implicit and mathematically describe the temperature for a given time and position within the multilayer roof. A numerical solution of the algebraic equations leads to the temperature profile throughout the roof insulation from which the heat transfer at the metal deck describes the thermal load for the building.

The STAR code is fully coupled to ambient weather conditions using an energy balance at the exterior surface of the roof (Fig. 27). The convection ($\hbar_L$), the mass transfer ($\bar{h}_m$), and the surface properties of solar reflectance (ρ) and infrared emittance (ε) affect the exterior temperature and, therefore, the heat flow in the following energy balance made at the roof surface:

$$q_{cond} = q_{roof\ surface}$$

$$-k\left(\frac{dT}{dz}\right)_S = (1-\rho)I_{solar} - \varepsilon\sigma\left(T_S^4 - T_{sky}^4\right) - \hbar_L\left(T_S - T_{air}\right) + \bar{h}_m i_{fg}\left(\omega_{air} - \omega_S\right) \qquad (2)$$

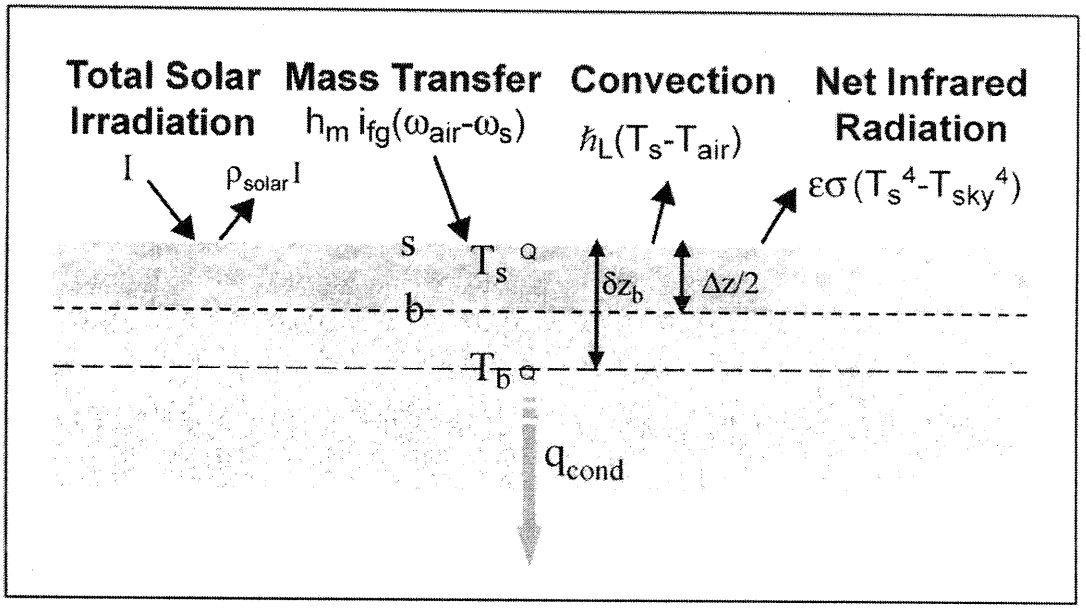

Fig. 27. Setup for integrating the roof energy balance into the numerical STAR computer code.

The roof temperature is therefore mathematically described by the roof's surface properties of solar reflectance (ρ) and infrared emittance (ε). Convection ($\hbar_L$) is also important. In the early morning, evaporation and, in the twilight, condensation, also affect the temperature and heat transfer through the roof. Increasing the reflectance or emittance will reduce the exterior temperature, which in turn results in reduced building load. Reflectance effects occur during the sunlight hours, while the effects of emittance occur continuously as long as there is a temperature difference between the roof surface and the radiant sky.

5.1.1 Formulation of Code

To model the exterior boundary condition (Fig. 27), the energy equation is integrated over small increments of time and space into the roof as follows:

$$\int_b^s \int_t^{t+\Delta t} (\bar{\rho} \cdot C_P)_{roof} \frac{\partial T}{\partial t} dt\, dz = \int_b^s \int_t^{t+\Delta t} \frac{\partial}{\partial z}\left(k \frac{\partial T}{\partial z}\right) dt\, dz \tag{3}$$

The integration leads to the following balance:

$$(\bar{\rho} \cdot C_P)_{roof} \{T_S^1 - T_S^0\} \frac{\Delta z}{2} = \int_t^{t+\Delta t} \left\{ \left(k \frac{\partial T}{\partial z}\right)_S - \left(k \frac{\partial T}{\partial z}\right)_b \right\} dt \tag{4}$$

The flux term $k(\partial T/\partial z)_S$ represents the heat flux incident on the roof surface (q_{roof}). Substituting the right-hand side of Eq. (2) into Eq. (4) accounts for the effects of the outdoor ambient weather. Taylor series expansions are applied to the radiation and mass-transfer terms to approximate them in linear formulations, and Eq. (4) is then integrated from time t to time t + Δt. The resultant, fully implicit equation becomes:

$$A_S T_S = A_b T_b + B \tag{5}$$

where

$$A_S = \left\{ A_S^0 + 4\varepsilon\sigma T_S^{*3} + \bar{h}_m i_{fg} \frac{d\omega_S^*}{dT} + \hbar_L + \frac{k_b}{\partial z_b} \right\}$$

$$A_b = \frac{k_b}{\partial z_b}$$

$$A_S^0 = (\bar{\rho} \cdot C_P)_{roof} \frac{\Delta z}{2\Delta t}$$

$$B = (1-\rho) I_{solar} + \varepsilon\sigma\left(T_{sky}^4 + 3T_S^{*3}\right) + \bar{h}_m i_{fg} \left\{ \omega_{air} - \omega_S^* + \frac{d\omega_S^*}{dT} T_S^* \right\} + \hbar_L T_{air} + A_S^0 T_S^0$$

Wilkes (1989) compiled an extensive literature review of convective-heat-transfer correlations for natural and forced convection. His compilation of correlations accounts for the effects of heat-flow direction, surface orientation, surface area, and temperature dependent fluid properties of the ambient air. The STAR code selects the appropriate correlation based on roof slope and also on the direction of heat flow. For laminar flow, the local heat-transfer coefficient is derived from the similarity solution of the Blasius equation [in honor of H. Blasius (1908)]. The coefficient takes the following form:

$$\frac{h_x x}{k} = 0.332 \, Re_x^{1/2} \, Pr^{1/3} \tag{6}$$

In turbulent flow, the boundary layer over a flat plate is affected more by random fluid fluctuations than by molecular diffusion (Incropera and DeWitt 1990). The momentum, thermal, and concentration boundary layers are essentially equal for moist air having a Pr number near unity. The heat-transfer coefficient can therefore be derived from the Chilton-Colburn analogy (i.e., Reynolds analogy). Thus, from the experiments by Schlichting (1960), who formulated a solution for the velocity-boundary-layer thickness, and by the Reynolds analogy relating momentum to heat transfer, the local heat-transfer coefficient for turbulent flow becomes

$$\frac{h_x x}{k} = 0.0296 \, Re_x^{4/5} \, Pr^{1/3} \tag{7}$$

Typically, a transition from laminar to turbulent flow occurs sufficiently upstream of the rear edge of the flat plate [i.e., low-slope roof ≅ 36 ft (11 m) long in direction of airflow]. Integrating the local laminar and turbulent coefficients over their respective domains by the following formula yields the average over the length of the roof:

$$\hbar_L = \frac{1}{L} \left\{ \int_0^{X_C} h_{lam} dx + \int_{X_C}^{L} h_{turb} dx \right\} \tag{8}$$

The overall average heat-transfer coefficient for a transition from laminar to turbulent flow at $Re_{x,C}$ = 500,000 is

$$\frac{\hbar_L L}{k} = \left\{ 0.37 \, Re_L^{4/5} - 871 \right\} Pr^{1/3} \tag{9}$$

The STAR code uses Churchill's technique to combine the natural-convection flows, which occur primarily during the daylight hours, with forced-convection flows (Churchill 1986). Given this formulation for the combined natural- and forced-convection coefficient ($\hbar_L$), the mass transfer coefficient ($\overline{h}_m$) is directly calculated from the Lewis (Le) number using the following equation:

$$\frac{\hbar_L}{\overline{h}_m\left(\overline{\rho}\cdot C_P\right)_{air}} = \left(\frac{\alpha}{D_{ab}}\right)_{air}^{2/3} \tag{10}$$

The model also uses ambient weather data to complete the physics of the problem. The dry bulb temperature, relative humidity, and barometric pressure are used to calculate the specific humidity of the ambient air. The radiant-sky temperature, used within the B term of Eq. 5, is derived from the global infrared irradiance measured by the BTC's field pyrgeometer and the equation for blackbody radiation: $q_{IR} = \sigma T_{sky}^4$. If pyrgeometer data are unavailable, STAR uses the Martin and Berdahl (1984) algorithm to calculate the radiant-sky temperature.

5.1.2 Validation against ESRA Field Data

The STAR code supports specified boundary conditions at the inside and outside surfaces of a roof and can also handle boundary conditions coupled to the outdoor weather and indoor environment. Initial validation attempts revealed that the model systematically over-predicted the measured membrane temperature and the heat flow measured between the two layers of wood fiberboard insulation. Both the temperature and heat flow were over predicted by about 10% of measurements collected at solar noon. The heat loss from the roof during the evening hours was also over-predicted by 23% of the measured heat flow.

Whenever a mismatch occurs between model and experiment, the analyst must scrutinize both the measurements and the computer code's algorithms to determine the source of error. An obvious source of error could be in the reflectance and emittance measurements. However, the Device and Services equipment were calibrated against ASTM standards and proven accurate, see Sects. 3.4.2 and 3.4.3.

Checks of Data Input

The thermal conductivity of the HFT is about 6 times larger than that of the wood fiberboard, and it will disturb the heat flow in the material around it so that the heat flow through the sensor is not equal to that through the wood fiberboard. Heat flow, like electrical current flow, follows the path of least resistance. The higher thermal conductivity of the HFT can therefore cause the sensor to over-predict the actual measured heat flow by almost 28% (Apthrop and Bligh 1985). To correct for the shunting of the heat flow around each transducer, each HFT was calibrated in a 12- by 12-in (0.305- by 0.305-m) guard, which was made from the same wood fiberboard as used in the roof construction(see Sect. 3.4.1). The capacitance of the HFT and wood fiberboard guard as measured by ASTM C518 (ASTM 1998) was 0.2693 Btu/(h·m^2·°F) [1.493 W/(m^2 ·K)]. Using inverse analysis and the field data for the membrane and deck temperature and heat flow yielded a capacitance of 0.264 Btu/(h·m^2·°F) [1.498 W/(m^2 ·K)] for the roof test sections. Hence, the measurements from the HFTs were properly calibrated for any shunting of heat flow around the device.

Given the confidence that the HFT were yielding accurate data, we compared the measured membrane temperature to a value back calculated from the heat flow measured from the HFT and from the temperature measured by a thermocouple adjacent to the HFT. The STAR code tracked the membrane temperature to within 1.3% of measurement for a full week of field data, which indicated

that the thermocouple measuring the membrane temperature was accurate. Similar simulations were made to predict the deck temperature given the heat flow and temperature measured atop the 1 in. (0.025 m) thick wood fiberboard. Results showed the simulated temperature was within 0.5% of measurement, which verified accurate operation of the deck thermocouple.

A check was then made of the BTC's weather station data by comparing the data to other weather stations on the ORNL campus. We found an error. The anemometer measuring the wind speed at the BTC campus had wind speeds that were almost 60% less than measures from anemometers stationed at other ORNL weather stations. The lower wind speed caused the convective heat transfer coefficient calculated by STAR to be under predicted as compared to values using the ORNL anemometer data (Fig. 28). The BTC anemometer was recalibrated and the STAR code predicted the daylight membrane temperature within 4% of field measurements for measures taken between 10 a.m. and 5 p.m. (Fig. 29). The heat flux however was predicted to within only 23% of field measurement for a full week of data due mainly to the under prediction of mass transfer condensing onto the roof in the evening hours.

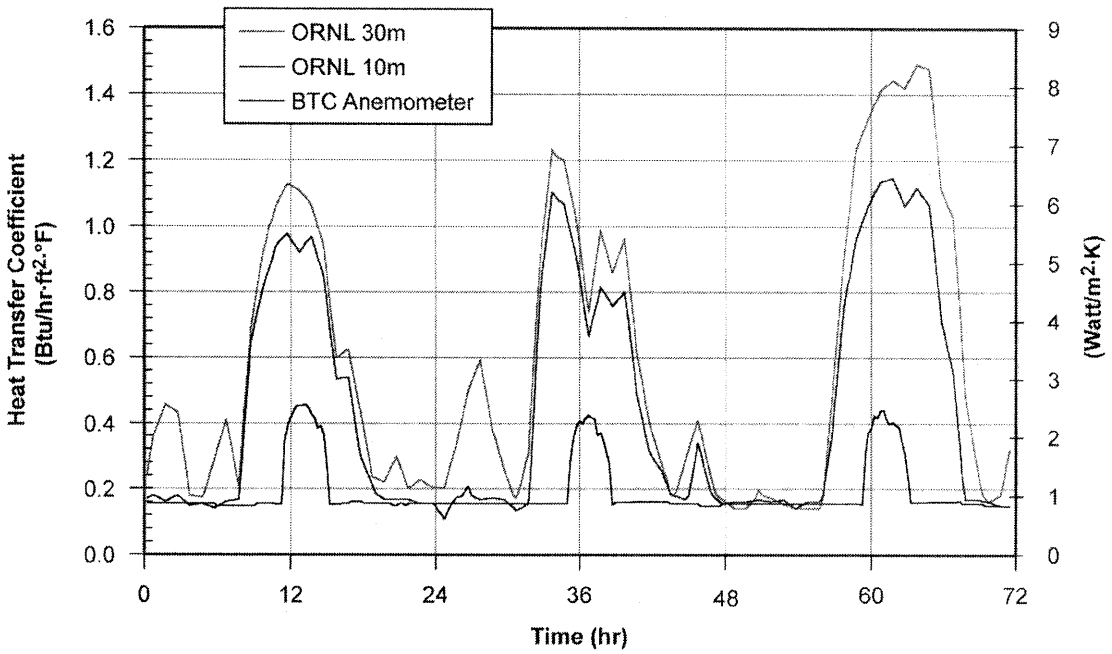

Fig. 28. The anemometer on the BTC campus was reading too low a wind speed and caused STAR to under predict convection heat transfer.

Weather conditions in east Tennessee seldom produce dry air. However, data for the week of September 3–9, 1999, had on the evening of September 8 and the morning of the 9th (hours 144 through 152 in Fig. 29), a dry roof. The membrane temperature of the test roofs exceeded the dew point temperature of the ambient air, and the roofs were dry. For these two particular periods, we observed a close match between the predicted and the measured temperature of several of the single-ply membranes over the late evening and early morning hours. On evenings when dew formed on the test roofs, the STAR code under predicted the measured membrane temperature by as much as 3F° (1.7C°) (Fig. 29).

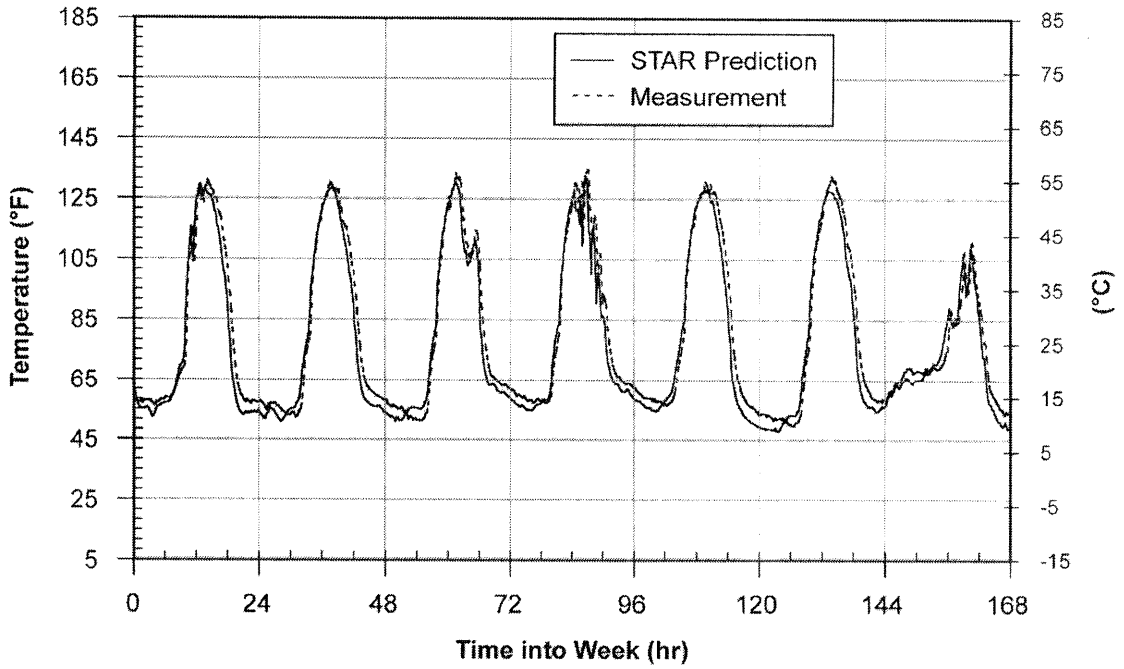

Fig. 29. Using the recalibrated anemometer helped STAR predict daylight membrane temperature within 4% of measurement.

Sensitivity to Condensation

Data for the week of September 3–9, 1999 of the air-to-membrane temperature gradient measured for the test roofs as well as the wind speed measured across the ESRA help reveal the uncertainties in accurately predicting the mass transfer (Fig. 30). From about 8 p.m. until 8 a.m. on these mild summer nights, the membrane is colder than the dew point temperature of the ambient air causing mass transfer to occur on the roof. During these evening hours, the convective-heat transfer is based almost solely on the wind flowing across the ESRA, and the mass-transfer coefficient is derived from Eq. (10) using the convective-heat-transfer correlations given in Eq. 6 and Eq. 9 dependent upon the strength of the Re number. However, the maximum temperature difference (Fig. 30) does not exceed 10F° (5.6C°), well below the limit for using the heat-and-mass-transfer analogy to reliably predict the mass transfer as recommended by Shah (1981). Further, the wind speed (Fig. 30) is less than 2 mph (0.89 m/s); therefore, the Reynolds (Re) number is less than 500,000, and the measured airflow is laminar, again below the limit stated by Shah (1981).

During the evening hours, natural convection is low because the air-to-membrane temperature gradient is less than about 10F° (5.6C°). The solid line in Fig. 31 represents forced-convection heat transfer that occurs from about 8 p.m. to 8 a.m. for the days of September 3–8, 1999; September 9 had some mild winds. The change in slope of the solid curve occurs as the heat transfer transitions from laminar to turbulent flow for Re numbers exceeding 500,000 (Fig. 31). The coefficient is largest around solar noon, when the wind speeds and buoyancy effects are largest; however, at night, as the roof cools and any ambient air turbulence settles, the coefficient decreases to its lowest value, it being only about 0.2 Btu/(h·ft^2·°F) [1.1 W/(m^2·°C)]. Solar irradiance increases as the sun reaches solar noon, and the membrane temperature exceeds the air temperature by about 40F° (22.2C°), warming the air within the boundary layer, which in turn increases the buoyancy forces atop the roof. Hence, the convection-heat transfer becomes a mix of forced- and natural-convection forces (data above forced convection curves in Fig. 31). Because of the additional component of natural convection, data for the

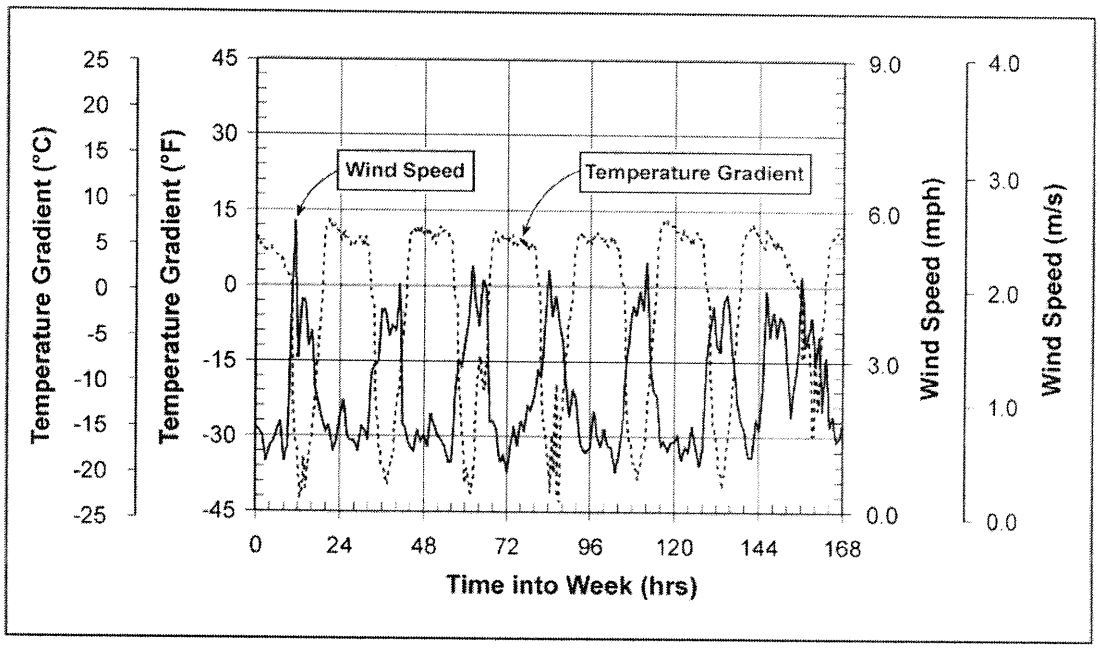

Fig. 30. The air-to-membrane temperature gradient and wind speed across the ESRA test roofs are monitored every 15 s, and 15 min averages are recorded by the data acquisition system.

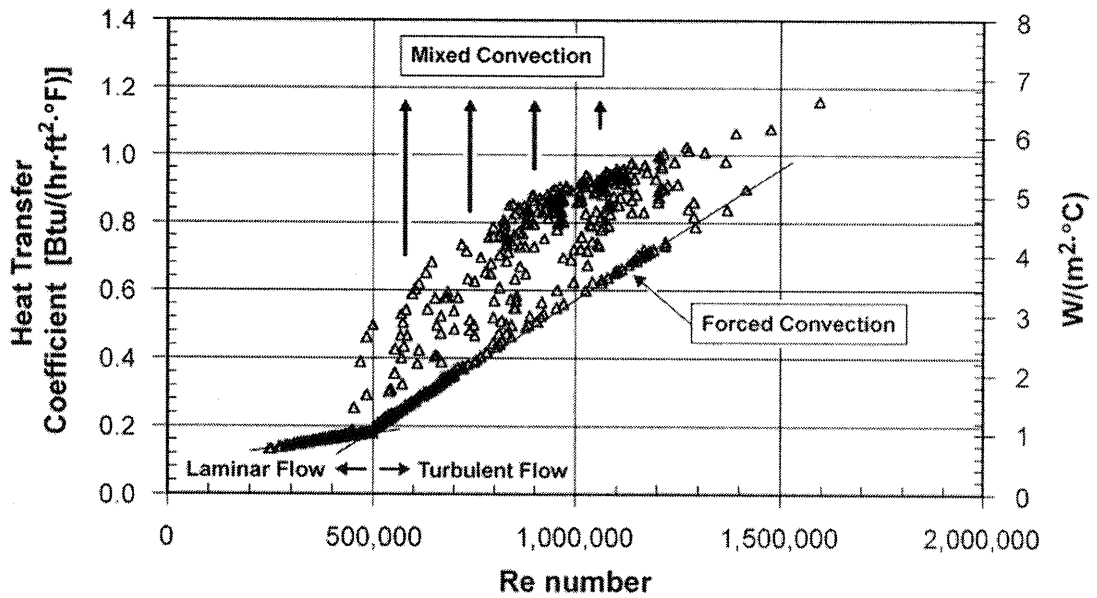

Fig. 31. The overall average convection heat transfer coefficient is calculated from the wind speed, the surface temperature and the outdoor ambient weather.

heat-transfer coefficients occurring around solar noon exceed those observed at night and are seen above the solid curves in Fig. 31 as mixed-convection heat transfer. The daylight predictions of the membrane temperature made by STAR are good, being within an average absolute error of 4% of field measurements. However, at night the prediction was accurate to only an average absolute error of 6% because of the mass transfer.

We compared the mass transfer predicted by STAR to that back-calculated from temperature measurements on the ESRA roof. The STAR code was run using the exterior membrane temperature and the deck temperature as boundary conditions to eliminate the uncertainties of weather. The code calculated the heat flux at the membrane using Fourier conduction, and the mass transfer was back calculated from this exterior flux using Eq. (2). The results showed that, as condensation begins around 8 p.m., the actual mass transfer is significantly higher than that calculated by the STAR code, which uses Eq. 10 to calculate a mass transfer coefficient ($\bar{h}_m$). Inspection of Fig. 30 shows that the largest air-to-membrane temperature gradients occur for roughly one hour past the start of condensation. Both the energy exchange from the mass transfer and the accumulation of liquid atop the roof cause the temperature gradient to drop (Fig. 30). The mass transfer therefore exponentially decays with time, and after about one to three hours from the onset of condensation it tends to follow the algorithm used by the STAR code. Overall coefficients do not account for the transients observed as humid air condenses onto the roof.

A correlation was formulated to better capture the transients at the start of condensation. A scaling of the energy equation for transient heat flow leads to a dimensionless time variable, the Fourier (Fo) number. Here we use the Fo number to compare the thermal diffusion from humid air to the length of the roof. The thermal diffusivity is based on the properties of saturated moist air evaluated at the average of the membrane and ambient air temperatures. The time in the Fo number was selected to be that time associated with the start of condensation.

Varma, Charan, and Soogappa (1978) as well as Yaghoubi, Kazeminejad, and Farshidiyanfar (1993) each formulated their correlation in terms of the Re number and moist-air gradients evaluated from the ambient air to the plate. However, regression analysis showed best fit using humid-air potentials rather than gradients. Because the potentials are a function of the ambient air and not the exterior roof temperature, the numerical procedure will also be more stable in calculating a convergent solution. The correlation fit takes the form

$$R \equiv \frac{h_{m,exp}}{h_{m,Le}} = C_1 \, Re_L^{C_2} \, Fo_L^{C_3} \left(\frac{\bar{P}_{WV}}{P_{atm}} \right)^{C_4} \qquad (11)$$

where

	C_1	C_2	C_3	C_4
for Fo ≤ 0.0009	9,529.0	-1.716	-1.250	-1.237
for Fo > 0.0009	13,568.4	-1.683	-0.189	-2.889

The multiplicative factor (R) is applied directly to Eq. (10). The correlation was programmed into the STAR code, and simulations were run for the week September 3–9, 1999. The correlation causes the simulated membrane temperature to better follow the measured data during times of condensation (Fig. 32). The day- and night-average predictive error is about 4% of the measured membrane temperature for the whole week of data (Fig. 32). As a result, the heat flux simulated by STAR does a better job in predicting the heat leakage from the roof during the evening hours. Previously, the simulation over-predicted the heat leakage because the analogy under-predicted the mass transfer. Using the correlation to support the analogy, the error in the total heat flow through the roof, integrated over the week of data for September 3–9, 1999, is about 5% of the experimental measurement as compared to 23% when using only the analogy (Fig. 32).

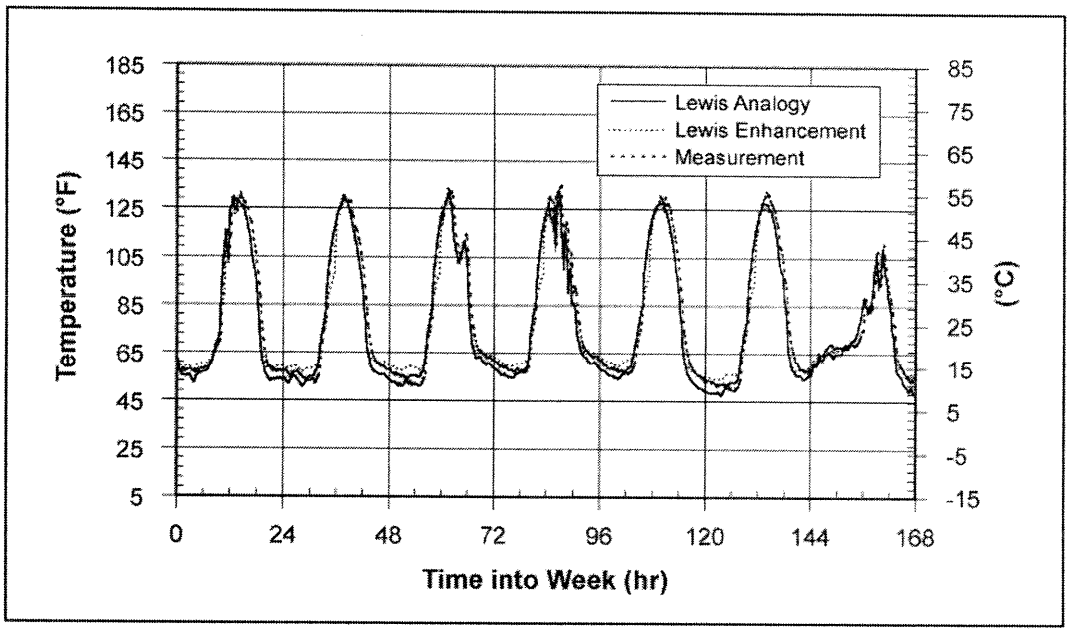

a. Comparison of the measurement and prediction for the membrane temperature.

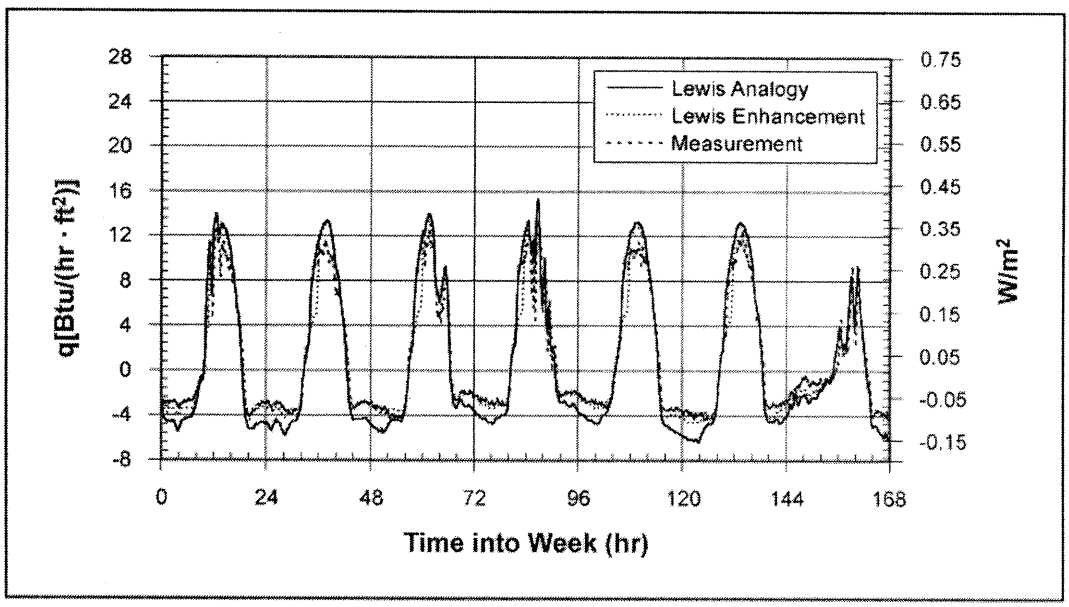

b. Comparison of the measurement and prediction for the heat flow.

Fig. 32. The correlation improves the STAR code's ability to predict the effects of mass transfer.

5.2 COUPLING TO WHOLE BUILDING CODE

DOE-2.1E is a public domain computer code that was designed by LBNL to support the thermal analysis for a multiplicity of buildings. The whole building code supports estimation of annual building heating and cooling loads and energy costs in response to weather data and the salient features of the building, the HVAC plant and utility rate structure. DOE 2.1E has a function routine feature that will read data from an external file. The function routine substitutes the value for the external roof, window or wall load that is internally calculated by DOE 2.1E, with the external load predicted by another code.

A building description was developed for a warehouse having 38,640 ft^2 of floor space. The simulated building has one story with 24-ft high walls. The walls are made of 6-in. thick concrete. A 2112 ft^2, one story office extension with 12-ft high walls is adjacent to the main warehouse area. The warehouse does not have any windows, but has nine 10-ft by 8-ft doors. The office exterior walls have a total of 282 ft^2 of glazing. The building occupancy is about 40 employees. As built, gas-fired unit heaters heat the warehouse area. During the summer, rooftop HVAC units provide comfort conditioning for the office and warehouse. Both the warehouse and the adjacent office area have low slope, insulated built-up roofs.

The building description was input into DOE 2.1E, and we substituted the external roof loadings from STAR with different reflectance single-ply membranes to put the energy savings for a better performing roof into the perspective of the whole building. The conditioned space was kept at 70°F (21°C) year round, and TMY2 typical meteorological year weather data for Oak Ridge, TN were input into DOE-2.1E for determining the whole building load. The warehouse simulations were conducted with membranes coded A, I, H, and C, Code C being the BUR. The reflectance and emittance data used for the membranes are listed in Table 6 of Sect. 4.1.

Building demographics generated by the Commercial Building Energy Consumption Survey (1995) showed that professional office buildings and warehouses are the predominant commercial building types in the United States. The largest concentration of these building types occurs in the southern states, where cooling loads are high and reflective roofs show best benefits. A warehouse building was selected for whole building simulation because the warehouse avoids the confounding variable of internal heat generation and because the energy savings are solely due to the reflective roof. Typically most warehouses have limited comfort control; all of the floor space in a warehouse is not conditioned for occupancy. The interested reader can refer to Petrie et al (2001a) who used DOE 2.1E (LBNL 1993) to compute net cooling and heating operating cost savings for a two-story, all-electric, office building with 6,000 ft^2 (560 m^2) of low-slope roof.

5.2.1 Warehouse Simulations

Simulation showed that the total heat flow through a BUR roof is about half of the total flow for the warehouse (see Fig. 33a and Fig. 33b). The roof is about 70% of the exterior surface area, and heat transmission through the roof appears to dominate the whole building heat flows. The only internal energy generation comes from occupancy and lighting. Therefore the trade-offs between heating and cooling are very similar between the roof loading and the whole building loading because the heat flows through the roof dominant the building load.

Increasing the reflectance from 0.05 for Code C to 0.865 for Code A caused the heat flux through the roof during the summer to drop from 25% to only 5% of the whole building load of 69 kBtu/(ft^2·yr). In the winter the higher reflectance penalized the building because the roof absorbed less solar irradiance as compared to the BUR (see blue bars in Fig. 33). The results reveal the trade-off between

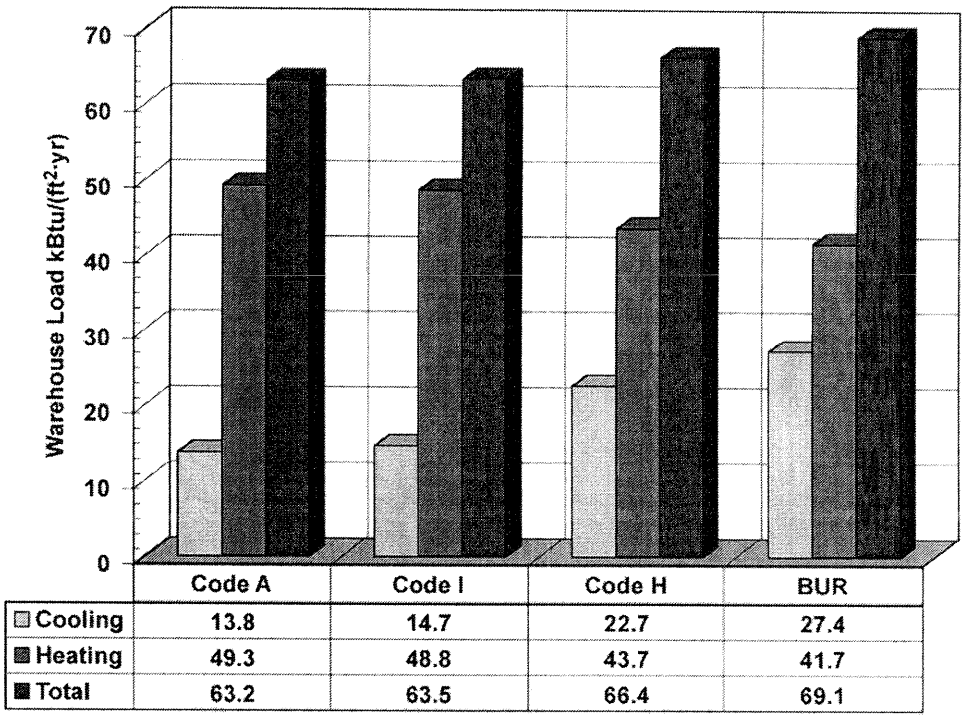

	Code A	Code I	Code H	BUR
Cooling	13.8	14.7	22.7	27.4
Heating	49.3	48.8	43.7	41.7
Total	63.2	63.5	66.4	69.1

a. Annual building loads for warehouse.

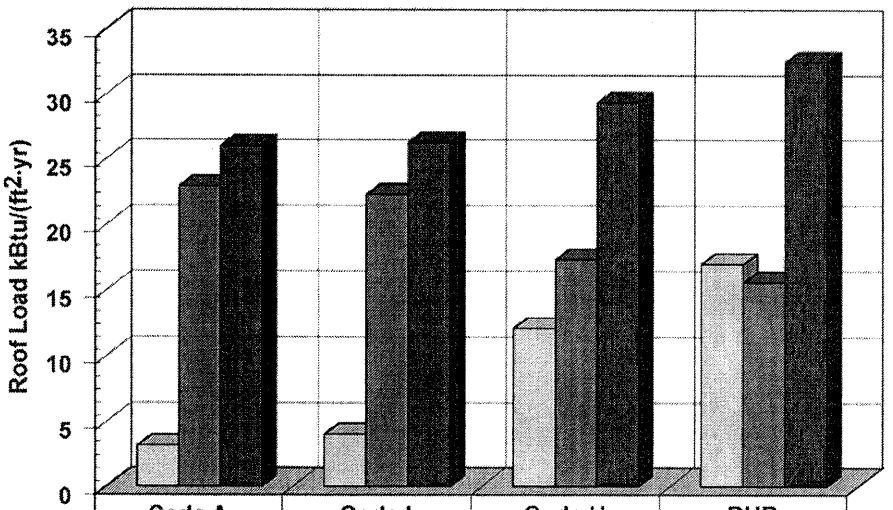

	Code A	Code I	Code H	BUR
Cooling	3.10	3.97	12.05	16.95
Heating	22.85	22.24	17.29	15.52
Total	25.9	26.2	29.3	32.5

b. Annual roof loads for warehouse with R5 insulation.

Fig. 33. The heat flux per year entering in cooling season and leaving the building in heating season.

heating and cooling seasons; however, for the moderate climate of Oak Ridge, TN., we observed the annual building load to drop 9% from the whole building annual load of 69 kBtu/(ft^2·yr). Hence, in moderate to predominantly hot climates, an exterior roof surface with a high reflectance and high infrared emittance will produce energy savings. These energy savings translate into cost savings, which are naturally dependent on the cost of energy and efficiency of its use.

Natural gas prices are roughly $5.50 per deca-therm, and electricity in the Tennessee Valley costs about $0.10 per kWh, which includes demand charges for commercial businesses. For these fuel prices, the annual energy savings are displayed in Fig. 34. The Code A membrane would produce a savings of about 12¢ per year per square foot of roof. The more moderate reflectance roof, Code H, would save about 5¢ per year per square foot of roof.

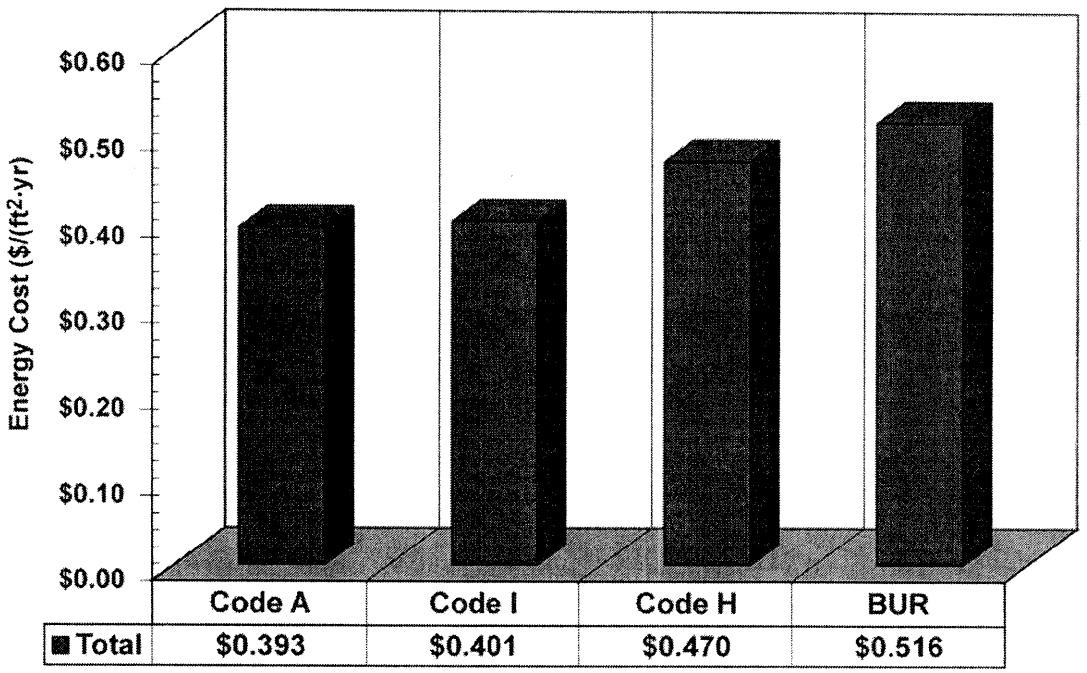

Fig. 34. Energy cost saving is based on R-5 roof insulation with HVAC rooftop air-conditioner having seasonal COP of 2.5.

An implicit assumption used to calculate these savings is the performance of the rooftop HVAC unit and the heating efficiency of the gas furnace. The coefficient of performance (COP) describes the performance of a rooftop HVAC system, which is the ratio of the machine's cooling capacity to the power needed to produce the cooling effect. The COP is mathematically described by:

$$COP_{HVAC} = \frac{\text{Cooling Capacity}}{\text{Power}_{HVAC}} \tag{12}$$

Because the HVAC unit is designed to meet the building load, the roof load (E_{cool} calculated by STAR) can be input into the "Cooling Capacity" term of Eq. 12. Given the COP of the rooftop HVAC unit, the power needed by the unit to match building load is calculated from Eq. 12. The COP can also be used to determine the annual cooling energy cost savings ($cool) by the formula:

$$\$cool = \frac{E_{cool} \cdot \$elec}{COP_{HVAC}} \tag{13}$$

The annual heating energy cost savings ($heat) require the efficiency of the furnace and are calculated by the formula:

$$\$heat = \frac{E_{heat} \cdot \$fuel}{\eta_{heat}} \tag{14}$$

5.2.2 Effect of Rooftop HVAC

The efficiency of a furnace is relatively constant; however, the cooling COP of HVAC equipment typically drops as the outdoor air temperature increases, as the heat exchangers foul, as mechanical wear occurs on the compressor valves and especially as the unit leaks refrigerant charge. Simulations were therefore conducted to show the effect of COP on cost savings for reflective roofing (Fig. 35). Roof insulation was set at R-5. The results show that increasing the COP of the rooftop HVAC unit diminishes the cost savings for a reflective roof. Savings vary from as high as 25¢ per square foot per year for a poorly performing HVAC unit with COP of 1.25 to a low of 10¢ per ft^2 per year for a high efficiency optimally performing HVAC unit. The results lead to the question, "What COP should one use to fairly access cost savings?"

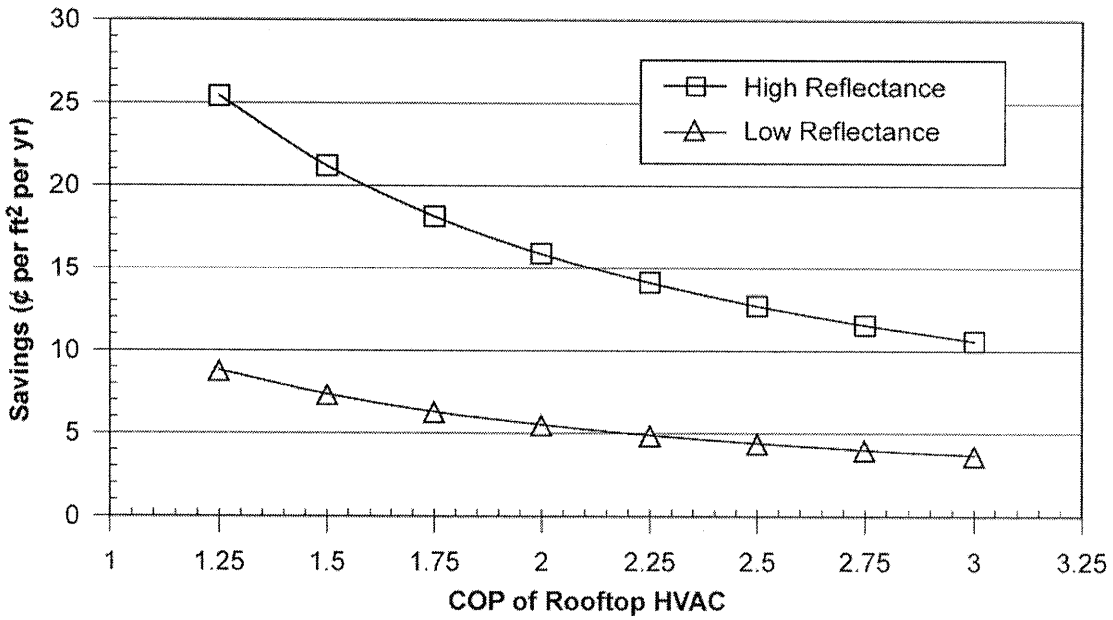

Fig. 35. COP of rooftop HVAV affects savings for reflective roofing.

Kelso and Kinzey (2000) state that the average performance of new rooftop HVAC equipment has a COP of about 2.5. Their statement is very broad, and does not account for differences in equipment nor for equipment faults. Breuker, Rossi and Braun (1998) identified electrical, mechanical and refrigeration faults from an insurance database for eight years of claims against HVAC equipment. Most failures were due to electrical components and mechanical components. Of the electrical failures, roughly 87% were caused by failures in the motor windings due to short cycling, refrigerant contamination or the loss of refrigerant. Breuker, Rossi and Braun (1998) experimentally showed that refrigerant leakage, compressor valve leakage, and condenser and evaporator fouling each could

degrade the COP roughly 5 to 20% of the COP for new equipment. A compounding of faults would lead to worse performance.

The author used the conservative approach in the simulations by assuming the COP of 2.5 for new equipment. However, a seasonal COP of 1.75 to 2.0 is more realistic because maintenance of most rooftop air-conditioners is typically ignored until the unit fails to provide cooling. This would increase the potential savings shown in Fig. 34 from \$0.13 to about \$0.18 per ft^2 per year for a high reflectance thermoplastic membrane.

6. BTC COOL ROOF CALCULATOR

The building's comfort cooling and heating energy, termed space conditioning, is directly related to solar insolation incident on a building; to the exterior temperature; to the level of roof, wall and foundation insulation; to the amount of fenestration; to the building's internal loads; and to the characteristics of the building's system and plant. Defining the component seasonal loads for a building through the roof, walls, windows, etc., is difficult because of the effect of the internal loads on the space conditioning requirements. Furthermore, averaging the component loads across all building types cannot be accurate because of the broad range of exterior surface area-to-building volume observed from one building to another and because of the diversity in building occupancy habits. Therefore a roof calculator was developed from the data for predicting the heat flow solely through the roof. The calculator has no interactions with the characteristics of the building and therefore eliminates confounding variables that can confuse the design of a roof.

Petrie et al. (2001a) formulated algorithms and implemented a cool roof calculator at the Internet location http://www.ornl.gov/roofs+walls/facts/RadiationControl.htm. The calculator is a useful tool for assisting building practitioners with the selection of a cost-effective, low-slope roofing system. Details of the formulation and validation of the algorithms used in the calculator are described in Petrie et al. (2001a). Accuracy of the calculator as compared to STAR is presented in Sect. 7.1 of this report. Here a step-by-step brief descriptive is given for each input and output of the calculator to assist users with proper use and interpretation of results.

6.1 COOLING AND HEATING LOADS

There are 235 different locations built into the pull-down list for the state and the city. If the exact location is not listed, use one with weather similar to the desired location.

State **Box 1.**

City **Box 2.**

6.2 PROPOSED ROOF DESIGN

The user inputs design details for the proposed low-slope roof, which is made of a metal deck, insulation laid atop the deck, and a fully adhered single-ply membrane. The user must specify the steady-state thermal resistance (R-value) of the roof, the solar reflectance, and the infrared emittance of the single-ply membrane. Further descriptive for these inputs follow:

R-Value [h·ft²·°F/Btu] **Box 3.**

Input the steady-state thermal resistance (R-value) of the roof, which is calculated from the thermal properties of the materials used in the roof. The metal deck and the single-ply membrane are very thin and do not significantly affect the R-value. The type and thickness of insulation is the primary contributor to the R-value. Many low-slope roofs have a plenum space, which will add thermal resistance to the roof. If a plenum space and dropped ceiling are present, one should increase the roof R-value by about 3 to represent this thermal resistance in the model.

ASHRAE (2001) lists the aged thermal properties of common insulating materials. For a roof made of composite layers of roof insulation, the R-value is calculated using the formula:

$$R_{total} = \sum_{i=1}^{n} \frac{t_i/12}{k_i} \equiv \frac{h \cdot ft^2 \cdot {}^{o}F}{Btu} \quad (15)$$

t_i (in) = the thickness of the i^{th} layer of insulation, and
k_i (Btu/(h·ft·°F) = the thermal conductivity of the i^{th} layer of insulation

Therefore a composite roof made with two layers of insulation, one layer being wood fiberboard[4] with a thickness of 1.5 in. (0.038 m) and the other layer having 2 in. (0.0508 m) of polyisocyanurate[5] foam insulation, and no other insulation, would have an R-value of about 17 h·ft²·°F/Btu [3 m²·K/W]. The example is not typical of roof construction, but is given to explain the use of Eq. 15. Representative R-values to help gage your input for typical insulations are high = 20; average = 10; low = 5 [h·ft²·°F/Btu].

Solar Reflectance [%] **Box 4.**

Table 12 provides the decimal equivalent of the solar reflectance of membranes fresh-from-the-factory and exposed to 3 full years of weathering on the ESRA located on the BTC campus in Oak Ridge, TN. Reflectance data for membranes exposed on the ESRA showed greater degradation than did samples exposed at the field sites (see Sect. 4.2). However, results also showed that the effect of weathering was similar across the country. Representative solar reflectance values that can help check your input are high = 85.0; average = 50.0; low = 5.0 %.

Infrared Emittance [%] **Box 5.**

The decimal equivalent of the infrared emittance is included in Table 12; however, weathering did not affect the emittance. Representative infrared emittance values that can help check your input are high = 90.0; average = 60.0; low = 10.0 %.

6.3 ENERGY COSTS AND HVAC EQUIPMENT EFFICIENCIES

The price of fuel, whether electric or gas, and the efficiency of the HVAC system are required to calculate affordable cost premiums for reflective roofing. The proposed roof design with the insulation R-value specified in box 3, the solar reflectance specified in box 4, and the infrared emittance specified in box 5 are used to calculate the cooling and heating energy. The energy costs and the potential savings are then calculated relative to a BUR having the same R-value as specified in box 3; however, the BUR has a fixed solar reflectance of 5.0%, and a fixed infrared emittance of 90.0%. The annual cooling and heating energy cost savings are calculated by the formulas:

$$\$cool = \frac{E_{COOL} \cdot \$elec}{COP_{HVAC}} \quad (16)$$

$$\$heat = \frac{E_{hest} \cdot \$fuel}{\eta_{heat}} \quad (17)$$

[4] Thermal conductivity of wood fiberboard is 0.0283 Btu/(h·ft·°F) or 0.049 W/(m·K).
[5] Polyisocyanurate insulation has a thermal conductivity of 0.01329 Btu/(h·ft·°F) or 0.023 W/(m·K).

Table 12. Solar reflectance and infrared emittance for the single-ply membranes

Code	Reflectance (ρ) of the thermoplastic and thermo-set membranes tested on the envelope systems research apparatus				Emittance (ε)
	New material	One-year exposure	Two-years exposure	Three-years exposure	
A	0.865	0.624	0.499	0.466	0.879
J	0.859	0.681	0.631	0.636	0.919
K	0.856	0.676	0.576	0.526	0.920
G	0.854	0.673	0.540	0.458	0.904
M	0.844	0.705	0.612	0.583	0.920
I	0.813	0.640	0.577	0.584	0.918
R	0.590	0.481	0.389	0.393	0.855
F	0.772	0.590	0.520	0.538	0.906
P	0.664	0.552	0.492	0.475	0.892
B	0.655	0.385	0.273	0.294	0.901
N	0.496	0.371	0.304	0.292	0.830
Q	0.368	0.272	0.233	0.232	0.904
E	0.140	0.150	0.146	0.153	0.900
S	0.210	0.219	0.220	0.221	0.900
H	0.282	0.282	0.263	0.251	0.805
O	0.179	0.181	0.179	0.170	0.860
L	0.075	0.069	0.070	0.061	0.867
C	0.049	0.037	0.037	0.033	0.900

Cooling season cost of electricity [$/kWh] **Box 6.**

The price of electricity for cooling ($elec) must be input to the calculator in the United States dollars (U.S.$) per kilowatt-hour. Local electricity pricing may vary significantly from statewide averages so the best source of information is local rates. If necessary, please consult the Energy Information Administration (EIA 2001) website http://www.eia.doe.gov/cneaf/electricity/epm/epmt53.txt before using the calculator to make a decision about an appropriate energy price for the location specified in box 1. Representative electricity costs that can help check your input are high = 0.20; average = 0.10; low = 0.05 [$/kWh].

Air conditioner efficiency [COP_{HVAC}] **Box 7.**

The coefficient of performance (COP) describes the performance of a rooftop HVAC unit. COP is the ratio of the machine's cooling capacity to the power needed to produce the cooling effect (see Sect. 5.2.1). The COP is used to determine the power consumption needed to meet the heat load penetrating through the roof in the summer (see Eq. 12). The effect of COP on the energy cost savings is very significant. Cost savings for a reflective roof drop as the COP of the rooftop HVAC unit increases (see Sect. 5.2.2). Kelso and Kinzey (2000) state that the average COP of new rooftop HVAC equipment is about 2.5. The authors believe this is too high and list the following as being more representative of annual seasonal COP: high = 2.0; average = 1.75; low = 1.5.

Energy source for heating [electricity or fuel] **Box 8.** ○ Electricity ○ Fuel

The calculator requires information on the fuel used for heating whether by electricity or by burning a fuel such as natural gas or fuel oil (choose one or the other).

Heating season cost of electricity [$/kWh] **Box 9.**

A heat pump or electrical resistance furnace uses electricity for heating. Input the price of electricity for heating in U.S.$ per kilowatt-hour. Local electricity pricing may vary significantly from statewide averages so the best source of information is local rates. Please consult the EIA (2001). Representative cost of electricity is high = 0.20; average = 0.10; low = 0.05 [$/kWh].

For electricity use: http://www.eia.doe.gov/cneaf/electricity/epm/epmt53.txt.

Heating Fuel Costs [$/kWh] **Box 10.**

A gas furnace commonly uses natural gas as fuel; input the price of natural gas in U.S.$ per Therm. A Therm is equivalent to 100,000 BTUs of heat. Natural gas prices are typically given in $/Therm or in $/MCF. If you have prices in $/MCF, divide by 10 to get the $/Therm. For example, natural gas with a price of $6.50 per MCF costs $0.65 per Therm. Furnaces in the northern United States use number two heating oil, and prices are usually given in $/gal. Multiply this number by 0.71 to get $/Therm. For example, heating oil at $1.20/gal would be $0.85/Therm. The EIA (2001) gives detailed information on state-by-state costs of heating fuels. Consult the EIA websites before using the calculator to make a decision about appropriate energy prices ($fuel) for your location.

For number 2 fuel oil use:
http://www.eia.doe.gov/pub/oil_gas/petroleum/data_publications/winter_fuels_report/current/pdf/table c3.pdf. Representative 2002 cost of fuel oil: East coast = 0.85; Midwest = 0.70 [$/Therm]

For natural gas use:
http://www.eia.doe.gov/pub/oil_gas/natural_gas/data_publications/natural_gas_annual/current/pdf/table_023.pdf. Representative cost of natural gas: high = 1.00; average = 0.70; low = 0.50 [$/Therm]

Heating system efficiency [COP or η_{heat}] **Box 11.**

The average seasonal heating efficiency depends upon the type of HVAC equipment and its operating condition. An electric heat pump uses electricity for both cooling and heating modes. Often the heating performance is characterized by the seasonal heating performance factor (SHPF). COP is used in the calculator and is related to the SHPF by COP = SHPF/3.413. Representative heating mode heat pump COP's are high = 2.0 for moderate climates; low = 1.5 for more severe heating climates.

An electrical resistance furnace converts electricity directly into heat with an efficiency of 1.0. Therefore input a heating COP of 1.0 if simulating comfort heating with an electric resistance furnace.

A fuel-burning furnace has a fractional efficiency (η_{heat}), ranging from 0.5 to 0.6 for old, inefficient equipment to 0.8 to 0.9 for new equipment. Condensing, natural gas furnaces may have seasonal heating efficiencies as high as 0.95. Enter the fractional seasonal efficiency for fuel-burning HVAC equipment. Representative heating η_{heat} is high = 0.9; average = 0.7; low = 0.5.

The calculator does not need the building's indoor temperature. It was validated for building temperatures of 67 and 78°F (19 and 26°C). Different set points in the summer and winter can be handled if the thermostat settings are the same with and without solar radiation control.

6.4 SAVINGS OUTPUT FROM CALCULATOR

The calculator shows two approaches for improving the roof to save the same amount of energy. The first approach is to install solar radiation control and that answer is shown in red in box 12 of the

calculator. The second approach is to add more insulation to your roof to show how much insulation is needed to save the same amount of energy as saved if you installed the solar radiation control.

Net Savings [$/ft² per year] **Box 12.** ⌜ ⌝

Net savings is the monetary sum of the annual cooling and heating energy cost savings as compared to the performance of a BUR having the same R-value, but with a reflectance of 5.0% and an emittance of 90.0%. If the user prefers to compare savings to a radiation control base other than the BUR, simply run the calculator twice, print or write down the results in boxes 12 through 14 and manually compute the difference for the two non-black roofs. The net savings is given in $ per ft^2 of roof area per year. If you want $ per 100 ft^2, multiply the $/$ft^2$ answer by 100. If you want $ per m^2, multiply it by 10.76.

Cooling savings [$/ft² per year] **Box 13.** ⌜ ⌝

The cooling savings is the annual cooling cost savings per unit area of roof as compared to a BUR. The calculator uses Eq. 16 in an algorithm to compute the savings.

Heating savings (penalty if negative) [$/ft² per year] **Box 14.** ⌜ ⌝

The heating savings is the annual heating cost savings per unit area of roof as compared to a BUR. The calculator uses Eq. 17 in an algorithm to compute the savings, $heat. A negative $heat implies a penalty because a dark absorptive roof loses less heat than does the more reflective roof. A negative $heat offsets somewhat the cooling savings as seen in the net savings (box 12). However, the results in boxes 12 through 14 show the trade-offs between summer and winter for reflective roofing.

Insulation in Black Roof to Yield Same Annual Savings

The second approach used by the calculator shows the amount of insulation that would be needed to save the same amount of energy as conserved by using the user input radiation control strategy. See the box 15 of the calculator for results.

Box 15. Upgrade from R- ⌜ ⌝ to R- ⌜ ⌝ [h ft^2 °F/Btu]

6.5 DETAILS OF COMPARISON

The heating degree-days and cooling degree-days and the average solar irradiance are written for the location selected in boxes 1 and 2. A degree-day is defined as the difference between the average temperature for the day and a base temperature of 65°F (18.3°C). The base temperature of 65°F (18.3°C) is the balance point temperature for a building, and has been documented as the average condition below which a building requires heat and above which a building requires cooling (ASHRAE 2000). The calculator uses 60°F (16°C) as the heating balance point and 75°F (24°C) for the cooling balance point.

The calculator was developed from hour-by-hour annual TMY2 weather data for each location and from the output of STAR for the annual roof heating and cooling loads. The heating and cooling loads computed by the calculator are then listed for a black roof and the proposed roof. These loads are annual sums of the heat flow per square foot through the deck of the roofs under simple heating and cooling conditions. They are only for the roofs. Depending upon how the building is operated, how its walls and windows are configured, and how much internal load it has due to equipment and occupants, the actual heating and cooling loads will be very different from the roof loads.

Heating degree-days [Annual °F-day] **Box 16.**

If the average for a time bin (calculated by averaging the maximum and minimum temperature within the bin) is less than the base value of 65°F (18.3°C), then the magnitude of the difference is designated as a heating degree-day. The summation of these days over the year is therefore the annual heating degree-days.

Cooling degree-days [Annual °F-day] **Box 17.**

If the average for the day is greater than the base value of 65°F (18.3°C), the difference is designated as a cooling degree-day. The summation of these days over the year is the annual cooling degree-days. The data were obtained from TMY2 data sets.

Solar load [Annual Average Btu/ft² per day] **Box 18.**

Solar load is the total solar irradiance that is incident on a horizontal surface. The data were obtained from TMY2 data sets.

Cooling load for black roof [Btu/ft² per year] **Box 19.**

The calculator predicts the annual cooling energy that will penetrate a BUR. The BUR has the same R-value as the proposed roof. Its solar reflectance is 5.0% and its infrared emittance is 90.0%.

Heating load for black roof [Btu/ft² per year] **Box 20.**

The calculator predicts the annual heating energy that leaves a BUR. The BUR has the same R-value as the proposed roof. Its solar reflectance is 5.0% and its infrared emittance is 90.0%.

Cooling load for proposed roof [Btu/ft² per year] **Box 21.**

The annual cooling energy is predicted by the calculator to penetrate the proposed roof.

Heating load for proposed roof [Btu/ft² per year] **Box 22.**

The annual heating energy is predicted by the calculator that leaves the proposed roof.

Suppose the practitioner wants to know the sole impact of increasing insulation for a highly reflective roof system (i.e., comparison is made to the highly reflective roof with R-5 insulation rather than the BUR with R-5). Here the individual runs the calculator first with R-5, and manually logs the cooling and heating loads and costs for the proposed roof (i.e., see box 21 and box 22). Then increase the R-value to R-10 and manually log the cooling and heating loads and the costs for this scenario. Subtract the cooling and heating loads of the proposed R-10 roof from the proposed R-5 roof to derive the terms Ecool and Eheat used in Eqs. 16 and 17. Now use these manually computed differences in Eqs. 16 and 17 to calculate the annual energy savings obtained by increasing the insulation for a set reflectance and emittance.

7. SEASONAL PERFORMANCE RESULTS

Marketing claims and testing done under widely varying conditions have confused consumers, who do not know how the claims apply to the roof design of their building. The cool roof calculator provides building owners, roofing contractors, architects, and engineers with an accurate estimate of the relative annual energy use of cool low-slope roofing membranes. The practitioner can use the calculator to weigh the trade-off between energy savings and first cost. Comparisons of increased reflectance and/or increases in roof insulation are easily made with the calculator to help evaluate economic and efficient roof design for various climates throughout the United States.

7.1 ANNUAL ROOF LOADS

Validations of STAR demonstrated the code's ability to predict the temperature and heat flow through the candidate low-slope roof membranes (see Sect. 4.1.2). Wilkes et al. (2000) input typical meteorological year (TMY2) data (NREL 1995) into STAR and showed excellent agreement between prediction and annual heat flow through a low-slope roof. Petrie et al. (2001a) therefore used STAR to generate the heat flux entering or leaving the conditioned space for a range of roof radiation properties, roof insulation levels, and deck constructions using the TMY2 database (NREL 1995). Petrie defined an annual cooling load (CL) as the heat flux entering the conditioned space through the low-slope roof when the outdoor air temperature exceeded 75°F (24°C). Similarly, the heating load (HL) was defined as the heat flux leaving the roof if the outdoor air temperature dropped below 60°F (16°C). Indoor air temperature was fixed at 72.5°F (22.5°C). Petrie proceeded to generate CLs and HLs for cooling-dominated and heating-dominated climates within the United States. Polynomials were selected to represent the results in order to produce a robust, interactive tool that would respond quickly to changes in input parameters.

Results from the STAR code and the cool roof calculator are presented to show the accuracy of results generated by the calculator. Simulations were run for test membranes coded A, I, and H, and the reflectance of new materials was input for the simulations. Insulation R-value was varied from R-5 through R-30.

The relative effects of different surfaces and different amounts of thermal insulation are generally the same using the calculator and the STAR code. The average error in heating load is of the order of 15% for the membranes Code A, I, and H simulated for insulation levels ranging from R-5 through R-20 (Fig. 36). For Minneapolis, MN, the heating loads are within 10% for an R-20 roof system using the Code A membrane. Using the Code H membrane, which has a more moderate reflectance, the discrepancy is only 2% of the load calculated by STAR.

In Phoenix, AZ, a warehouse typically has a roof R-value of about 5 or less. Here the error is only 2% for simulations conducted with the Code A membrane (Fig. 37). Increasing the amount of insulation causes the discrepancy between the calculator and STAR to increase. With R-5 insulation the calculator prediction is slightly less that that made by STAR. However, as the R-value is increased, the calculator predicts a value that exceeds STAR's prediction. Petrie et al. (2001a) used thermal property data for polyisocyanurate insulation in STAR in his development of the loads data for the roof calculator. The simulations conducted for the SPRI study used wood fiberboard, which is an order of magnitude denser than polyisocyanurate insulation. We believe thermal mass effects are causing the slight inconsistency.

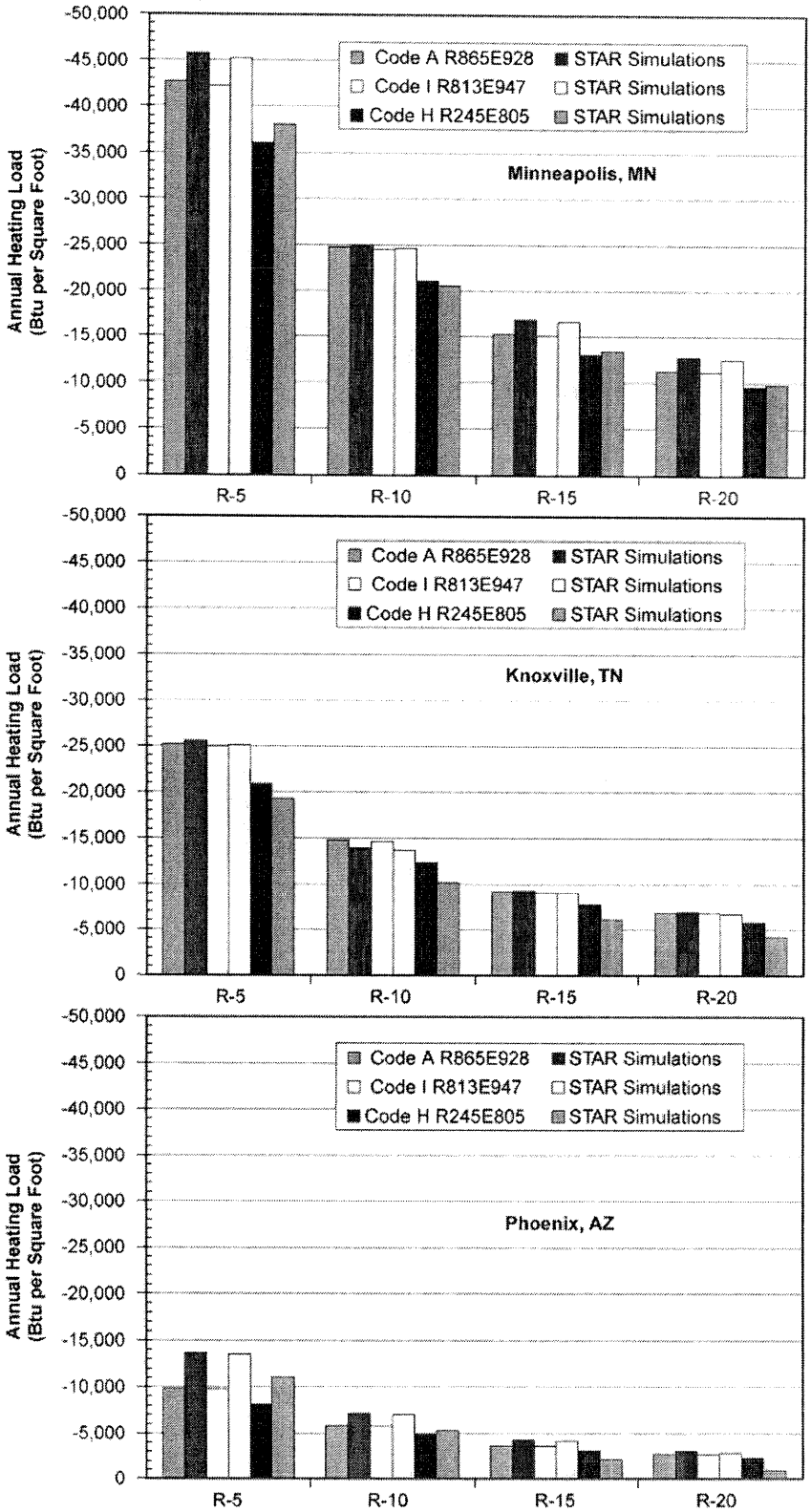

Fig. 36. Annual heating loads for reflective roofing.

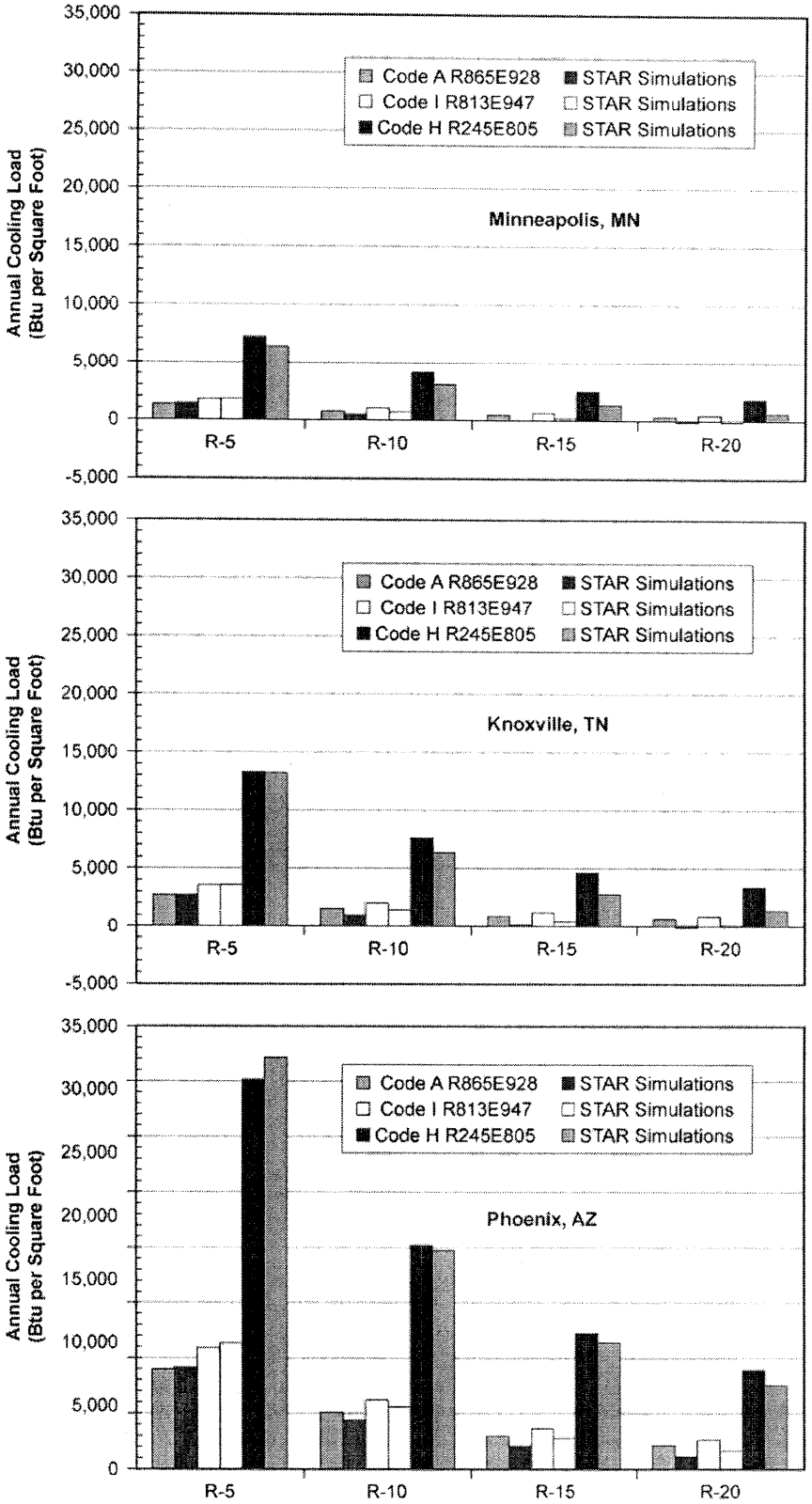

Fig. 37. Annual cooling loads for reflective roofing.

Yet, the results show that the calculator does an adequate job (±10%) of predicting the cooling and heating loads of roofs exposed to predominantly cooling and also predominantly heating climates. The calculator is also accurate for insulation levels ranging from about R-5 through R-32, Petrie et al. (2001a).

7.2 AFFORDABLE PREMIUMS

The monetary value of energy savings for a low-slope roof covered with membranes coded A, I, and H were calculated relative to a dark BUR. Simulations did not include the effect of the membranes being soiled. Only fresh-from-the-factory reflectance measures were used for the simulations shown in Table 13 and Fig. 38. Using Eq. 16, we multiplied the energy savings by the appropriate average price for electricity and divided by the average COP for a rooftop HVAC unit. Similarly, the penalty for heating energy losses was calculated using Eq. 17 for the proposed reflective roofs. A highly reflective roof will incur a heating energy penalty because the reflective roof does not absorb solar irradiance, as does a BUR during the winter months. We multiplied the heating energy penalty by an appropriate average price for heating energy and divided by the average efficiency for the heating furnace. The sum of the cost for cooling energy savings and for the heating energy penalty is the net annual operating cost savings. For the purpose of this example, the average of 2000 national prices for electricity and natural gas were used (see Sect. 6.3). The seasonal COP for the HVAC unit was assumed to be 1.75 and the heating equipment efficiency was 85%.

For the cooling-dominated climate of Phoenix, AZ, and the mixed climate of Knoxville, TN, the highly reflective membrane Code A yielded the maximum energy savings (Fig. 38). With a roof insulation level of R-5, energy savings are about $\$0.37/ft^2$ per year and $\$0.13/ft^2$ per year for Phoenix AZ, and Knoxville, TN, respectively. When the R-value level is increased to R-15, energy savings are reduced to $\$0.13/ft^2$ per year and $\$0.05/ft^2$ per year. Increasing the insulation level reduces the effectiveness of the reflective roof, Table 13. None of the reflective membranes offer an energy cost savings $\geq \$0.05/ft^2$ per year for the heating-dominated climate of Minneapolis, MN (Table 13). The results help demonstrate the regions where reflective roofing is profitable and can make significant market penetration.

A practitioner or building owner might choose a dark absorptive roof and would like to know how much insulation is needed in the roof for the same savings as a cool roof offers. The cool roof calculator is designed to support this need, and Table 13 shows the level of insulation needed by the dark roof to have the same annual operating cost as a high-reflectance roof. In Phoenix, a dark absorptive BUR would need an R-Value of 15.6 as compared to an R-5 roof covered with the reflective membrane Code A. In the more moderate climate of Knoxville, the BUR would need R-10 as compared to the R-5 covered with Code A. From Table 13 one sees that ignoring radiation control causes the amount of insulation to almost double for the cooling-dominated climate of Phoenix and the mixed climate of Knoxville. Hence the manufacturer's representative can use the calculator as a sales tool to demonstrate the trade-off in the material costs for reflective roofing as opposed to the material cost of additional insulation needed to offset the increase in annual roof energy if the roof cover is a dark absorptive BUR.

A SPRI affiliate supplied wholesale costs for polyisocyanurate insulation sold in Phoenix, AZ, Knoxville, TN, and Minneapolis, MN (Table 14), to help demonstrate this feature of the roof calculator. These cost data were used along with the equivalent R-value data from Table 13 to compare material costs for two roof systems—one, having a cool roof membrane with polyisocyanurate insulation and the other having a dark, absorptive BUR with the equivalent R-value of polyisocyanurate insulation that would force both roofs to have the same annual operating cost for roof energy. As example, a BUR cover needs an R-34.7 to have the same annual operating cost as a

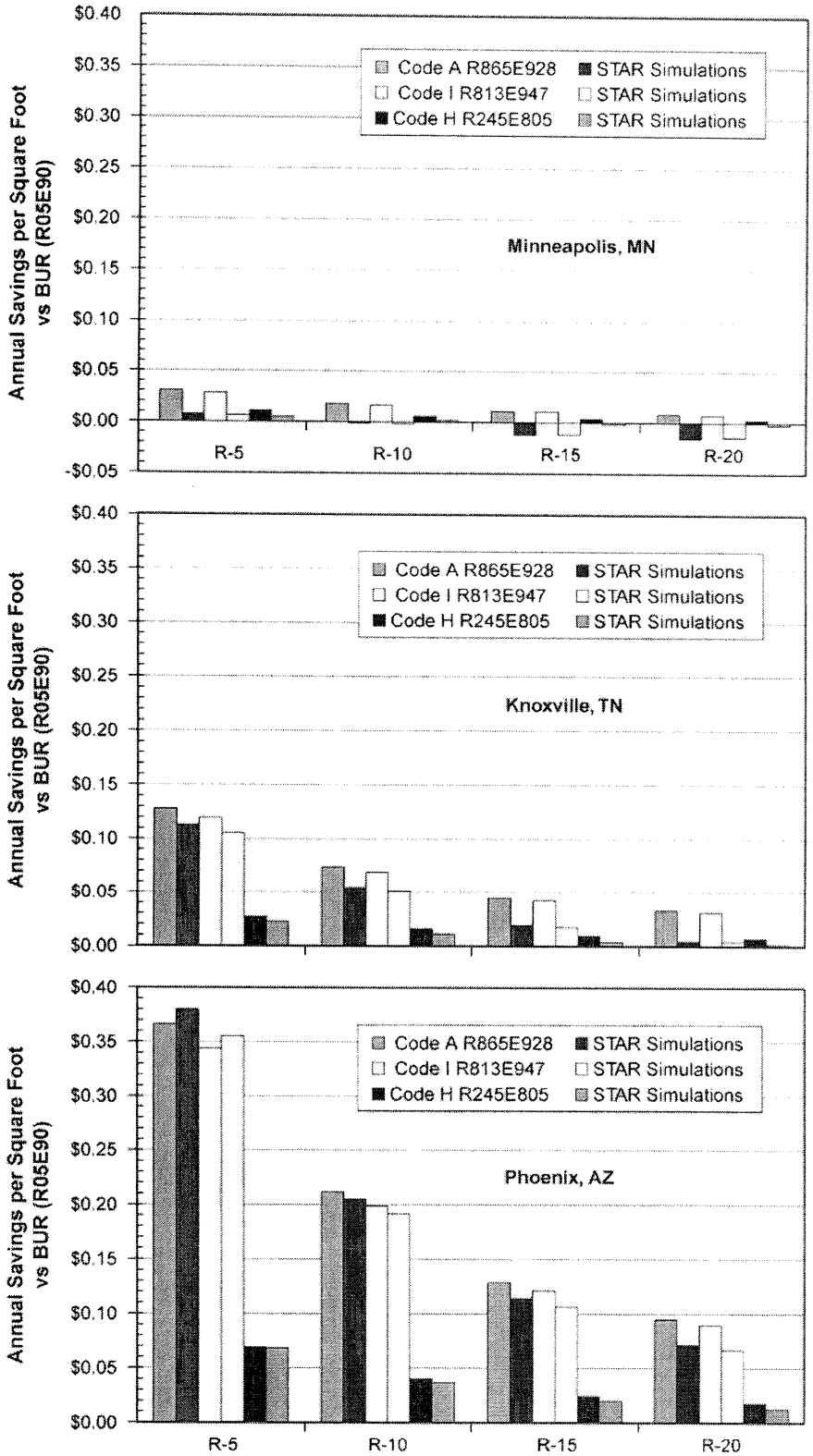

Fig. 38. Annual energy savings for reflective roofs as compared to a BUR.

Code A membrane with R-15 insulation (Table 13). The difference in R-value (R-34.7 minus R-15) is translated into the cost of additional insulation using the cost data of Table 14 and is then plotted in Fig. 39 against a cool membrane with different R-values of polyisocyanurate insulation. The curves for Phoenix, Knoxville and Minneapolis

therefore represent the affordable cost premium for cool membranes as compared to the material cost for the additional insulation. This affordable cost premium reaches a maximum as R-value increases but then diminishes with further increase in R-value (Fig. 39). There is a synergy between R-value and reflective roofing as R-value increases from R-5 up to about R-20; however, continuing to increase R-value beyond R-20 causes the effect of insulation to mask the effect of a reflective roof. Also, the peak in cost premium shifts to higher R-values as the climate changes from a hot to a cold climate (i.e., the cooling climate of Phoenix versus the heating climate of Minneapolis). Note that we did not constrain the annual operating cost of energy transferred across the roof; it drops as R-value increases and is at its lowest value at R-30 (Fig. 39).

For Phoenix and Knoxville, the maximum affordable cost premium of \$0.90 per ft^2 occurs at about R-15 and R-18 respectively (Fig. 39 a and b). By ASHRAE Standard 90.1 (1999), the minimum level of insulation for nonresidential, low-slope roofing is R-15. Also single-ply membranes of about 40-mil thickness cost about \$0.40 per ft^2; a thicker 80-mil membrane costs about \$0.75 per ft^2. Therefore based solely on material costs, a consumer could easily afford in Phoenix and Knoxville a cool membrane (Code A or Code I) with R-15 level of polyisocyanurate insulation. However, in Minneapolis, the membrane with R-20 insulation would have to cost less than about \$0.20 per ft^2 to have the same material cost as a BUR with about R-23. The state energy code in Minneapolis requires R-30 for low-slope commercial roofs, which makes the cost effectiveness of cool roofing even more prohibitive in Minnesota. The Code H membrane has a low reflectance, and

Table 13. Annual energy savings and the R-value of BUR with equivalent energy costs of reflective roofs*

	Net annual savings (\$ per ft^2) vs R05E90 (BUR)			BUR equivalent R-value for net savings = 0		
	Code A R865E928	Code I R813E947	Code H R245E805	Code A R865E928	Code I R813E947	Code H R245E805
Phoenix, AZ						
R-5 (h·ft²·°F)/Btu	\$0.366	\$0.344	\$0.069	R-15.6	R-14.3	R-6.2
R-10 (h·ft²·°F)/Btu	\$0.211	\$0.199	\$0.040	R-30.7	R-28.0	R-11.2
R-15 (h·ft²·°F)/Btu	\$0.129	\$0.121	\$0.024	R-34.7	R-34.1	R-16.7
R-20 (h·ft²·°F)/Btu	\$0.095	\$0.089	\$0.018	R-35.7	R-35.4	R-26.1
R-30 (h·ft²·°F)/Btu	\$0.075	\$0.070	\$0.014	R-36.3	R-36.1	R-32.0
Knoxville, TN						
R -5 (h·ft²·°F)/Btu	\$0.128	\$0.119	\$0.027	R-10.3	R- 9.8	R-5.9
R-10 (h·ft²·°F)/Btu	\$0.073	\$0.069	\$0.015	R-16.0	R-15.3	R-10.9
R-15 (h·ft²·°F)/Btu	\$0.045	\$0.042	\$0.009	R-30.3	R-29.2	R-16.2
R-20 (h·ft²·°F)/Btu	\$0.033	\$0.031	\$0.007	R-33.6	R-33.3	R-23.6
R-30 (h·ft²·°F)/Btu	\$0.026	\$0.024	\$0.005	R-34.9	R-34.7	R-31.5
Minneapolis, MN						
R-5 (h·ft²·°F)/Btu	\$0.030	\$0.028	\$0.010	R- 5.8	R- 5.8	R- 5.3
R-10 (h·ft²·°F)/Btu	\$0.017	\$0.016	\$0.006	R-10.8	R-10.8	R-10.3
R-15 (h·ft²·°F)/Btu	\$0.011	\$0.010	\$0.003	R-16.1	R-16.1	R-15.3
R-20 (h·ft²·°F)/Btu	\$0.008	\$0.008	\$0.003	R-23.5	R-23.2	R-20.8
R-30 (h·ft²·°F)/Btu	\$0.006	\$0.006	\$0.002	R-31.4	R-31.3	R-30.5

* These simulations do not include soiling of the membranes.

Table 14. Wholesale cost of polyisocyanurate insulation per square of insulation (one square = 100 ft^2)

Insulation thickness (in.)	Cost data for polyisocyanurate insulation ($/square)		
	Phoenix, AZ	Knoxville, TN	Minneapolis, MN
1	$27.80	$25.50	$24.75
2	$39.15	$33.55	$34.00
3	$56.65	$54.00	$54.60
4	$76.25	$75.70	$81.35

shows that the membrane must cost less than $0.30 per ft^2 to economically justify its use over a BUR with additional polyisocyanurate insulation (Fig. 39c).

7.3 COST OF BUILDING ENERGY INCURRED DUE TO SOILING OF ROOF

Simulations were also conducted to determine the increase in cost of building roof energy caused by soiling of the single-ply membranes. Weather databases for Phoenix, AZ, Knoxville, TN, and Minneapolis, MN, were derived from the TMY2 data (NREL 1995) to contain 3 years of hourly data for the ambient dry bulb temperature and relative humidity, wind speed, wind direction, solar insolation, cloud cover and precipitation. STAR read the data and calculated the hourly heat flux entering or leaving the conditioned space. Simulations were conducted for a low-slope roof with insulation levels ranging from R-5 through R-30 exposed to the climates of Phoenix, Knoxville, and Minneapolis. Membrane soiling was forecast using algorithms predicting the loss of reflectance (Sect. 4.3).

An annual roof load was calculated by summing the CL and the HL roof energies, which were previously defined in Sect. 7.1. The annual roof energy for a soiled membrane was scaled by the annual roof energy for the identical clean membrane. Therefore subtracting one from the scaled factor represents the percentage increase in roof energy as compared to the same clean membrane whose reflectance remains constant (Fig. 40). A scaled roof energy factor of one represents no net change in energy, trends exceeding one represent penalties in increased roof energy, and trends falling below one represent decreases in roof net energy (Fig. 40).

For a roof having R-15 insulation in Phoenix, AZ, the results show significant increases in roof energy. One year of soiling causes a 24% increase in the annual roof energy for the Code A membrane with R-15 insulation. After 2 years, the roof incurs a 51% increase. The increase in energy levels out through 3 years of exposure, and the net increase in annual roof energy plateaus at about 60%. For the Code I membrane compared against a clean Code I membrane, a 31% increase is observed after 3 years of exposure in Phoenix (Fig. 40).

The predominant heating in Minneapolis causes the annual roof energy for the highly reflective membranes to drop slightly because the soiling of the Code A and I membranes lessens the heating-energy penalty.

Knoxville's climate is more moderate. The heating degree-days (HDD) for the Knoxville climate are about 3662°F·days as calculated from the TMY2 database; cooling-degree days (CDD) are about 1366°F·days. However, despite the fact that Code A and I membranes soil, the net effect on annual roof energy is a wash (Fig. 40). For the Code A and I membranes with insulation levels exceeding R-10, the cooling energy savings are offset by the heating-energy penalty. The result for Knoxville is very interesting because its ratio of CDD to HDD of (0.37) may roughly represent a boundary for the

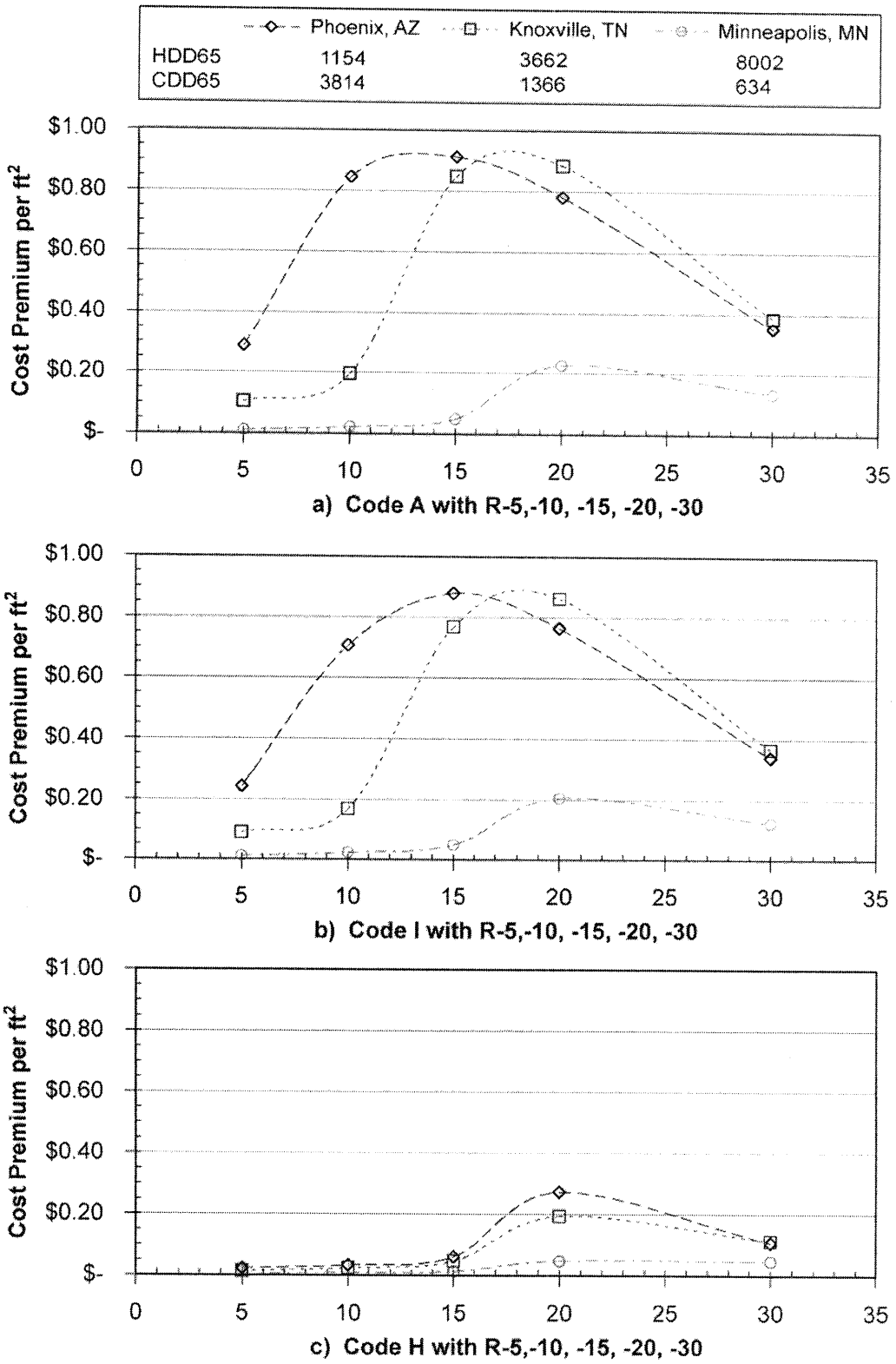

Fig. 39. Cost of additional insulation needed for a smooth BUR roof to have the same annual operating cost as a cool roof membrane.

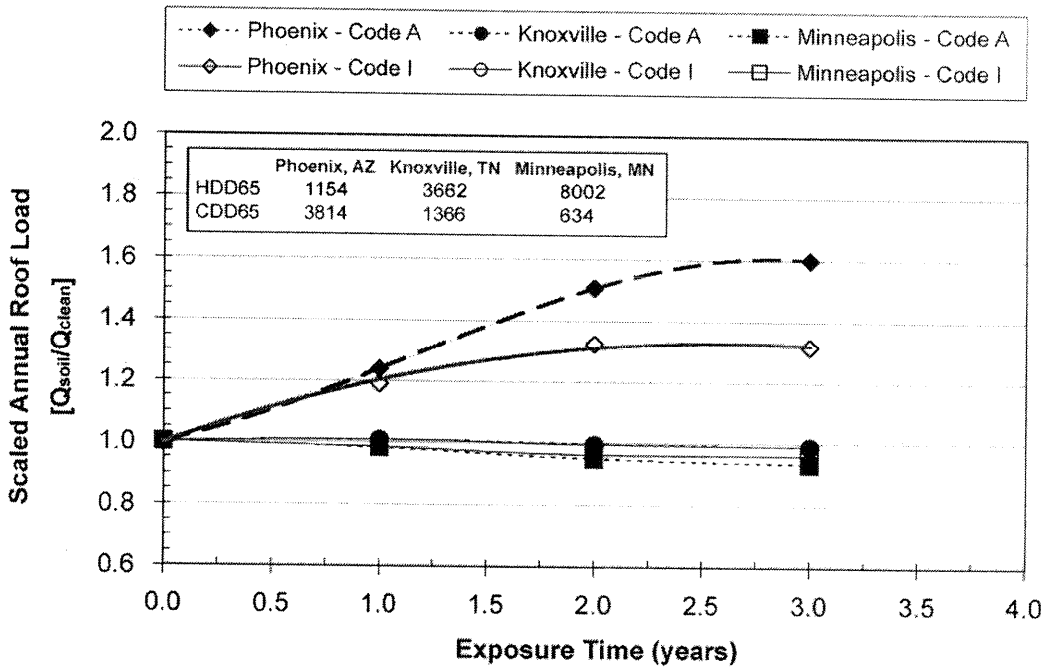

Fig. 40. The scaled annual energy transmitted through a low-slope roof having R-15 insulation is shown for different thermoplastic membranes. Qsoil represents the annual energy transmitted through a soiled membrane with R-15 insulation. Qclean represents the same membrane with no loss of reflectance.

benefit of periodically washing cool roof membranes. In Phoenix the advantage for washing is obvious, while for Knoxville there is no clear advantage for periodically washing the roof.

Cost estimates were calculated by subtracting the roof energy for a thermoplastic membrane that soils with time from the roof energy for the same membrane that remains clean. Service charges for electricity and natural gas, HVAC COP and gas furnace efficiencies used in the analysis are discussed in Sects. 5.2.1 and 5.2.2, respectively. The cost data are listed in Table 15 for different levels of roof insulation for exposure in the climates of Knoxville and Phoenix. The negative currency values represent the cost of energy that the building owner incurs as the roof soils. It can be compared to the cost for commercial washing to economically justify washing the roof.

An independent contractor would charge about 1¢ per square foot to wash a roof with a power washer. The cost of additional roof energy for Phoenix clearly justifies power washing a roof with insulation as high as R-30 for the Code A membrane. In fact, the building owner can realize a net savings of about 6¢ per square foot if he washes the roof every other year for a roof with Code A membrane with R-15 insulation. The cost advantage is not as great for the Code I membrane because Code I loses only about 25% of its original reflectance as compared to the 50% loss observed for Code A membrane, (see Sect. 4.1). Yet, the building owner can still save about 4¢ per square foot by washing the Code I membrane that has R-15 insulation every other year. Washing every third year increases the saving to about 11 and 7¢ per square foot of the Code A and Code I membranes, respectively.

In the more moderate climate of Knoxville, the advantage for washing the roof is only about 1¢ per square foot after 3 years of exposure for the Code A membrane with R-15 insulation. Once again,

Table 15. Cumulative cost penalty $/(ft^2·yr) for the building roof energy observed as the highly reflective membranes Code A and Code I soil with exposure time. The negative currency values reflect the cost the building owner pays in increased utility services because the thermoplastic membranes soil the roof and increase the annual roof energy

R-Value	Code A membrane Exposure time (years)			Code I membrane Exposure time (years)		
(h·ft^2·°F)/Btu	1	2	3	1	2	3
Exposure in Phoenix, AZ, climate						
5	-$0.067	-$0.219	-$0.400	-$0.057	-$0.162	-$0.266
10	-$0.037	-$0.120	-$0.218	-$0.031	-$0.088	-$0.145
15	-$0.021	-$0.068	-$0.123	-$0.018	-$0.050	-$0.082
20	-$0.014	-$0.043	-$0.077	-$0.012	-$0.031	-$0.051
30	-$0.008	-$0.027	-$0.048	-$0.007	-$0.020	-$0.032
Exposure in Knoxville, TN, climate						
5	-$0.023	-$0.070	-$0.125	-$0.019	-$0.052	-$0.083
10	-$0.011	-$0.035	-$0.062	-$0.010	-$0.026	-$0.041
15	-$0.004	-$0.013	-$0.023	-$0.004	-$0.010	-$0.015
20	-$0.001	-$0.004	-$0.006	-$0.001	-$0.003	-$0.004
30	-$0.001	-$0.002	-$0.004	-$0.001	-$0.002	-$0.002

cooling energy savings are partially offset by the heating-energy penalty. A slight cost penalty is observed in the Knoxville climate because of the difference in costs of electricity as compared to cost of natural gas. However, as discussed earlier, washing shows no clear cost advantage to the building owner in a moderate climate like Knoxville having a $^{CDD}/_{HDD} \approx 0.37$.

8. REFERENCES

Apthorp, D. M., and Bligh, T. P. 1985. "Modeling of Heat Flux Distortion Around Heat Flux Sensors." Building Applications of Heat Flux Transducers, ASTM STP 885, E. Bales, M. Bomberg, and G. E. Courville, Eds., American Society for Testing and Materials, Philadelphia, 1985, pp. 45–64.

Armstrong, S. 2002. "The Fundamentals of Fungi." ASHRAE Journal, Nov. 2002. 18–24.

ASHRAE. 2001. "Thermal and Water Vapor Transmission Data." ASHRAE Fundamentals, Vol. 25, pp.25.5–25.8.

ASHRAE Standard 90.1-1999. "Energy Standard for Buildings Except Low-Rise Residential Buildings." ASHRAE, 1999.

ASTM. 1995. Designation E1918-95: Standard Test Method for Measuring Solar Reflectance of Horizontal and Low-Sloped Surfaces in the Field. American Society for Testing and Materials, West Conshohocken, PA.

ASTM. 1996. Designation E903-96: Standard Test Method for Solar Absorption, Reflectance, and Transmittance of Materials Using Integrating Spheres. American Society for Testing and Materials, West Conshohocken, PA.

ASTM. 1997. Designation C 1371-97: Standard Test Method for Determination of Emittance of Materials Near Room Temperature Using Portable Emissometers. American Society for Testing and Materials, West Conshohocken, PA.

ASTM. 1998. Designation C518-98: Standard Test Method for Steady-State Thermal Transmission Properties by Means of the Heat Flow Meter Apparatus. American Society for Testing and Materials, West Conshohocken, PA.

ASTM. 2002. Designation C1549-02: Standard Test Method for Determination of Solar Reflectance near Ambient Temperature Using Portable Solar Reflectometer. American Society for Testing and Materials, West Conshohocken, PA.

Bååth, E., M. Díaz-Raviña, A. Frostegård, and C.D. Campbell. 1998. Effect of metal-rich sludge amendments on the soil microbial community. Appl. Environ. Microbiol. 64:238–245.

Baker, M. C. 1980. Roofs. Polyscience Publications Inc., Montreal, Quebec, Canada.

Balkwill, D. L., F. R. Leach, J. T. Wilson, J. F. McNabb, and D. C. White. 1988. Equivalence of microbial biomass measures based on membrane lipid and cell wall components, adenosine triphosphate, and direct counts in subsurface sediments. Microbial. Ecol. 16: 73–84.

Berdahl, P. H., and Bretz, S. E. 1997. "Preliminary survey of the solar reflectance of cool roofing materials." Energy and Buildings, Vol. 25, 149–158.

Bligh, E. G., and W. J. Dyer. 1959. A rapid method of total lipid extraction and purification. Can. J. of Biochem. and Phys. 37:911–917.

Brueker, M., Rossi, T., and Braun, J. 2000. "Smart Maintenance for Rooftop Units." ASHREA Journal, Nov. 2000. 41–47.

Byerley, A. R., and Christian, J. E. 1994. "The Long Term Thermal Performance of Radiation Control Coatings." *ACEEE Summer Study on Energy Efficiency in Buildings*, 5.59–5.71, Washington, D.C., American Council for an Energy Efficient Economy.

Childs, P. W., T. W. Petrie, and J. A. Atchley. 2001. Comparison of techniques for in situ, non-damaging measurement of infrared emittances of low-slope roof membranes. Submitted for review and publication in proceedings, Thermal Performance of the Exterior Envelopes of Buildings VIII Conference, December 2–6, 2001, Clearwater Beach, Florida.

Churchill, S. W. 1986. "Mixed Convection Heat Transfer." J. Heat Transfer, Vol. 108, 835–840.

EIA. 2001. Form EIA-826, Monthly electric utility sales, and Form EIA-176, Annual report of natural and supplemental gas supply and disposition. Internally search for EIA-826 and EIA-176 on Internet web site http:// www.eia.doe.gov/. Washington, DC: U.S. Energy Information Admin.

Frostegård, A., A. Tunlid, and E. Bååth. 1996. Changes in microbial community structure during long-term incubation in two soils experimentally contaminated with metals. Soil Biol. Biochem. 28:55–63.

Griffin, E. R. 2002. Introducing Stability at the Molecular Level. *Roofing Technology Magazine*, Vol. 2 Issue 2.

Guckert, J. B., C. P. Antworth, P. D. Nichols, and D. C. White. 1985. Phospholipid, ester-linked fatty acid profiles as reproducible assays for changes in prokaryotic community structure of estuarine sediments. FEMS Microbiol. Ecol. 31:147–158.

Incropera, F. P., DeWitt, D. P. 1990. Fundamentals of Heat and Mass Transfer. 3rd ed. John Wiley & Sons, New York.

Kelley, J. J., M. Häggblom, and R. L. Tate III. 1999. Changes in soil microbial communities over time resulting from one time application of zinc: a laboratory microcosm study. Soil Biol. Biochem. 31:1455–1465.

Kelso, J., and Kinzey, B. 2000. "BTS Core Data Book." DOE's Office of Building Technology, State and Community Programs.

Kollie, T.G., Weaver, F.J., McElroy, D.L. 1990. "Evaluation of a Commercial, Portable, Ambient-Temperature Emissometer." Rev. Sci. Instrum. Vol. 61, 1509-1517.

Martin, M., and Berdahl, P. H. 1984. "Characteristics of Infrared Sky Radiation in the United States." Solar Energy, Vol. 33, 321–336.

NREL. 1995. TMY2s. Typical meteorological years derived from the 1961–1990 national solar radiation database. Data Compact Disk. Golden, CO: National Renewable Energy laboratory.

Patankar, S. V. 1984. Numerical Heat Transfer and Fluid Flow. Hemisphere, New York.

Petrie, T. W., Childs, P. W., Christian, and J. E. 1998. "Radiation Control Coatings on Rough-Surfaced Roofs at a Federal Facility: Two Summers of Monitoring plus Roof and Whole Building Modeling." ASHRAE Proceedings, Thermal Performance of the Exterior Envelope of Buildings VII, Atlanta, GA., 353–371.

Petrie, T. W., Atchley, J. A., Childs, P. W., and Desjarlais, A. O. 2001a. "Effect of Solar Radiation Control on Energy Costs—A Radiation Control Fact Sheet for Low-Slope Roofs," *Proceedings, Performance of the Exterior Envelopes of Whole Buildings VIII: Integration of Building Envelopes*. December 2001. Paper 146, CD ISBN 1-883413-96-6. Atlanta, GA: American Society of Heating, Refrigeration and Air-Conditioning Engineers, Inc.

Petrie, T. W., Desjarlais, A. O., Robertson, R. H., and Parker, D. S. 2001b. Comparison of techniques for in-situ, non-damaging measurement of solar reflectance of low-slope roof membranes. Presented at the 14th Symposium on Thermophysical Properties and under review for publication in International Journal of Thermophysics, Boulder, CO: National Institute of Standards and Technology.

Quinn, T. J., and Fröhlich, C. 1999. "Accurate radiometers should measure the output of the Sun." Nature, 28 October 1999. vol. 401, p. 841.

Reagab, J. A., and Acklam, D. M. 1979. "Solar reflectance of common building materials and its influence on the roof heat gain of typical southwestern US residences." Energy Building, Vol. 2., 237.

Ringelberg, D. B., S. Sutton, and D. C. White. 1997. Biomass, bioactivity and biodiversity: microbial ecology of the deep subsurface: Analysis of ester-linked phospholipid fatty acids. FEMS Microbiology Reviews. 20:371–377.

Schlichting, H. 1960. Boundary Layer Theory. 4th ed. McGraw-Hill, New York.

Shah, M. M. 1981. "Estimation of Evaporation from Horizontal Surfaces." ASHRAE Trans., Vol. 87, pt. 1. 35–51.

Taha, H., Sailor, D., and Akbari, H. 1992. High-albedo materials for reducing building cooling energy use, LBL-31721, Lawrence Berkeley National Laboratory, Berkeley, CA.

Varma, H. K., Charan, V., and Soogappa, P. 1978. "Simultaneous Heat and Mass Transfer to a Flat Plate in Humid Air Stream Under Frosting Conditions." Letters in Heat and Mass Transfer, Vol. 5, 297–305.

White, D. C., and D. B. Ringelberg. 1998. Signature lipid biomarker analysis. In Techniques in Microbial Ecology. Burlage, R. S., R. Atlas, D. A. Stahl, G. Geesey, and G. Sayler (Eds). Oxford University Press, New York.

White, D. C., W. M. Davis, J. S. Nickels, J. D. King, and R. J. Bobbie. 1979. Determination of the sedimentary microbial biomass by extractable lipid phosphate. Oecologia 40: 51–62.

Wilkes, K. E. 1989. Model for Roof Thermal Performance. ORNL/CON-274. Oak Ridge, TN, Oak Ridge National Laboratory

Wilkes, K. E., T. W. Petrie, J. A. Atchley, and P. W. Childs. 2000. "Roof heating and cooling loads in various climates for the range of solar reflectance and infrared emittance observed for weathered coatings." *Proceedings 2000 ACEEE Summer Study on Energy Efficiency in Buildings,* pp. 3.361–3.372. Washington, DC: American Council for an Energy Efficient Economy.

Yaghoubi, M. A., Kazeminejad, H., and Farshidiyanfar, A. 1993. "Heat and Mass Transfer with Dehumidification in Laminar Boundary Layer Flow Along a Cooled Flat Plate," J. Heat Transfer, Vol. 115, 785–788.